Stony Brook University

Design and Simulation of Single-Electron Molecular Devices

A Dissertation Presented

by

Nikita Simonian

to

The Graduate School

in Partial Fulfillment of the Requirements

for the Degree of

Doctor of Philosophy

in

Physics

Stony Brook University

December 2012

Stony Brook University

The Graduate School

Nikita Simonian

We, the dissertation committee for the above candidate for the Doctor of Philosophy degree, hereby recommend acceptance of this dissertation.

Konstantin K. Likharev – Dissertation Advisor
Distinguished Professor, Department of Physics and Astronomy

Philip B. Allen – Chairperson of Defense
Professor, Department of Physics and Astronomy

Marivi Fernandez-Serra
Assistant Professor, Department of Physics and Astronomy

Dominik Schneble
Associate Professor, Department of Physics and Astronomy

Andreas Mayr
Professor, Department of Chemistry

This dissertation is accepted by the Graduate School.

Charles Taber
Dean of the Graduate School

Abstract of the Dissertation

Design and Simulation of Single-Electron Molecular Devices

by

Nikita Simonian

Doctor of Philosophy

in

Physics

Stony Brook University

2012

This work presents a study of molecular single-electron devices that may be used as the basic building blocks in high-density resistive memories and hybrid CMOS/nanoelectronic integrated circuits. It was focused on the design and simulation of a molecular two-terminal nonvolatile resistive switch based on a system of two linear, parallel, electrostatically-coupled molecules: one implementing a single-electron transistor and another serving as a single-electron trap. To verify the design, a theoretical analysis of this "memristive" device has been carried out, based on a combination of *ab-initio* calculations of the electronic structures of the molecules, Bardeen's approximation for the rate of tunneling due to wavefunction overlap between source/drain electrodes and the molecular device, and the general theory of single-electron tunneling in systems with discrete energy spectra. The results show that such molecular assemblies, with a length below 10 nm and a footprint area of about 5 nm^2, may combine sub-second switching times with multi-year retention times and high ($> 10^3$) ON/OFF current

ratios, at room temperature. Moreover, Monte Carlo simulations of self-assembled monolayers (SAM) based on such molecular assemblies have shown that such monolayers may also be used as resistive switches, with comparable characteristics and, in addition, be highly tolerant to defects and stray offset charges. An important and unexpected finding in this work is that the simulated I-V curves in a few molecular junctions exhibit negative differential resistance (NDR) with the origin so fundamental, that the effect should be observed in most molecular junctions where the sequential single-electron transfer limit is valid. Another important by-product of this work is a more complete understanding of some shortcomings of the existing density functional theory approximations, including their advanced versions such as the ASIC method.

Contents

List of Figures

List of Tables

Acknowledgements

This work would not be possible without a massive amount of computations performed on the supercomputers provided by DOD's HPCMP program.

Personally I would like to thank Professor Marivi Fernandez-Serra for her continuous help and support with the SIESTA package. Professors Andreas Mayr and Philip B. Allen, for their time clarifying and giving excellent suggestions to many important questions that were raised in the course of this project. Professor Dominik Schneble for taking time out of his busy schedule to serve on my oral and defense committee.

My advisor, Professor Konstantin K. Likharev, whose high standards, intellectual rigor, enthusiasm, perspective and input were extremely valuable to get this work done.

Out of the office, the many friends who I've met in Stony Brook over the years have made my stay here eventful. Yelena, for her patience, kindness, joy and love.

Lastly, my parents have provided inexhaustible encouragement and support throughout my Ph.D. route, and I wish to thank them here for all of their help.

Chapter 1

Introduction

1.1 Motivation

Complementary metal-oxide-semiconductor (CMOS) technology, arguably the most influential integrated circuit (IC) technology of the modern era, has seen an unprecedented performance growth at a steady exponential rate known as "Moore's Law" over the past 40+ years. The ability to sustain this growth has largely come from a continued shrinkage of the circuit components: smaller devices allow faster switching between their states, with more devices per die. Traditionally the IC industry has employed the "top-down" approach to create nanoscale devices by using larger, externally-controlled processes like patterning by optical lithography to direct their assembly. In essence the whole CMOS technology relies on a single device: the metal-oxide-semiconductor field-effect transistor (MOSFET), which in order to have identical properties need to have well defined geometries, in particular the length and the width of the conduction channel. Miniaturization of this electronic device to critical feature dimensions at or below 10 nm requires atomically precise patterning in order to control the rising quantum mechanical fluctuations [1–4]. Even if such patterning precision is achieved, the cost of a semiconductor fabrication plant will become prohibitively expensive leading to the stall of the "Moore's-Law".

Alternatively a "bottom-up" approach that has received much attention over a course of more than a decade (see, e.g., [5–13]), suggests to use specifically tailored molecules that naturally come in identical size and composition as the basic building blocks in integrated circuits. Wired single molecules that perform functions similar to those of a transistor have been demonstrated by several research groups [8, 9]. However, experiments were plagued by unacceptably low yield of working devices, low reproducibility as well as quick device degradation. The most common source of problems in such devices

is a poor ability to control the contacts and interfacial chemistry between a single molecule and a metallic electrode, resulting in a wide sample-to-sample variation of several orders of magnitude of the contact resistance and hence a large variation of the current flowing through a molecular device. In addition in three-terminal single-molecule devices that mimic the operation of a transistor, there is also little control over the distance from the molecular junction to the gate electrode since the placement of a single molecule in the gap between the two electrodes is completely random. Good control over this distance is essential because the electric field of the gate electrode exponentially decays in the narrow gap between source and drain electrodes (see Sec. 3.6) and therefore depending on where the molecular device is located in the gap, different gate voltages are needed to control the passing source to drain current. Moreover such devices can hardly amplify the signal; for example, the voltage gain of a 1-nm-scale transistor, based on any known physical effect (e.g., the field effect, quantum interference, or single-electron charging), can hardly exceed one, i.e. the level necessary for sustaining the operation of virtually any active digital circuit, and hence even if other problems are solved at a single device level, very large scale integrated (VLSI) circuits entirely built using such miniature devices can hardly ever be viable.

In spite of these limitations, it is still feasible to pursue more robust molecular devices that alone or as self-assembled monolayers (SAM) have simple functional properties for example of a two terminal resistive switch - see e.g. [14–16]. If such devices can be built, they may be used in hybrid CMOS/nanoelectronic circuits [17, 18] that according to recent studies are one of the most promising architectures that can extend the exponential pace of semiconductor integrated circuit scaling for as much as 10 to 15 years [14]. In such a hybrid circuit (Fig. 1.1a) the usual CMOS "stack" (consisting of a layer of silicon MOSFETs at the wafer surface and several layers of metallic interconnects) is complemented with a dense nanoelectronic add-on, namely a nanowire crossbar with identical nanodevices at each crosspoint (Fig. 1.1b). The crosspoint device may include a single-bit memory cell whose state controls the connection of two nearby nanowires.

The purpose of this dissertation was to design molecular assemblies with a built-in resistive switching functionality that can be used as two-terminal crosspoint devices in the CMOS/nanoelectronic circuits, and to simulate the electronic transport and charging in these molecular devices alone and in their self-assembled-monolayers (SAM)s. The devices were designed in such a way that their key electronic states (participating in charging and transport) are weakly coupled to the source and control electrodes [1]. In this limit the dy-

[1]Generally the electric charge of each molecular component can be a multiple of the

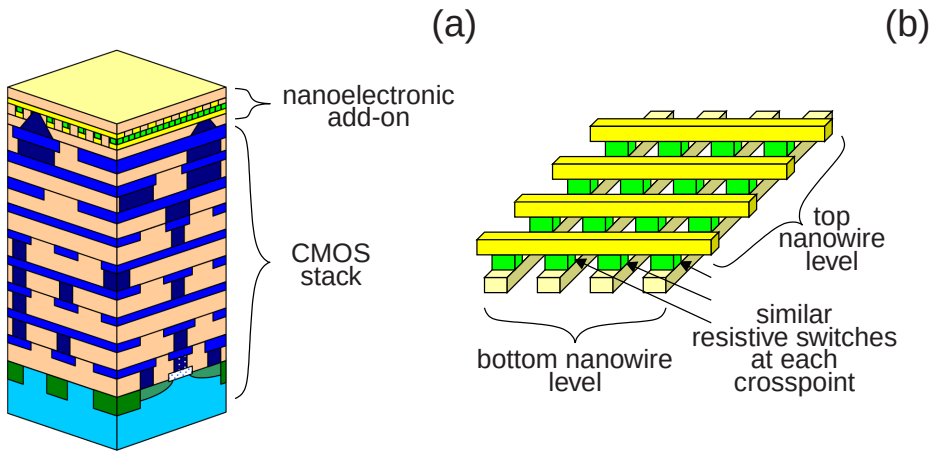

Figure 1.1: (a) The general idea of the hybrid CMOS/nanoelectronic circuit (b) the crossbar add-on.

namics of the electrons in the system may be described by the theory of single-electron charging and transport in systems with discrete energy spectra [19–22].

In the reminder of this chapter I will review recent progress in the studies of various device designs (both molecular and solid state) that have built in resistive switching functionality. Some of these devices already have most characteristics suitable for the initial push towards the crossbar based electronic architectures. Since the molecular assemblies that we have designed work in the single-electron limit, we will give a concise overview of the basic physics of single-electron phenomena and review the key single-electron devices that are relevant to this work. Chapter 2 of the dissertation is devoted to the novel designs of candidate component molecules of a molecular single-electron resistive switch. In Chapter 3 I introduce an adequate theoretical model that is used in subsequent chapters to calculate transport and charging properties of candidate molecules. Chapter 4 discusses the results of calculations of components of initially suggested molecules: surprisingly, the resulting current voltage ($I-V$) curves show negative differential resistance (NDR). A simple yet previously missed universal negative differential resistance mechanism is proposed, that may be observed at single-electron charging and transport in single atoms and simple molecules. In Chapter 5 the results of a calculation of electronic transport and charging in the final molecular single-electron re-

fundamental charge e at any instant (the weak coupling limit that we have adopted in our designs) or may be continuous (the strong coupling limit) — see Sec. 1.3 for a more detailed explanation.

sistive switch and results of Monte-Carlo simulations of SAMs based on such switches are presented. The thesis is concluded (Chapter 6) with a summary of the results and possible future directions. In Appendix A it is shown on a simple example that the effect of self-interaction in the modern density-functional-theory (DFT) calculations (that were heavily relied on in this work) may significantly offset the resulting properties of the system such as electronic energy spectrum, and hence give wrong predictions. In Appendix B another self-interaction induced problem with the DFT theory is addressed — the level "freezing" at voltages above certain thresholds in component molecules of the molecular switch, this DFT deficiency in particular creates difficulties in the calculation of charging and discharging rates of the trap component of the molecular switch — see Sec. 3.3.1 for details and the resolution. In Appendix C a simple derivation of a Bardeen's approximation is given, which is used in calculations of electron transfer rates between source/drain electrodes and the attached molecules — see Sec. 3.4.

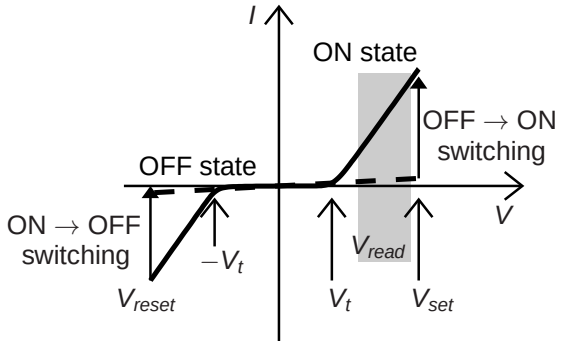

Figure 1.2: Schematics of the $I-V$ curve of a bipolar resistive switch.

1.2 Resistive Switches

The most critical component of the hybrid CMOS/nanoelectronic circuit (Fig. 1.1a) is the resistive switch (alternatively called either "latching switch" or "programmable diode") — a two-terminal electronic device with a resistive bistability. Figure 1.2 schematically shows a possible (bipolar) switching scenario. In the ON state the dc $I-V$ curve is similar to that of the usual diode, with a fast increase of current above a certain voltage V_t. The device may be switched into another (OFF) state, with a very low current, by crossing the threshold V_{reset}, and switched back by its biasing with voltage $V > V_{set}$. Such resistive bistability has been repeatedly observed, since the middle of the past

century, in thin layers of many materials including several organic compounds (with or without embedded metallic clusters), metal oxides, amorphous silicon, and self-assembled molecular monolayers.

In order to be compatible with the crossbar architecture, candidate devices must meet certain requirements.
(1) Their retention τ_r and set/reset τ_{set}, τ_{reset} times (of switching from OFF to ON and from ON to OFF) must satisfy relations $\tau_{set}/\tau_r \approx \tau_{reset}/\tau_r \geq 10^{10}$. Devices that feature the rentention time τ_r of the order of a few seconds can be considered candidates for dynamic-random-access-memory (DRAM) applications, while devices with $\tau_r \approx 10^8$s or higher are good candidates for nonvolatile memory applications.
(2) The ON/OFF current ratio[2] (Fig. 1.2) should be sufficiently high ($\geq 10^3$) to suppress current "sneak paths" in large crossbar arrays [23, 24].
(3) The signal provided by a single crosspoint device should be able to control either a MOSFET transistor of the CMOS sub-system or a sense amplifier of the resistive memory block. This is only possible if the total ON current of the crosspoint is higher (or at least not much lower) than the leakage current of transistor's gate, currently approaching 100 A/cm^2 [25].
(4) Ideally these devices should be easily scaled to below 10 nm.
(5) Device switching endurance should above $\sim 10^5$ program-erase cycles, i.e. be comparable (or at least not much lower) than modern flash memory cells.

Clearly, designing a resistive switch that features all of the above characteristics is extremely challenging. The final molecular device presented in this work (see Chapter 5 for details) does satisfy many of the requirements outlined above, however much additional work is still needed towards practicable single-electron molecular resistive switches.

1.2.1 Organic compounds, inorganic/organic nanocomposites.

A number of devices based on relatively thick organic layers ($\sim$ 100 nm) sandwiched between various metallic electrodes — see Table 1.1, as well as hybrid organic/inorganic devices, where a semiconductor (ZnO, CdSe, Si, CuO, etc.) or metal (Au, Ag, FeNi, etc.) nanoparticle layer [26–31] is sandwiched between layers of organic molecules have been recently studied. Most of these materials provide a rather high ON/OFF current ratios in the range of $10^2 - 10^6$; however, only one publication [32] has reported good sample-to-sample reproducibility of switching voltage thresholds, and the layer thickness in that work was very large ($\sim$ 200 nm). It remains to be seen whether it may be scaled

[2]Taken at the read voltage V_{read}

Base electrode	interlayer (nm)	Top electrode	ON/OFF ratio	Switching time(s)	Retention time (s)	Endurance (cycles)	Reproducibility	Refs.
metal - organic compound - metal								
Al	AIDCN	Al	$> 10^4$	$< 10^{-8}$	$> 10^4$	?	?	[33]
InSnO	eosin (100)	Al	$> 10^5$	?	$> 10^4$	$\gg 1$	?	[34]
Al	Au-DT	Al	$> 10^3$	$< 10^{-7}$	?	$\gg 1$	?	[35]
Cu	DDQ	Ti (200)	$\sim 10^3$	$< 10^{-6}$	$> 10^5$	?	?	[36]
Au	Cu-TCNQ (200)	Al	~ 10	< 1	$> 10^4$	$> 10^3$	$< 20\%$	[32]

Table 1.1: Some recently reported results for organic compound based resistive switches

down while keeping good switching properties.

1.2.2 Metal oxide, Sulphides, Silicon Oxide, Amorphous Silicon

Resistive switching in metal-oxide-metal junctions has been extensively studied for the last 50 years, with the apparently first observation of negative resistance in thin anodic oxide films reported in 1962 [37]. More recently a number of different oxide materials such as TiO_2 [38–40], MoO_x [41], CuO_x [42, 43], SiO_2 [44] were used with various metallic electrodes to produce very promising results, (For the summary of results see Table 1.2.)

There is still some degree of uncertainty regarding the exact physical mechanism behind the observed bistability effects in both organic and inorganic interlayer materials. Most such materials show bipolar switching operation - see Fig. 1.2 some - feature unipolar switching, yet others have simultaneously both bipolar and unipolar switching operations. Most authors suggest (see e.g., the recent review [45]) that at least the bipolar operation of these devices is due to the reversible formation of a conducting filament between the junction electrodes, due to ion drift in the interlayer material caused by applied electric fields - see Figure 1.3. A recent paper [16] suggests on the atomic level that the unipolar switching may be possible due to the existence of temperature gradients in the interlayer materials that induces drift of positively charged oxygen ions.

A summary of recent results in this field (see Table 1.2), indicate that such devices may enable fabrication of CMOS/nanoelectronic hybrids with the crossbar parameter F_{nano} (the crossbar half-pitch) above the 10nm limit. Still

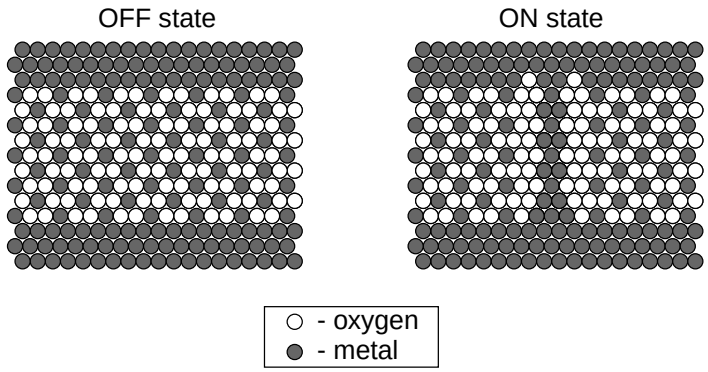

Figure 1.3: A cartoon of the apparent nature of resistive bistability in metal oxide junctions.

however, most publications do not give much quantitative information about the achieved device reproducibility. Even if the reproducibility concerns are solved in the near future, the apparent operation mechanism make metal oxide based devices hardly scalable to or below the 10nm limit, where the crosspoint junction area becomes comparable to or smaller than the cross-section of the switchable filament, and hence device-to-device reproducibility would require a system uniformity on the atomic level, which will hardly be ever possible.

1.2.3 Single molecules and self-assembled molecular monolayers

It appears that the only practical way towards integrating identical resistive switches in crossbar architectures beyond the 10 nm crossbar frontier is to use specially synthesized molecules. As was mentioned in Sec. 1.1, wiring single molecules is a daunting task, plagued by low yield and irreproducibility. However molecular two-terminal crosspoint devices (see Fig. 1.1b) may use self-assembled-monolayers of identical molecules — see Fig. 1.4. The footprint of a typical molecule in such a monolayer is very small (~ 1 nm^2), so that even with the low-limit pitch values of F_{nano} the number of molecules per node would be in the hundreds, and hence such devices may in principle be quite reproducible.

In the beginning of crossbar circuit research, there was a substantial effort toward the implementation of molecular resistive switches using self-assembled monolayers (SAM) of mechanically interlocked organic molecules such as catenanes [55, 56] and rotaxanes [57]; the former molecular assembly was suggested to have two distinct conducting regimes depending on the position of the macrocycle molecule, which in turn may be controlled by applying voltages

Base electrode	interlayer (nm)	Top electrode	ON/OFF ratio	Switching time(s)	Retention time (s)	Endurance (cycles)	Reproducibility	Refs.
M_1	MO_x (?)	M_2	$> 10^2$	$< 10^{-8}, 10^{-5}$	?	?	$> 50\%$	[41]
Cu	CuO_x (12)	TiN	$\sim 10^3$	$< 10^{-7}$	$> 10^6$	> 600	$\sim 40\%$	[42]
Ag	Ag_2S (?)	Ag/Pt	~ 30	$< 10^{-6}$	?	$> 10^5$	?	[46]
Cu	$Cu_{2-x}S_x$ (?)	Pt	$\sim 10^3$	?	?	?	?	[47]
Ni	NiO_x (40)	Pt	$\sim 10^2$	?	?	?	$\sim 15\%$	[48]
Pt	CuI_xS_y (700)	Cu	$> 10^3$	< 0.1	$> 10^3$	$> 10^2$	?	[49]
Pt	CuS_x (?)	Cu/Pt	$\sim 10^3$	?	?	30	?	[50]
Si	ZrO_2 (50)	Au	$\sim 10^3$	?	$> 10^3$	$> 10^2$	?	[51]
W	SiO_2 ($<$ 50)	Cu	$\sim 10^3$	10^{-6}	$> 10^4$	$> 10^7$	?	[44]
Cu	CuO_x (7)	Ni,Co	$> 10^3$	$< 10^{-7}$	?	?	$\sim 30\%$	[43]
Pt	TiO_2 (27)	Pt	~ 5	?	?	> 30	?	[38]
Si	a-Si (~ 5)	Ag	$> 10^4$	$< 10^-7$	$> 10^6$	$> 10^4$	$\sim 15\%$	[52]
Ti/Pt	ZrO_2 (43)	Cu	$\sim 10^6$	$\sim 10^-7$	$> 10^4$	$> 10^4$	$\sim 30\%$	[53]
p-Si	a-Si (80)	Ag	$\sim 10^4$	$< 10^{-9}$	10^7	10^6	$\sim 10\%$	[54]
Ti/Pt	TiO_2 (15)	Ti/Pt	$\sim 10^4$	?	?	?	?	[39]
Ti/Pt	TiO_2 (50)	Ti/Pt	$\sim 10^3$	$< 10^-8$	?	> 50	?	[40]

Table 1.2: Some recently reported results for resistive switches based on metal oxides, sulphides, silicon oxide, and amorphous silicon

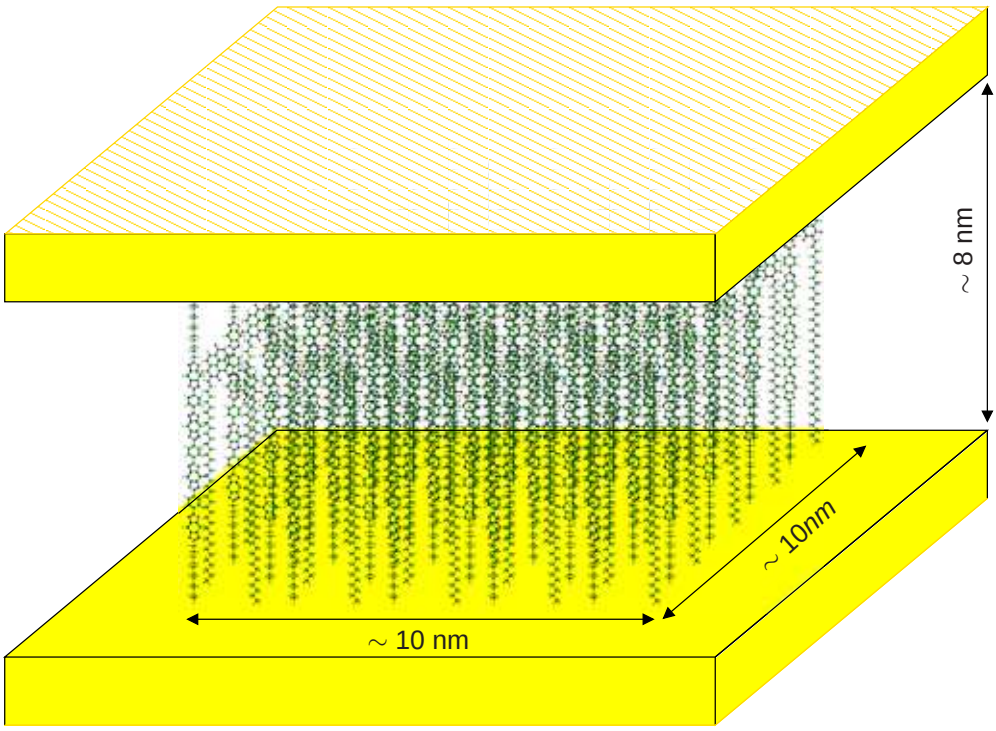

Figure 1.4: Schematic view of a 5 × 5-switch SAM sandwiched between two electrodes.

beyond a certain threshold. However, it has been noticed in at least some studies that the memory effects do not change much if the SAM is removed from the junction altogether, and hence may be explained by the same conducting filament formation as discussed in the Sec. 1.3.

Still, possibilities for using other physical mechanisms of resistive switching in molecules have not yet been thoroughly investigated. One such possibility, presented in this thesis, is to use a molecular version of the device called the single-electron resistive (or "latching") switch.

1.3 Single-electron devices

1.3.1 Basics

The basic concept of single electronics is illustrated in Fig. 1.5, where two parts of a conductor are separated by some interface. It turns out that depending on the strength of this interface (its effective tunnel resistance R) the electric charge of each conductor may be a multiple of the fundamental charge $e \approx$

1.6×10^{-19} C (this is natural for the particle picture of matter) or may be continuous (the wave picture allows this, because the wavefunction of each electron may be split between the two parts). The particle picture is more adequate when the tunnel resistance R is high

$$R \gg R_Q \equiv \hbar/e^2 = 4.1k\Omega, \tag{1.1}$$

where R_Q is the quantum unit of resistance; the wave picture is more natural in the opposite limit.

This relation may be derived and explained in numerous ways; perhaps the simplest interpretation is as follows. In a closed ("Hamiltonian") quantum system, the characteristic energy of quantum fluctuations per degree of freedom is $E_Q \sim \hbar\omega$, where ω is a characteristic frequency. In contrast, each part of the conductor we are discussing, concerning its electric charge degree of freedom, is an "open" system, strongly interacting with its environment (corresponding to an RC relaxator, rather than an LC oscillator). For such a system, $\hbar\omega$ should be replaced by $\hbar/\tau$, with $\tau = RC$, where C is the capacitance between the two conducting parts. Transfer of a single electron between the parts causes an electrostatic energy change of the order of $E_C \sim e^2/2C$. Comparing E_C and E_Q we notice that C cancels, and hence if $R \ll R_Q$, quantum fluctuations smear out the electrostatic energy difference which tries to keep the electric charge of each part constant, in the opposite limit if $R \gg R_Q$, the electrostatic charge in each conducting part is a multiple of the elementary charge e.

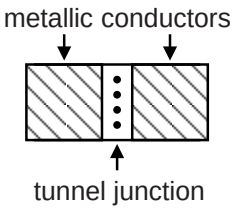

Figure 1.5: The basic concept of single-electronics; two conductors separated by a tunnel barrier.

1.3.2 Single-electron box

The most generic single-electron device, called the "single-electron box" is schematically shown in Fig. 1.6a. The basic physics of this device was first understood by Lambe and Jaklevic [58] on the basis of their experiments with disordered granular structures, while the first quantitative theory of the box was developed by Kulik and Shekhter [59]. The device consists of just one

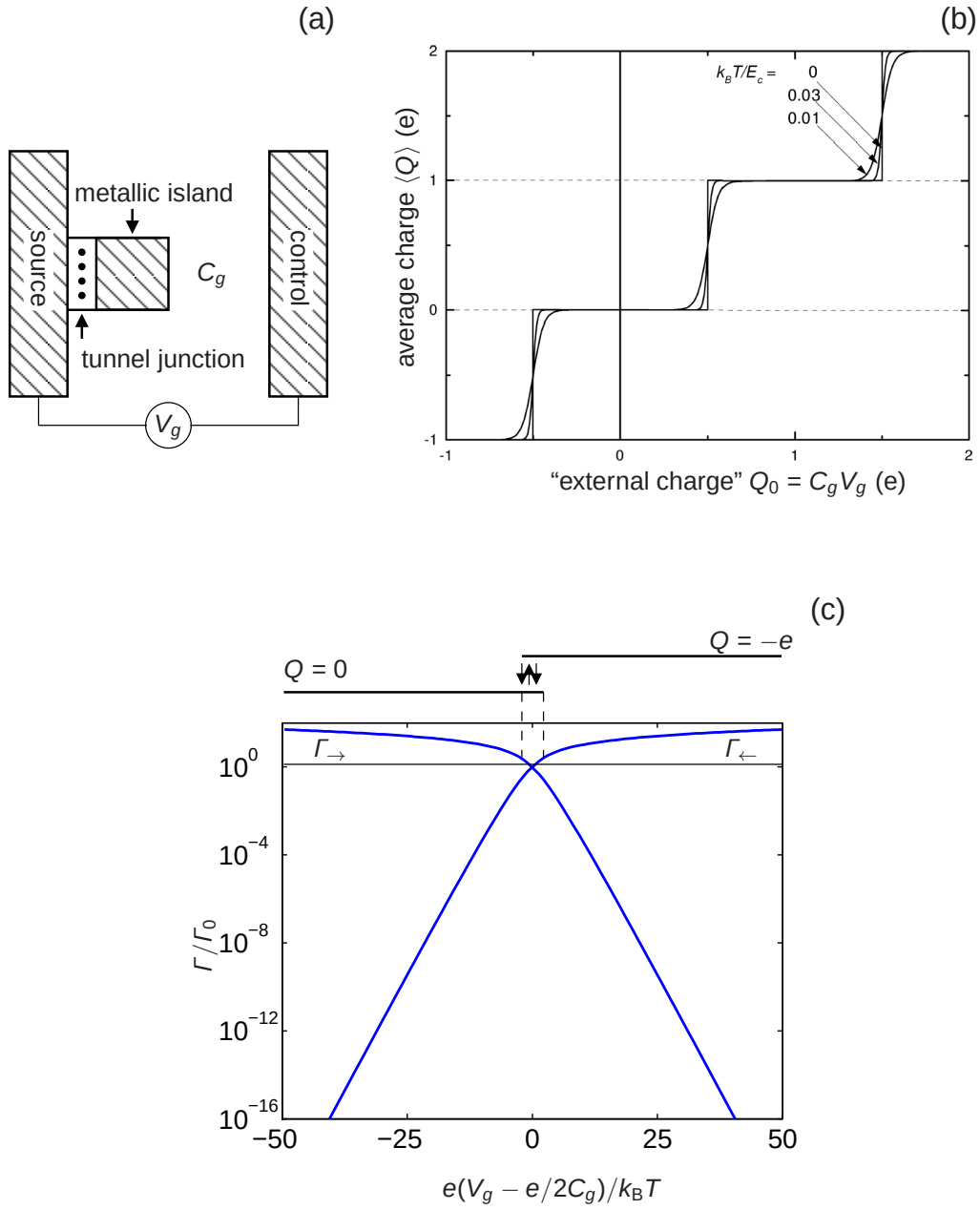

Figure 1.6: Single-electron box: (a) schematics, (b) the "Coulomb staircase", i.e. the step-like dependence of the average charge Q of the island on the gate voltage V_g, for several values of relative temperature, and (c) electron tunnel rates $\Gamma_\leftarrow$ (in) and $\Gamma_\rightarrow$ (out) of the single-electron box.

small conductor ("island") separated from an external electrode by a tunnel

barrier with a high resistance

$$R \gg R_Q \tag{1.2}$$

An external electric field may be applied to the island using a capacitively coupled gate electrode. The field changes the local Fermi level of the island and thus determines the conditions of electron tunneling. Elementary electrostatics shows that the energy of the system may be presented as

$$E = (Q_0 - ne)^2/2C_\Sigma + const,\ Q_0 \equiv C_g V_g, \tag{1.3}$$

where n is the number of uncompensated electrons on the island, C_g is the island-gate capacitance, while C_Σ is the total capacitance of the island (including C_g). The parameter Q_0 is usually called the "external charge", in contrast to the discrete island charge $-ne$, the variable Q_0 is continuous, and may be a fraction of the elementary charge e. At sufficiently low temperatures,

$$k_B T \ll E_C,\ E_C \equiv e^2/C_\Sigma, \tag{1.4}$$

the stationary number n of electrons in the island corresponds to the minimum of E; a simple calculation using Eq. 1.3 shows that Q is a steplike function of Q_0, i.e. of the gate voltage V_g (Fig. 1.6b), jumping by e when

$$Q_0 = e(n + 1/2),\ n = 0, \pm 1, \pm 2, ... \tag{1.5}$$

The physics of the "Coulomb staircase" in Fig. 1.6b is very simple: the increasing gate voltage V_g tries to attract more and more electrons to the island. The discreteness of the electron charge, provided by low transparency barriers (satisfying Eq. 1.2) ensures that the changes may only be discrete. If the temperature is increased to $k_B T \sim E_C$, the system has a non-vanishing probability to be in other charge states. A straightforward calculation of the average charge yields the pattern shown in Fig. 1.6b: the step-like dependence of charge on gate voltage is gradually smeared out by thermal fluctuations.

By itself, the single-electron box is not a very useful electronic circuit component. First, it does not have internal memory: the number of electrons in the box is a unique function of the applied voltage V_g so that it cannot be used for information storage.[3] And another way to see this is to look at Fig. 1.6c where we show the rates of tunneling in and out of the single-electron box. Clearly there is no possible charge state metastability (unlike in the case of the single-electron trap — see Sec. 1.3.4 and compare Figures 1.6c and 1.9c).

[3] In Sec. 1.3.4 we introduce a modification of the single-electron box: the single electron-trap that allows a metastable charge storage.

Second, the box cannot carry dc current, so that an ultrasensitive electrometer is necessary to measure its charge state.

1.3.3 Single-electron transistor

By simply splitting the electrode of the single-electron box into two parts (source and drain), turns it into a much more useful device: the single-electron transistor — see Fig. 1.7a for a geometry of this device. It was first suggested in 1985 [60, 61] and first implemented in 1987 [62].

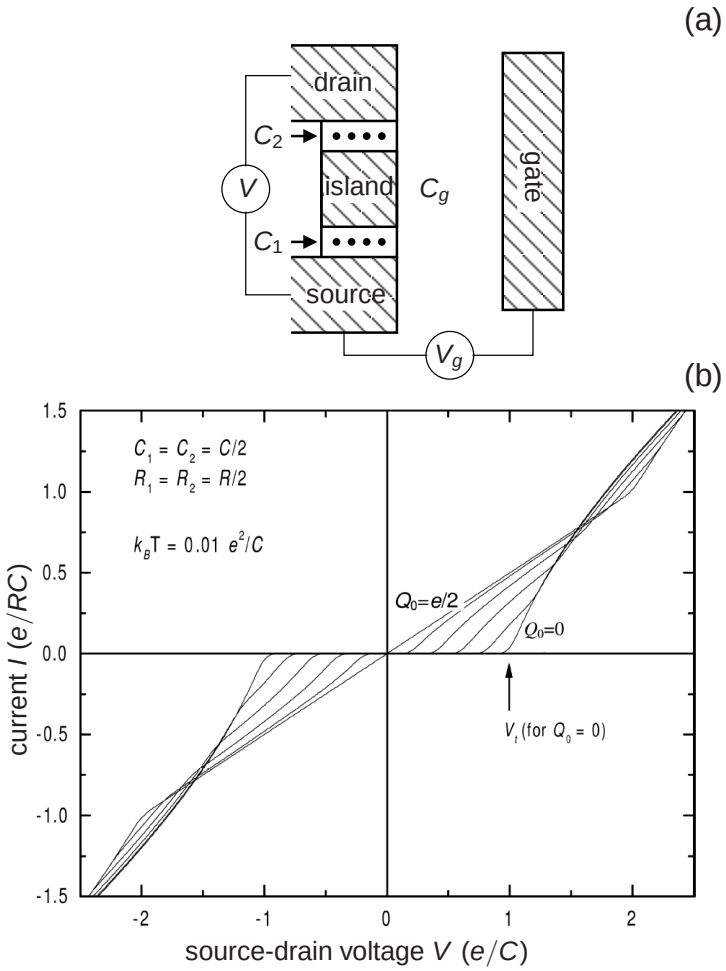

Figure 1.7: Single-electron transistor: (a) schematics, and (b) a typical set of source-drain $I - V$ curves of a symmetric transistor for several values of the "external charge" Q_0, i.e. of the gate voltage V_g, calculated using the "orthodox" theory of single-electron tunneling.

Figure 1.7b shows a typical set of dc $I-V$ curves of such transistor, for several values of the "external charge" Q_0, defined in the same way as in the single-electron box in Sec. 1.3.2. One can see that at small drain-to-source voltage V, there is virtually no current, except at the special values of Q_0 given by Eq. 1.5. The physics of this phenomenon (the "Coulomb blockade") is easy to understand: even if $V > 0$, and thus it is energy-advantageous for a electron to go from source to drain, on its way the electron has to tunnel into the island first, and change its charge Q by $\Delta Q = -e$. Such charging would increase the electrostatic energy E of the system

$$E = (Q_0 - ne)^2/2C_\Sigma - eV(n_1C_2 + n_2C_1)/C_\Sigma + const,\ C_\Sigma = C_g + C_1 + C_2 \quad (1.6)$$

(where n_1 and n_2 are the numbers of electrons passed through the tunnel barriers 1 and 2, respectively, so that $n = n_1 - n_2$), and hence at low enough temperature ($k_B T \ll E_C$) the tunneling rate is exponentially low.

At a certain threshold voltage V_C the Coulomb blockade is overcome, and currents starts to grow with V. The most important property of the single-electron transistor is that V_C is a periodic function of V_g, vanishing in special values of gate voltage, given by Eq. 1.5 — see Fig. 1.8. The reason for these so-called "Coulomb blockade oscillations" can be understood from the discussion of the single-electron box: in the special points (1.5), one electron may be transferred to the island from either drain or source without changing the electrostatic energy of the system even at V = 0. Hence, an electron can tunnel from the source to the island and then to the drain even at negligible V , so that $V_C = 0$. As can be shown from Eq. (1.6), at low temperatures the dependence of V_C on V_g is piecewise-linear, with its lower and upper branches forming the so-called "diamond diagram" (Fig. 1.8) [60].

1.3.4 Single-electron trap

Another key device, the "single-electron trap", may also be understood as a generalization of the single-electron box. Let me replace the single tunnel junction in Fig. 1.6a with an array of islands separated by tunnel barriers — Fig. 1.9a. The main new feature of this system is its internal memory. Within a certain range of applied gate voltage V_g the system may be in one of two charged states of its edge island — see the inset in Fig. 1.9b. With sufficiently small intermediate islands (such that the charging energy e^2/C of each such island is large) the state retention time τ_r[4] of the single-electron trap can be made much longer than the short switching times $\tau_\leftarrow, \tau_\rightarrow$ of the trap (see Fig.

[4]The time may be defined as the inverse of the rate Γ_r of spontaneous switching between two adjacent charge states at the bias point $V = V_e$ which equilibrates their energies.

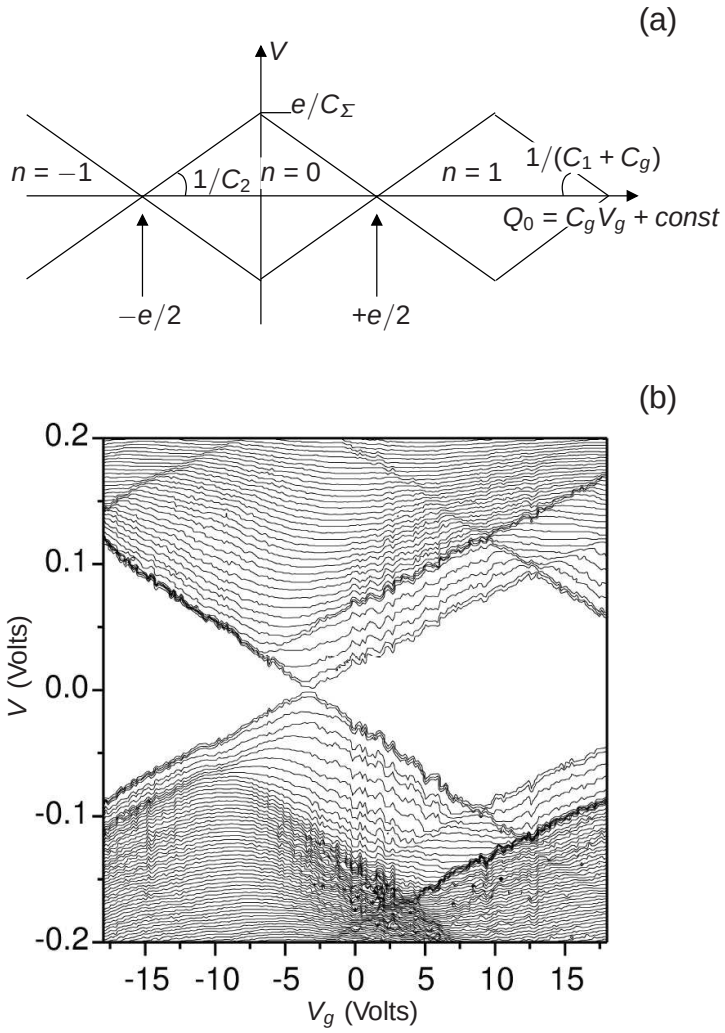

Figure 1.8: Coulomb blockade threshold voltage V_C as a function of Q_0: (a) theoretical dependence at $T \sim 0$ K, and (b) experimental contour plots of current on the $[V\ ,\ V_g]$ plane for an aluminum SET with $E_c \approx 100$ meV at $T = 4.2$ K — taken from Ref. [63]

1.9b) unlike the single-electron box, where those times are comparable (see Fig. 1.6c). The design similar to the one schematically shown in 1.9a has been used, in particular, for a successful implementation of aluminum-based latching switch prototypes (see Sec. 1.3.5) with long retention times at low (sub-1-K) temperatures [64, 65].

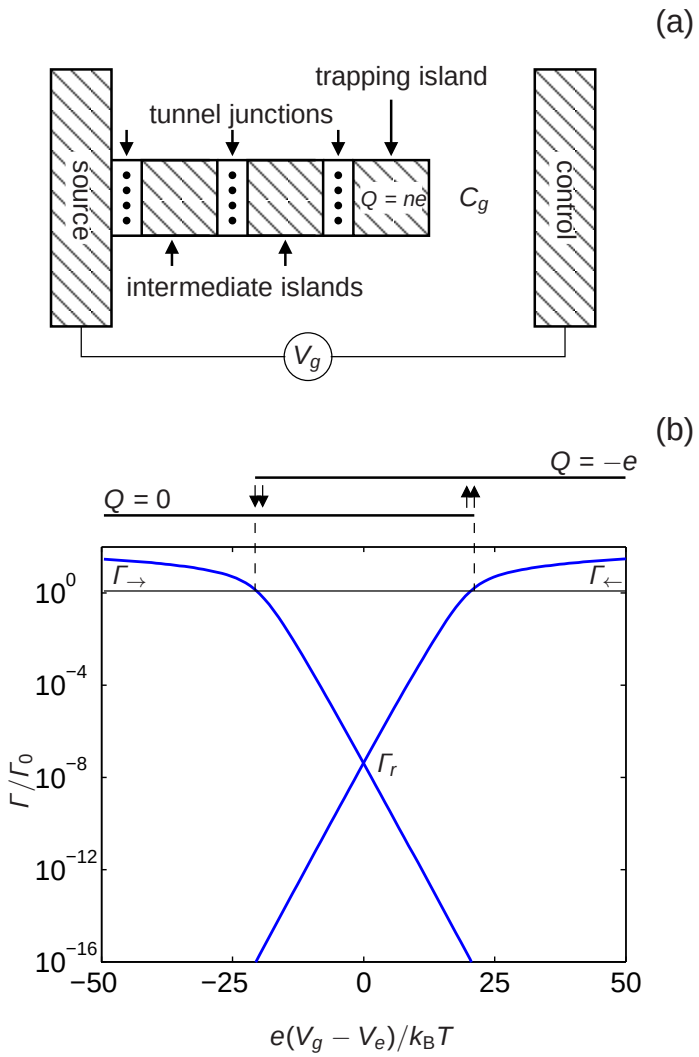

Figure 1.9: Single-electron trap: (a) schematics, and (b) electron tunnel rates in and out of the single-electron trap with the charging energy $e^2/C = 20k_{\rm B}T$.

1.3.5 Single-electron switch

One may combine a single-electron transistor and a single-electron trap into a single two terminal electrostatically-coupled device placed in parallel between two electrodes[5] — see Fig. 1.10a. When the charge state of the trap island is electroneutral ($Q = 0$), the Coulomb blockade threshold V_C of the transistor is large (Fig. 1.10b), so that at all applied voltages with $|V| < V_C$ the transistor

[5]In the switch, the third (gate) terminal of the single-electron transistor is replaced by the single-electron trap

carries virtually no current — the so-called OFF state of the switch. As soon as the voltage exceeds a certain threshold value $V_{\leftarrow} < V_C$, the rate of tunneling into the single-electron trap island increases sharply (1.9b), and an additional elementary charge q (either a hole or an electron) enters the trap island from the source electrode, charging it to $Q = q = \pm e$. The electrostatic field of this charge shifts the background electrostatic potential of transistor's island and as a result reduces the Coulomb blockade threshold of the transistor to a lower value V_C'. This is the ON state of the switch, with a substantial average current flowing through the transistor at $V > V_C'$. The device may be switched back into the OFF state by applying a reverse voltage in excess of the trap-discharging threshold $|V_{\rightarrow}|$. As was experimentally demonstrated for metallic, low-temperature prototypes of the single-electron switch [64], its retention time may be very long [6]. However, for that the scale $e^2/2C$ of the single-electron charging energy of the trap island, with effective capacitance C, has to be much higher than the scale of thermal fluctuations, $k_B T$. For room temperature, requires few-nm-sized islands [66], and so far the only way of reproducible fabrication of features that small has been the chemical synthesis of suitable molecules — see, e.g., [67, 68].

[6] A resistive switch with a sufficiently long (a-few-year) retention time at $V = 0$ may be classified as a nonvolatile memory cell.

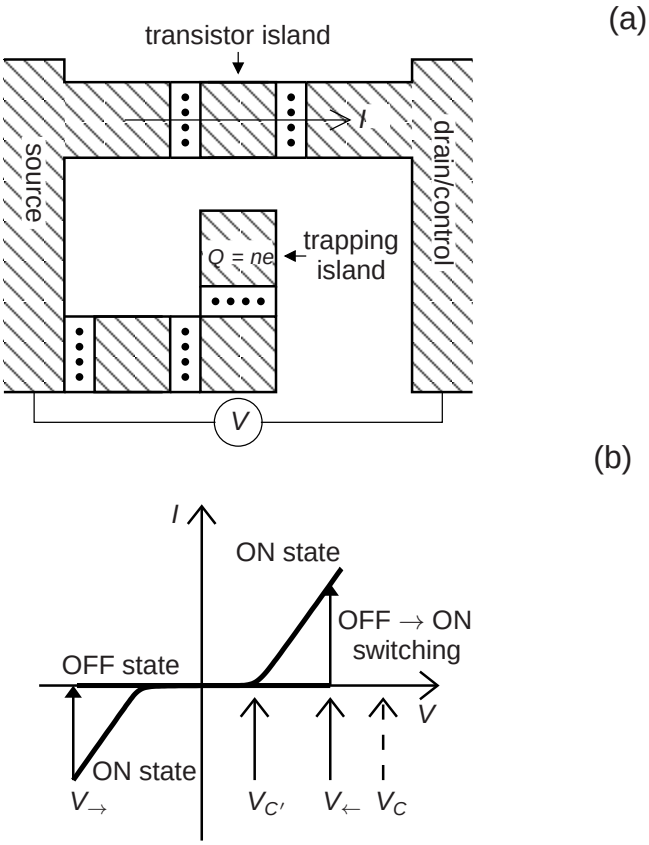

Figure 1.10: Single-electron switch: (a) schematics, and (b) its $I - V$ curve (schematically).

Chapter 2

Designing the molecular single-electron switch

2.1 General design guidelines and components

In the usual design of the single-electron trap (see Sec. 1.3.4 and Fig. 1.9) a long charge retention time is achieved by incorporation of several additional single-electron islands into the trap charging path. Such multi-island design of the trap is inconvenient for its molecular implementation. Indeed, the final island of the trap has to be physically close to the transistor island, in order to ensure a substantial electrostatic coupling between them. If the trap molecule includes several intermediate islands, it becomes much longer than the transistor molecule, and has to be bent approximately as shown in Fig. 1.10a, creating substantial difficulties for the chemical synthesis of the molecules and their self-assembly on electrode surfaces, and increasing the device footprint on the electrode (and hence chip) area.

Fortunately, the long molecular chains used in molecular electronics [67, 68] as tunnel barriers, have a band structure which enables their use not only as tunnel barriers, but as intermediate islands as well. Figure 2.1a shows the original design of the single-electron molecular switch, proposed by A. Mayr [69]. The design consists of a linear molecular rod featuring a central electron acceptor group (namely, naphthalenediimide or perylenediimide groups as transistor or trap islands) and terminal surface attachment groups such as oligo(phenylene ethynylene) (OPE) chains. The two molecules are locked together by non-conducting support groups that ensure their spatial separation. However, already the first quantitative density-functional-theory (DFT) simulations (see Fig. 2.2 and Chapter 3 for a concise review of this theory) have shown that the relatively narrow HOMO-LUMO bandgap of the OPE chains

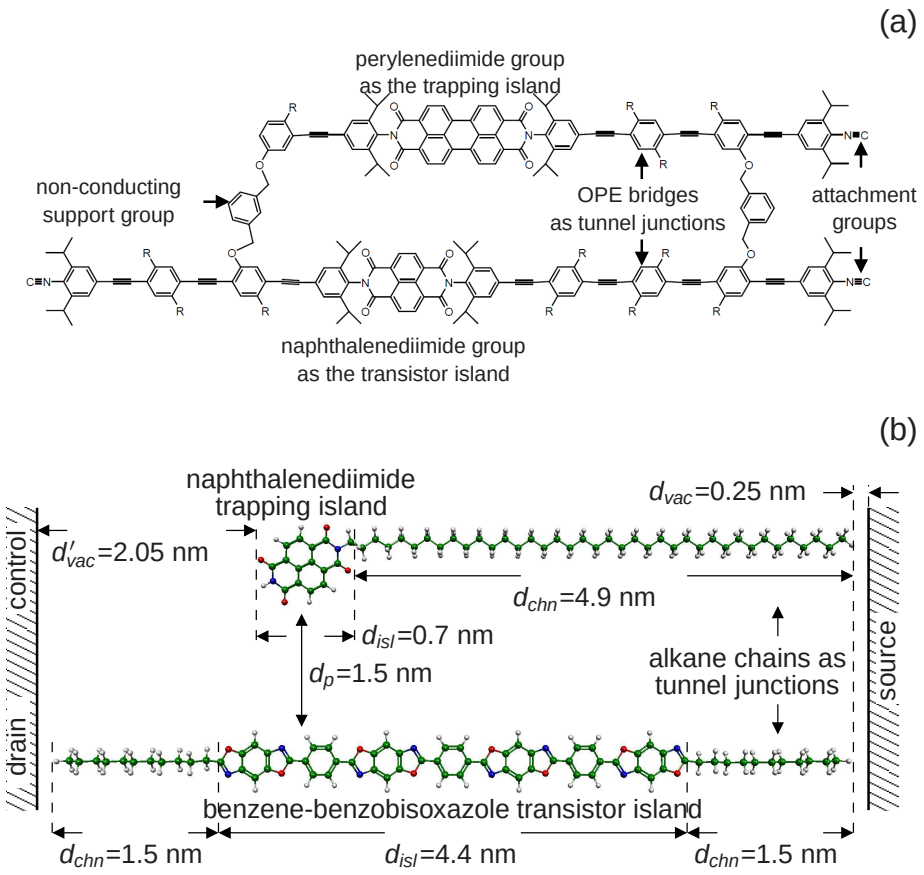

Figure 2.1: In (a) the early, OPE-tunnel chain based version of the molecular resistive switch, and in (b) our final version of a molecular resistive switch featuring an alkane-naphthalenediimide single-electron trap electrostatically coupled to an alkane-benzobisoxazole-benzene single-electron transistor.

(of the order of 1.5 eV, in agreement with [70]) cannot provide a tunnel barrier high enough to ensure sufficiently long electron retention times in traps with acceptable lengths. Moreover, DFT calculations predict that the energies of the orbitals, most important for device operation and spatially localized at either naphthalenediimide or perylenediimide groups (what I call the "working" orbital(s) in Sec. 2.2 and in Fig. 2.3b), do not fit into the HOMO-LUMO gap of the OPE chains: depending on the charge state of those molecules, the eigenenergies are either above the LUMO or below the HOMO energy of the OPE chain. As a result, it was concluded that alkane chains (CH_2-CH_2-...), with a bandgap of ~ 9 eV [71] — see Fig. 2.2, are much better resistive switch components. There is also substantial experience in the chemical synthesis of molecular electronic devices and SAMs using such chains as tunnel barriers

[67, 68]. Figure 2.1b shows a possible realization of such a device, based on benzene-benzobisoxazole and naphthalenediimide acceptor groups (playing the role of single-electron islands), and alkane chains playing the roles of tunnel barriers in both trap and transistor molecules and a set of intermediate islands in the molecular trap.

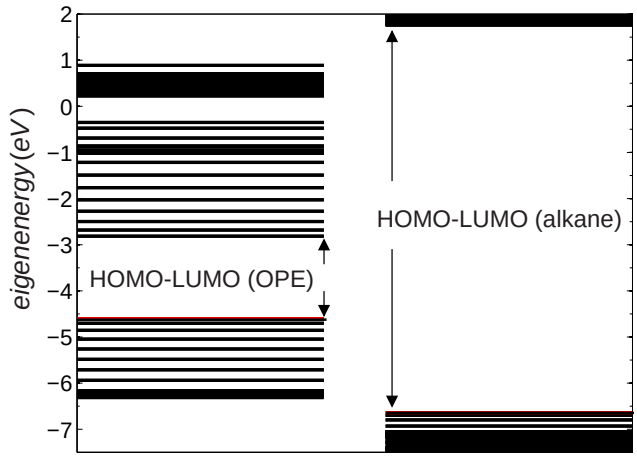

Figure 2.2: Comparison of the Kohn-Sham electron energy eigenspectra of long (> 6 nm) OPE and long (> 5 nm) Alkane chains.

2.2 Designing the molecular trap

2.2.1 Two roles of molecular chains

In order to explain the novel approach of using molecular chains simultaneously as tunnel barriers and as intermediate islands, let me again review the role of intermediate islands in the conventional design of the trap (see Fig. 1.9a and Sec. 1.3.4). If a single-electron island is so large that the electron motion quantization inside it is negligible, its energy spectrum, at a fixed net charge Q, may be treated as a continuum. Elementary charging of the island with either an additional electron or an additional hole raises all energies in the spectrum by $e^2/2C$, where C is the effective capacitance of the island [66, 72]. As a result, the continua of the effective single-particle energies of the system for electrons and holes are separated by an effective energy gap e^2/C — essentially, the "Coulomb gap" [73]. If this gap is much larger than $k_B T$ at applied voltages V close to the "energy-equilibrating" voltage V_e (see the middle panel of Fig. 2.3a), it may ensure a very low rate Γ_r of single-charge tunneling in either direction and hence a sufficiently long retention time $t_r = 1/\Gamma_r$ of the trap. The

energy gap may be suppressed by applying sufficiently high voltages $V \sim e/C$ of the proper polarity, enabling fast switching of the device into the counterpart charge state — see the left and right panels of Fig. 2.3a.

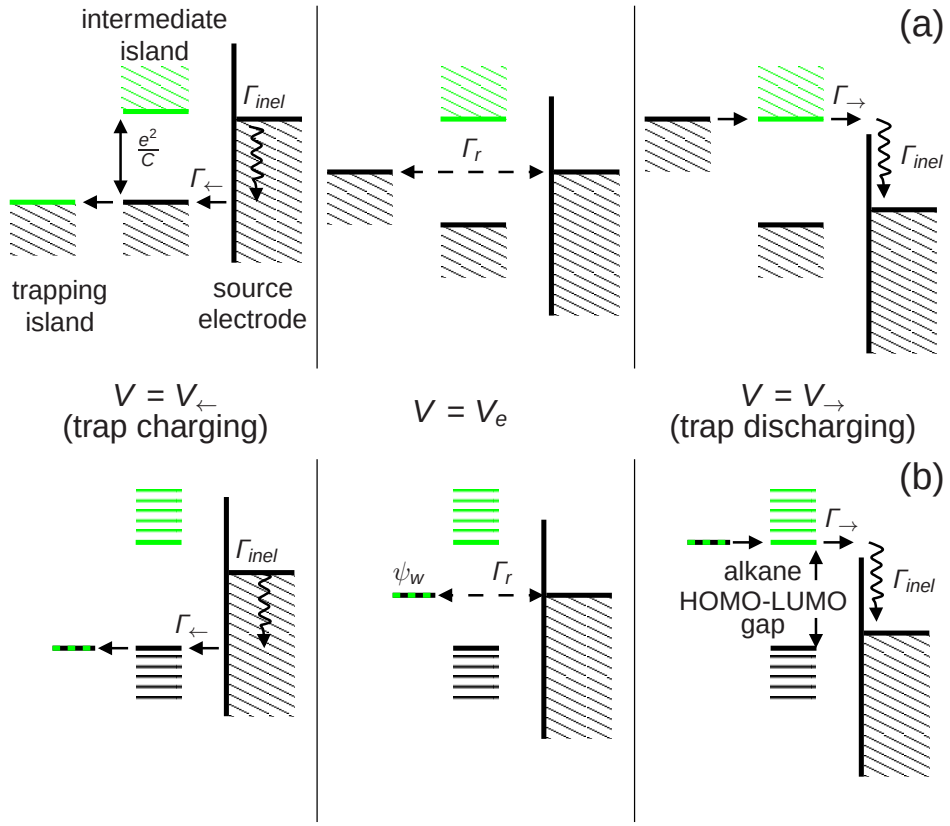

Figure 2.3: Schematic single-particle energy diagrams of (a) the usual single-electron trap shown in Fig. 1.9a (for the sake of simplicity, with just one intermediate island) and (b) A possible design of a molecular trap, each for three values of the applied voltage V. Occupied/unoccupied energy levels are shown in black/green. (The dotted green/black line denotes the energy level of the "working" orbital that is either empty or occupied during the device operation, defining its ON/OFF state.) Horizontal arrows show (elastic) tunneling transitions, while vertical arrows indicate inelastic relaxation transitions within an island, a molecule, or an electrode.

In a manner similar to the conventional single-electron trap design, in the molecular single-electron trap shown in Fig. 2.1b, the "energy-equilibrating" voltage V_e aligns the Fermi energy of the source electrode with the lowest unoccupied level of the acceptor group that is, by design, located in the middle of the HOMO-LUMO gap of the alkane chain (instead of the e^2/C "Coulomb

gap" of the intermediate island). As a result, an electron from the source electrode may elastically tunnel into the group only with a very low rate Γ_r — see the middle panel in Fig. 2.3b[1]. The reciprocal process (at the same voltage) may be viewed as electron tunneling from the HOMO of the singly-negatively charged molecule. (To simplify the terminology, I call this molecular orbital the "working orbital" (indexed W), instead of HOMO or LUMO of the counterpart molecular ions, to make the name independent of the charge state of the device.) The energy-balance condition of both processes is similar, and may be expressed via the effective single-particle energy ε_W of the working orbital:

$$\varepsilon_W = \Delta E(n) \equiv E_{gr}(n) - E_{gr}(n-1), \tag{2.1}$$

where $E_{gr}(n)$ is the ground-state energy of the molecular ion with n electrons. (In the case of singly-negative ion, $n = n_0 + 1$, where n_0 is the number of protons in the molecule.) In this notation, the energy-balance (level-alignment) condition, which defines the voltage V_e, is

$$\varepsilon_W = W - e\gamma V_e, \tag{2.2}$$

where W is the work function of the source electrode material, and γ is a constant factor imposed by the geometry of the junction; $0 < \gamma < 1$. (Its physical meaning is the fraction of the applied voltage, which drops between the trapping island and the source electrode.) At the charging threshold voltage $V_{\leftarrow}$, the energy ε_W crosses the valence band of the chain, allowing a fast charging of the molecule — see the left panel in Fig. 2.3b. Similarly, as shown on the right panel in Fig. 2.3b, at $V_{\rightarrow}$ this energy crosses the conduction band of the chain, allowing a fast discharging of the molecule.

2.2.2 Molecular trap operation

As an example, Fig. 2.4 shows the atomic self-interaction corrected (ASIC) [74] Kohn-Sham electron eigenenergy spectrum $\varepsilon_i^{\rm ASIC}(n)$ of the alkane- naphthalenediimide molecule used as the final trap design (Fig. 2.1b), with the net charge $Q(n) = -e(n-n_0) = -e$, as a function of the applied voltage V. (Here i is the spin-orbital index; see Chapter 3.) Point colors in Fig. 2.4 crudely represent the spatial localization of the orbitals: blue corresponds to their localization at the trapping (acceptor) group, while red marks the localization at the alkane chain's part close to the source electrode. Figure 2.5 shows the

[1]The large $\sim$ 2nm vacuum gap between the control electrode and the trapping island is sufficient to prohibit unwanted electron tunneling between that electrode and the molecular trap.

probability density of the working orbital $\psi_W^{\rm ASIC} = \psi_{n_0+1}^{\rm ASIC}(n_0+1)$ of the molecular trap, integrated over the directions perpendicular to the molecule's axis, with blue lines corresponding to the probability density at the most negative applied voltage. At the equilibrating voltage $V_e \approx 2.2$ V, the working orbital is well localized at the acceptor group, and is isolated from the source electrode by a ~ 4.5-eV-high energy barrier. However, as Fig. 2.5 shows, the probability density of the orbital decays into the alkane group rather slowly, with the exponent coefficient $\beta \approx 0.4 a_{\rm B}^{-1}$, corresponding (in the parabolic approximation of the dispersion relation) to the effective electron mass[2] $m_{ef} \approx 0.1 m_0$. As a result, a long (~ 5 nm) alkane chain is needed to ensure an acceptable retention time of the trap. (The 2-nm free-space separation between the other side of the molecule and the control/drain electrode, shown in Fig. 2.1b, is quite sufficient for preventing electron escape in that direction.)

At a sufficiently high forward/reverse bias voltage, the working orbital energy ε_W crosses into the conduction/valence band of the alkane chain, so that the group localized electron can propagate in the periodic potential of the alkane chain, that can be seen by the rise of $|\psi_W|^2$ at larger values of z — see Fig. 2.5. This rise enables fast electron tunneling to/from the source electrode, i.e. a fast switching of the device to the counterpart charge state, in a manner similar to that of the conventional single-electron trap, as shown schematically on the left and right panels of Fig. 2.3b. Thus the long molecular chain, with a sufficiently large HOMO-LUMO gap, may indeed play the roles of both the tunnel junction and intermediate islands of the conventional (see Sec. 1.3.4 single-electron trap.

2.3 Designing a compatible molecular transistor

As was already mentioned in the introduction, for the design of the second component of the switch, the molecular single-electron transistor, the most important challenge is to satisfy the ON and OFF state current requirements. In particular, the ON current should not be too large to keep the power dissipation in the circuit at a manageable level, but simultaneously not too small, so that the device's output does not vanish in the noise of a sense amplifier (for memory applications [76, 77]) or the CMOS inverter (in hybrid logic circuits

[2] Experiments (for a recent summary, see, e.g., Table 1 in [75]) give for the exponent coefficient β a wide range $(0.26-0.53)a_{\rm B}^{-1}$ corresponding to the effective mass range $(0.05-0.2)m_0$ (assuming a rectangular, 4.5-eV-high energy barrier). It has been suggested [75] that such a large variation is due to a complex dispersion law inside the alkane bandgap, making β a strong function of the tunneling electron energy

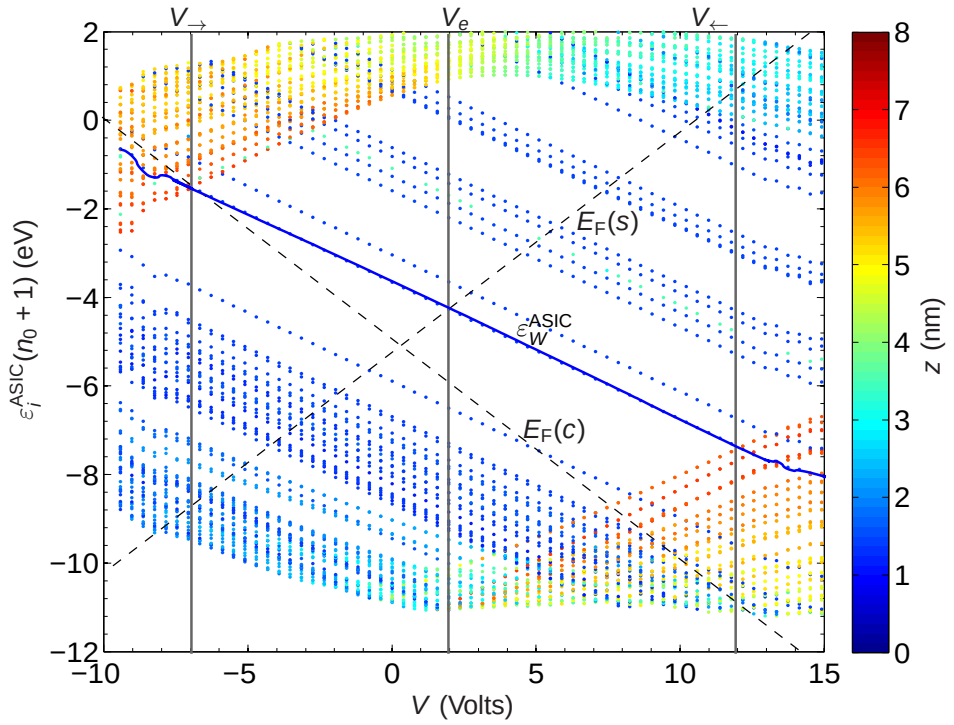

Figure 2.4: ASIC DFT Kohn-Sham energy spectrum (corrected for level "freezing" at high positive and negative voltages — see Chapter 3 for details) for the singly-negatively charged alkane-naphthalenediimide trap molecule, as a function of the applied voltage V, with colors representing the spatial localization of the corresponding orbitals — see the legend bar on the right. The vertical lines mark voltage values $V_\leftarrow$, V_e, and $V_\rightarrow$ corresponding to the left, middle, and right panels of Fig. 2.3b. The dashed lines labeled $E_F(s)$ and $E_F(c)$ show the Fermi levels of the source and control/drain electrodes whose work function was assumed to equal 5 eV.

[78]). Also, the ON/OFF current ratio should be sufficiently high to suppress current "sneak paths" in large crossbar arrays [77, 79]. In addition, the transistor molecule should be geometrically and chemically compatible with the trap molecule, enabling their chemical assembly as a unimolecular device, with their single-electron island groups sufficiently close to provide substantial electrostatic coupling (without it, the charge of the trap would not provide a substantial modulation of the transistor current.). At the same time, the molecules must not be too close, in order to prevent a parasitic discharge of the trap via electron cotunneling through the transistor into one of the electrodes — see Sec. 3.7 for a more detailed discussion. The chemical compatibility

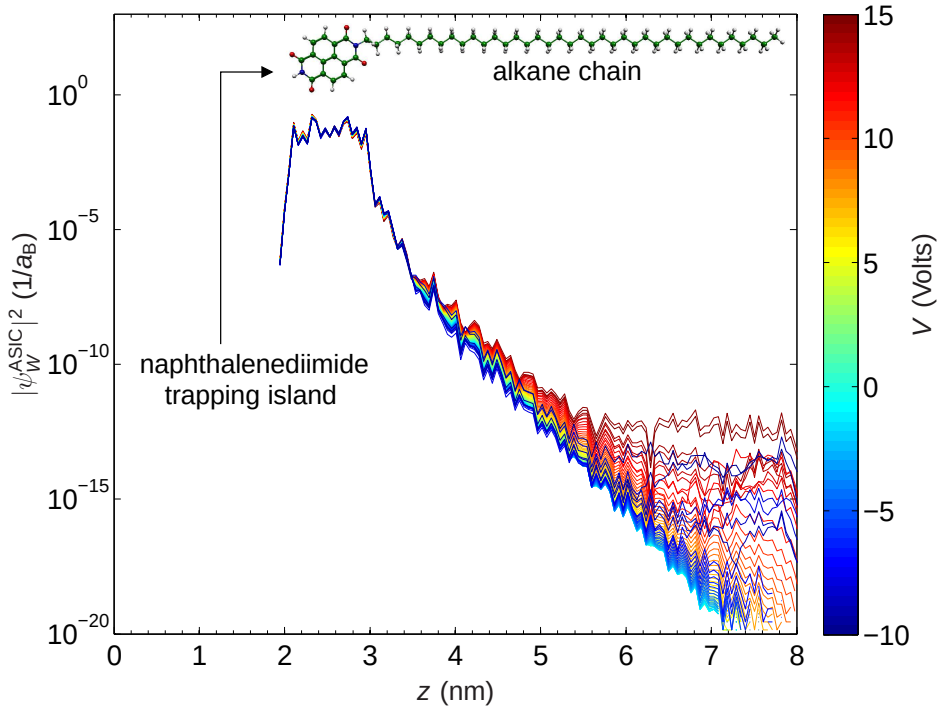

Figure 2.5: ASIC Kohn-Sham "working" orbital's probability density for the singly-negatively charged alkane-naphthalenediimide trap molecule, integrated over the directions perpendicular to molecule's axis, for a series of applied voltages V — see the legend bar on the right of the panel.

strongly favors the use of similar chains as the transistor's tunnel junctions.

In the course of this study several alkane-chain based transistor devices with naphthalenediimide, perylenediimide and benzobisoxazole acceptor groups as transistor islands have been analyzed. However, in all these cases the long alkane chains, needed to match the lengths of the transistor and trap molecules, make ON currents too low. Finally, it was decided to use an unusually long ($\sim$ 4.3-nm) benzene-benzobisoxazole [80] island group — see Fig. 2.1b and Fig. 2.7. Figure 2.6 shows the Kohn-Sham electron eigenenergy spectrum $\varepsilon_i^{\mathrm{ASIC}}(l_0+1)$ of this molecule as a function of voltage V (where l_0 is the number of protons in the transistor molecule). Blue/red colored points correspond to the orbitals localized at the left/right alkane chain, while green color points denote the orbitals extended over the whole acceptor group. This extension is clearly visible in Fig. 2.7, which shows the probability density of the working orbital $\varepsilon_{W'}^{\mathrm{ASIC}} = \varepsilon_{l_0+1}^{\mathrm{ASIC}}(l_0+1)$ of the transistor molecule. During transistor operation, the tunneling electron may populate any of several group-localized orbitals, resembling the operation of the usual (metallic) single-electron tran-

sistor. As a result of such island extension, alkane chains of the transistor could be substantially shortened, to $\sim$ 1.5-nm-long $C_{11}H_{25}$, enabling low but still acceptable ON currents of the order of 0.1 pA, even if a small (0.25-nm) vacuum gap between the alkane chain and the source electrode is included into calculations to give a phenomenological description of the experimentally observed current reduction due to unknown interfacial chemistry — see Sec. 3.4 for a more detailed discussion.

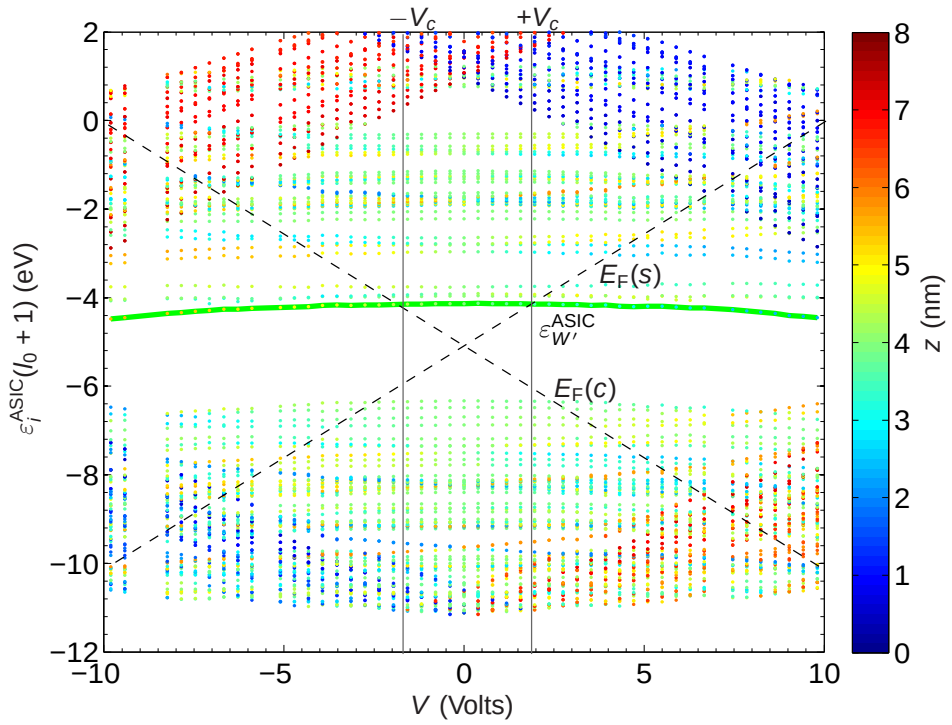

Figure 2.6: ASIC Kohn-Sham energy spectrum for the single-negatively charged benzene-benzobisoxazole transistor molecule, as a function of the applied voltage V, with colors representing the spatial localization (within the junction) of the corresponding orbitals — see the legend bar on the right. The dashed lines labelled $E_F(s)$ and $E_F(c)$ show the Fermi levels of the source and control/drain electrodes whose work function was assumed to equal 5 eV.

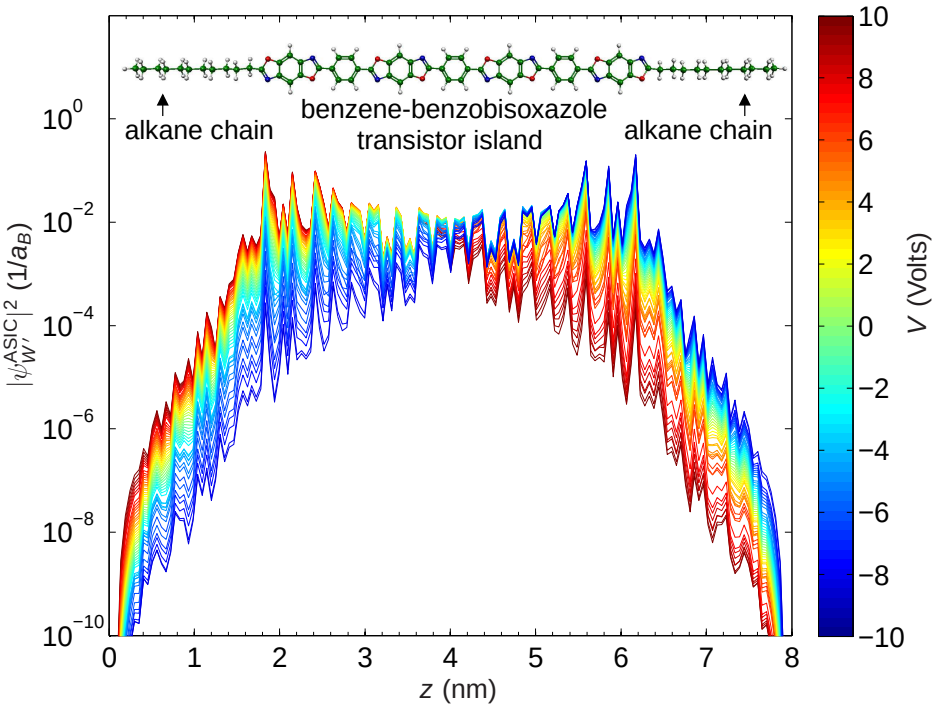

Figure 2.7: ASIC Kohn-Sham probability density of the working orbital for the single-negatively charged benzene-benzobisoxazole transistor molecule, integrated over the directions perpendicular to the molecular axis, for a series of applied voltages — see the legend bar on the right.

Chapter 3

Theoretical model and approximations

3.1 Master equations of electronic transport in single-electron transistors

3.1.1 Applicability conditions, assumptions and prior work

The general theory of single-electron transistors with a substantially discrete spectrum of electron states of the island ("quantum dot") has been developed by Averin and Korotkov [20, 22]. The main condition of its applicability is that the rates $\Gamma_{k\to k'}$ of electron tunneling in and out of the island need to be sufficiently low:

$$\hbar\Gamma_{k\to k'} \ll |E_k - E_{k'}|\,, \tag{3.1}$$

for eigenenergies E_k of all quantum states substantially involved in the transport. For most applications in hybrid integrated circuits with acceptable energy dissipation, the single-molecule current I should be below ~ 100 nA (and much less than that at the current, initial stage of the development of this technology - see, e.g., Ref. [81]), so that $\hbar\Gamma_{k\to k'} \sim \hbar I/e$ should be below $\sim 10^{-3}$ eV, while the typical differences between the adjacent energy levels of molecules of interest are much larger (~ 1 eV), so that this condition is well fulfilled.

In Ref. [20], the island energy E_k has been considered dominated by single-electron charging:

$$E_k \approx U(n) = \frac{(en - Q_0)^2}{2C_\Sigma}, \tag{3.2}$$

where $Q_0 = C_g V_g +$ const, $n = n(k)$ is the number of electrons on the island in its quantum state number k, and C_g and $C_\Sigma = C_s + C_d + C_g$ are the transistor capacitances [60, 61] which have been assumed to be independent of n and of the applied voltages V and V_g. For molecular-size single-electron islands, small enough for room-temperature operation of single-electron transistors (with the single-electron charging energy well above ∼100 meV [82]), this model cannot give quantitatively correct results. For example, Fig. 3.1 shows the differences of ground energies $E_g(n)$ of adjacent ions of a single Na atom, calculated using an *ab initio* density-functional theory (DFT) software package NRLMOL, optimized for massively-parallel computation — see Ref. [83] and references therein [1]. Within the approximation given by Eq. (3.2), such a difference should be a linear function of n, with the slope given by the single-electron addition energy e^2/C. Instead, two very different slopes corresponding to the effective capacitances of the filled second electron shell (at $n \leq 10$) and the third shell (for $n \geq 10$) are seen.

In the subsequent work [22], deviations of E_k from $U(n)$ have been allowed, but assumed to follow a simple quasiparticle model:

$$E_k = U(n) + \sum_i \varepsilon_i p_i, \tag{3.3}$$

where ε_i is the kinetic energy of the electron on i-th quasiparticle level, and $p_i = 0$ or 1 are level occupancies (with the sum of all p_i's equal to n). However, for general systems with strongly interacting electrons even this approximation is invalid, and the eigenenergies E_k and corresponding orbitals have to be calculated from an *ab initio* approach to the electronic structure, for example DFT. Unfortunately, the Kohn-Sham equations, which are the basis for the DFT approach, do not provide an accurate account of single-electron charging effects. Literally interpreted, they describe the Coulomb and exchange interaction of each electron of a molecule with all n electrons, including itself, which contradicts the principles of quantum mechanics. (See a nice discussion of this problem in the beginning of Ref. [85]. I will come back to this in a greater detail in Sec. 3.3.1). This is why great care should be taken when applying the DFT approach to the sequential single-electron transport, and this has not been done in any work I am aware of.

As an example, Feng *et al.* [86] have carried out DFT-based calculations

[1] This package was used for early *ab initio* calculations (described in Chapter 4), later I adopted the SIESTA [84] package whose performance (with the "standard" double-Zeta polarized basis set) for *ab initio* calculations of large molecules (such as those shown in Fig. 2.1b) is substantially higher, though the results obtained from NRLMOL may be slightly more accurate.

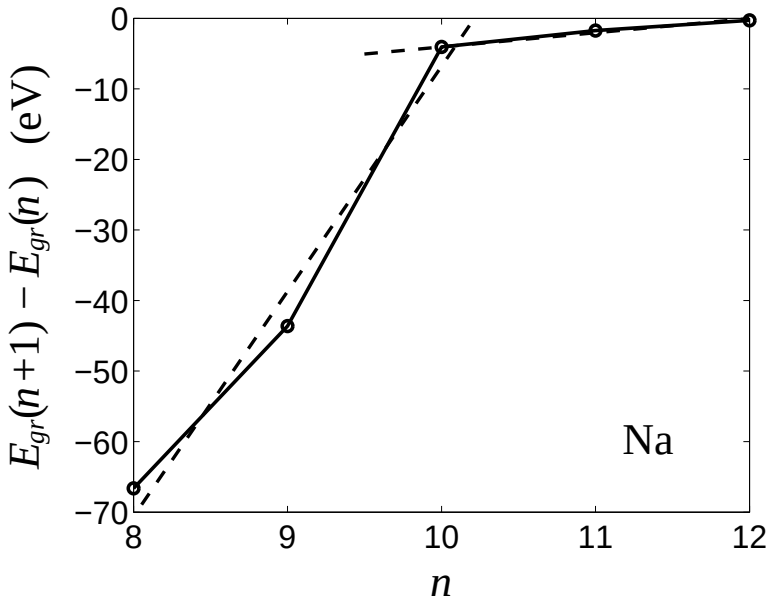

Figure 3.1: The difference between total energies of adjacent sodium atom ions as a function of the total number of electrons, as calculated using the DFT-based NRLMOL software package [83]. (The difference does not include the free electron energy, i.e. corresponds to a single ionization step.) Case $n = 11$ corresponds to the neutral atom. Two dashed straight lines show two linear approximations given by Eq. (3.2) with two sharply different values of the single-electron charging energy: ~ 30 eV for $n \leq 11$ and ~ 3 eV for $n \geq 11$.

of single-electron tunneling through short carbon nanotubes, but limited these calculations to ε_i, still using the simple approximation (3.3) for the description of charging effects. Moreover, they used the WKB approximation, without accounting for the barrier transparency change due to finite source-drain voltage V, and thus missed the negative differential resistance (NDR) effects which were discovered in this work by using a more complete description of tunneling in molecules.

Toher *et al.* [85] were more careful in their calculation of the barrier transparencies, but still used a phenomenological approach to the single-electron charging description.

An important next step has been taken by Hedegard and Bjornholm [87] who have used the fixed-capacitance model (3.2) only for the description of the molecule interaction with its electrostatic image in the electrodes, while calculating the rest of the molecular energy change at tunneling as the difference of the DFT ground state energies $E_g(n)$ of the molecule, for two values of n, before and after tunneling. For the purposes of that paper, focused only on the location of the conduction peaks in the limit of vanishingly small applied voltage, their approach is close to the one described here. However, in order to calculate the magnitude of the conductance peaks or the electric current at a finite voltage, an adequate treatment of excited states and tunneling rates has to be developed as well. Such a full analysis was one of the objectives of this thesis.

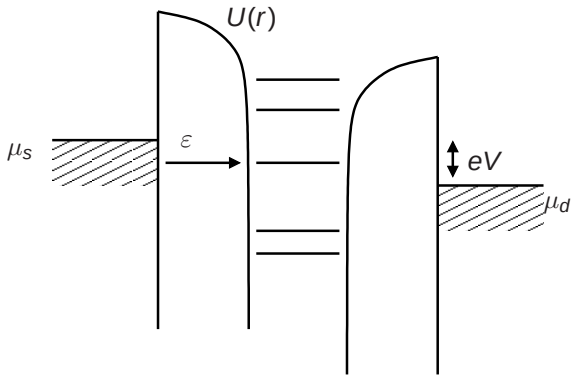

Figure 3.2: Schematic energy diagram of the molecular single-electron transistor.

3.1.2 Master equations generalized for molecular single-electron transistors

To extend the approach [22] to the general case of interacting electrons, I should translate it from the language of quasiparticle energies ε_i to that of total eigenenergies E_k of the system, including the effects of source-drain and gate voltages. The general theory of single-electron tunneling [22, 60] shows that condition (3.1) allows one to neglect the coherence of sequential quantum transitions in the system, and reduce the quantum-mechanical equations for the evolution of its density matrix $\rho_{k,k'}$ to a set of "master" equations for its diagonal components:

$$\dot{\rho_k} = \sum_{\substack{k' \\ n'=n\pm1,n}} w_{k'\to k}\rho_{k'} - w_{k\to k'}\rho_k, \tag{3.4}$$

where $\rho_k \equiv \rho_{k,k}$ is the probability to find the system in a quantum state number k, and the summation is over all states k' which are connected to k by either tunneling of one electron to/from the source or drain ($n' = n\pm1$), or an internal quantum transition (say, energy relaxation) inside the molecule ($n' = n$). The tunneling rates $w_{k\to k'}$ may be decomposed into two parts describing mutually incoherent processes of tunneling to/from the source and drain electrodes:

$$w_{k\to k'} = w^s_{k\to k'} + w^d_{k\to k'}, \tag{3.5}$$

and each of these parts may be presented as products of "unconditional" rates $\Gamma^{s,d}_{k\to k'}$, times the electrode state occupancy factors:

$$w^{s,d}_{k\to k'} = \begin{cases} \Gamma^{s,d}_{k\to k'} f(\varepsilon_{k\to k'} - \mu^{s,d})\Big|_{n'=n+1}, \\ \Gamma^{s,d}_{k\to k'} \left[1 - f(\varepsilon_{k\to k'} - \mu^{s,d})\right]\Big|_{n'=n-1}. \end{cases} \tag{3.6}$$

Here $\varepsilon_{k\to k'}$ is the energy of the tunneling electron, while $\mu^{s,d}$ is the Fermi level of the corresponding electrode - source or drain. The difference between these Fermi levels is determined by the applied source-drain voltage: $\mu^s - \mu^d = eV$, see Fig. 3.2. In all realistic cases, the source and drain remain in thermal equilibrium, and their occupancy factors $f(\varepsilon - \mu)$ are given by the Fermi distribution.

Let me now follow Ref. [22] in assuming that the speed of internal transitions is much faster than that of tunneling:

$$\Gamma^{int} \gg \Gamma^{s,d}. \tag{3.7}$$

Actually, the internal relaxation times in typical organic molecules range from a few tens of femtoseconds to a few picoseconds (see, e.g., Ref. [88]), while for the transistor currents, the shortest time interval e/I between the tunneling events is above 1 ps. Thus, the above condition is readily satisfied in most cases; but even if it is not, the effects of the finite speed of relaxation on transistor characteristics are very limited - see, e.g., Fig. 1 in Ref. [20]. Under the assumption (3.7), eigenstates with the same number of electrons have time to thermalize and their conditional probability may be described by the Gibbs distribution:

$$\rho_k = \sigma(n) p_k(n),\ p_k(n) = Z^{-1}(n) e^{-E_k/T},\ Z(n) = \sum_k e^{-E_k/T}, \tag{3.8}$$

where the summation is carried over all states with the number of electrons (n) fixed. Now, summing Eqs. (3.4) over each of such state subsets, we get a master equation for the dynamics of the total probabilities $\sigma(n)$ to have n electrons on the island:

$$\frac{d\sigma(n)}{dt} = [w_{\rightarrow}(n+1)\sigma(n+1) - w_{\leftarrow}(n)\sigma(n)] + [w_{\leftarrow}(n-1)\sigma(n-1) - w_{\rightarrow}(n)\sigma(n)]\,, \tag{3.9}$$

where $w_{\pm}(n)$ is the total rate of tunnel transitions in and out of the state with n electrons:

$$w_{\leftrightarrows}(n) = w^s_{\leftrightarrows}(n) + w^d_{\leftrightarrows}(n), \tag{3.10}$$

with

$$\begin{aligned} w^{s,d}_{\leftarrow}(n) &= \sum_k p_k(n) \sum_{\substack{k' \\ n'=n+1}} w^{s,d}_{k\to k'}, \\ w^{s,d}_{\rightarrow}(n) &= \sum_k p_k(n) \sum_{\substack{k' \\ n'=n-1}} w^{s,d}_{k\to k'}. \end{aligned} \tag{3.11}$$

Equation (3.9) is equivalent to Eq. (12) of Ref. [22], and has a steady state solution described by similar recurrent relations

$$\sigma(n+1) = \frac{w_{\leftarrow}(n)}{w_{\rightarrow}(n+1)}\sigma(n), \tag{3.12}$$

plus the normalization condition $\sum_n \sigma_n = 1$. The solution of the set of these equations enables one to calculate the transistor current:

$$I = I^s = I^d = \mp e \sum_n \sigma(n)[w^{s,d}_{\leftarrow}(n) - w^{s,d}_{\rightarrow}(n)]. \tag{3.13}$$

The only difference between the results presented here and those of Ref. [22] is that the full tunneling rates are calculated by a more regular and general formula (3.11) which is valid for the case of strongly interacting electrons. The price to pay for this generalization is that the summation should be carried over all possible quantum states of the molecular island, rather than the quasiparticle states as in Eq. (11) of Ref. [22].

Equations (3.10, 3.11, 3.12, 3.13) may be directly used to calculate single-electron transport in single molecules. In the molecular switch, however, one must be careful as each transistor molecule electrostatically couples to the complementary molecular trap. This coupling influences its charging rate(s). To take this influence into account one must add an extra index l that distinguishes between the charge states of the complementary molecular island. The following notation is adopted throughout the remainder of the thesis: l is the number of electrons on the transistor island and n is the number of electrons on the trap island, the tunnel rates in and out of the transistor are hence $w^{s,d}_{n,\leftrightarrows}(l)$, while the conditional probabilities $\sigma_n(l)$ of certain charge states l of the transistor island provided that the trap is in the n-electron charge state, satisfy the following normalization condition:

$$\sum_l \sigma_n(l) = 1. \tag{3.14}$$

3.1.3 Charging rates in single-electron molecular traps

A crucial difference between the trap and the transistor molecules (that was already briefly mentioned in Chapter 2) is that the molecular transistor has similar but much more frequent single-charge transitions. This rate hierarchy allows the molecular trap to be described by averaging rates Γ of tunneling events in it over a time interval much longer than the average time period between tunneling events in the molecular transistor, but still much shorter than $1/\Gamma$. These average rates may be calculated as

$$\langle \Gamma_{\leftarrow}(n) \rangle = \sum_l \sigma_n(l) w_{l,\leftarrow}(n), \tag{3.15}$$

for electron tunneling from the source into the trap molecule, and

$$\langle \Gamma_{\rightarrow}(n+1) \rangle = \sum_l \sigma_{n+1}(l) w_{l,\rightarrow}(n+1), \tag{3.16}$$

for the reciprocal event. See for example Chapter 5 Fig. 5.2, where in particular I show the effect of such averaging taken into the account, compared to rates calculated without the transistor effect. (Rather surprisingly, for our

design, the effect of the tunneling events in the transistor on the charging and discharging rates in the trap has turned out to be quite mild, while the reciprocal effect is quite substantial.)

3.1.4 Elastic cotunneling in molecular traps

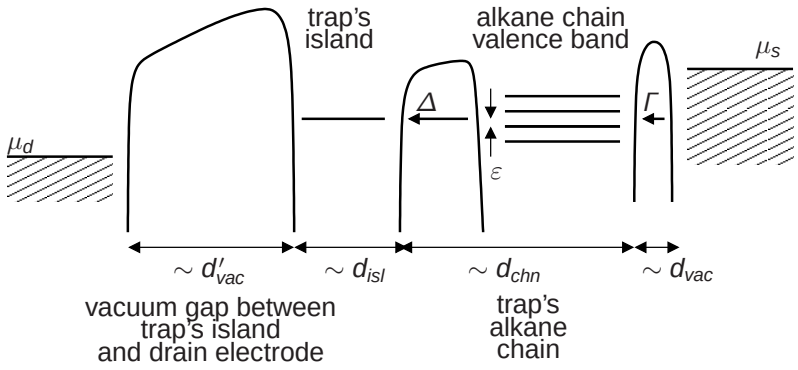

Figure 3.3: Mechanism of elastic cotunneling into the molecular trap's acceptor group (schematically).

In complex molecules (such as the molecular trap) there are two mechanisms of changing the charge state of the acceptor group. First is the direct tunneling between the orbitals (indexed i'), localized at the acceptor group and the metallic electrode(s). As was mentioned in Sec. 2.2.2, tunnel times between these orbitals and the metal are significantly reduced at high forward/reverse bias voltage, when their energies $\varepsilon_{i'}$ cross into the conduction/valence band of the alkane chain and hence the group localized electrons are allowed to propagate in the periodic structure of the molecular chains — see. Fig. 2.5.

Second, within the same voltage ranges, the group's charge state may be also changed via elastic cotunneling[2] through chain localized orbitals see Fig. 3.3. The contribution of this effect to the charging rate may be estimated using the following formula [89, 90]:

$$\Gamma^{\text{cot}} = \frac{\Delta^2 \Gamma}{\hbar^2 \Gamma^2 + 2\Delta^2 + 4\varepsilon^2}, \tag{3.17}$$

[2]A process where an electron charges the trap, violating the energy conservation law, by briefly occuping (allowed by the Heisenberg uncertainty principle) an orbital in the alkane chain valence band that generally has an energy different from that of the electron addition energy.

where Δ is the matrix element of electron tunneling between the trap-localized orbital and the chain-localized orbital, ε is the difference between eigenenergies of these states, and Γ is the rate of tunneling between the source electrode and the chain localized orbital. In our trap molecule, the parameters participating in this formula have the following values: $\Delta \sim 10^{-8}$ eV (see Appendix B), $\hbar\Gamma \sim 10^{-3}$ eV, while the typical value $\varepsilon \sim 10^{-1}$ eV is given by the scale of the distance between the chain-localized levels (see Fig. 2.4).

As a result, the contribution described by Eq. 3.17 gives very sharp peaks at voltages that align energies of the group and chain localized orbitals ($\varepsilon = 0$), with the peak height of the order of $\Gamma^{\rm cot} \sim 10^2$ 1/s, and a much lower background $\Gamma^{\rm cot} \sim 10^{-2}$ between these peaks (each peak may be spit in two due two the charge shaking of the single-electron transistor.) As will be shown in Chapter 5, in the voltage ranges in question, this background is substantially lower than the rate due to the first mechanism (the direct tunneling between the electrodes and the acceptor group orbital).

Because of this fact, our final results (shown in Fig. 5.2) take into account only the direct tunneling mechanism.

3.2 Density Functional Theory

3.2.1 Introduction

Because of the large size and complexity of the molecules used in my design — see Fig. 2.1, the only practical way to calculate their electronic structure is to use a software package (such as NRLMOL or SIESTA [84]), based on the density-functional-theory (DFT). What follows is a brief overview of this theory. Let us consider an N-electron system in a state described by the wavefunction $\Psi(x_1, x_2, ..., x_N)$, where x_i represents both the electron position $\mathbf{r}$ and electron spin ς degrees of freedom. The non-relativistic Hamiltonian operator for this system (including the electron self-interaction) is

$$\widehat{H} = \sum_{i=1}^{N} \left(-\frac{1}{2}\nabla_i^2 + v_i(\mathbf{r}) + \frac{1}{2}\sum_{j=1}^{N} \frac{1}{r_{i,j}} \right), \tag{3.18}$$

where $-\frac{1}{2}\nabla_i^2$ is the electronic kinetic energy, $v_i(\mathbf{r}) = \sum_{g=1}^{K} \frac{Z_g}{r_{i,g}}$ is the electrostatic interaction with all the nuclei and $\frac{1}{2}\sum_{j=1}^{N} \frac{1}{r_{i,j}}$ is the electron-electron interaction. It may be shown that — see e.g., [91] the total energy of this system may be written as

$$E = \int \left[\left(-\frac{1}{2}\nabla^2 \right) \rho(\mathbf{r}, \mathbf{r}') \right]_{\mathbf{r}=\mathbf{r}'} d^3r + \int v(\mathbf{r})\rho(\mathbf{r})d^3r + \int\int \frac{1}{r_{1,2}} \rho_2(\mathbf{r}_1, \mathbf{r}_2) d^3r_1 d^3r_2 \tag{3.19}$$

where $\rho(\mathbf{r}, \mathbf{r}')$ is the spinless one-electron density matrix that may be calculated from

$$\rho(\mathbf{r}, \mathbf{r}') = \int \left[N \int \Psi(x, x_2, ..., x_N)\Psi^*(x', x_2, ..., x_N) dx_2 ... dx_N \right]_{\varsigma=\varsigma'} d\varsigma, \tag{3.20}$$

$\rho(\mathbf{r})$ is the electron density

$$\rho(\mathbf{r}) = [\rho(\mathbf{r}, \mathbf{r}')]_{\mathbf{r}'=\mathbf{r}}, \tag{3.21}$$

and $\rho_2(\mathbf{r}_1, \mathbf{r}_2)$ is the two-electron density

$$\rho_2(\mathbf{r}_1, \mathbf{r}_2) = \int \left[\frac{N(N-1)}{2} \int \Psi(x_1, x_2, ..., x_N)\Psi^*(x_1, x_2, ..., x_N) dx_3 ... dx_N \right] d\varsigma_1 d\varsigma_2, \tag{3.22}$$

normalized to the number of electron pairs $N(N-1)/2$. Equation (3.19) suggests that the expectation value of $\widehat{H}$ for an N-electron system may be evaluated without knowing the full N-electron wavefunction, and explicit expressions for the two-electron density (3.22) and the one-electron density matrix (3.20) will suffice.

3.2.2 The Hohenberg-Kohn Theorem

In 1964 Hohenberg and Kohn showed [92] that the ground state total energy of an N-electron system is a functional of the electron density $\rho(\mathbf{r})$

$$E_{gr} = E[\rho]. \tag{3.23}$$

The proof of the theorem goes as follows: construct two N-electron Hamiltonians $\widehat{H}$ and $\widehat{H}'$ for two different external potentials $v(\mathbf{r})$ and $v'(\mathbf{r})$. Then, their difference is

$$\widehat{H} - \widehat{H}' = \sum_{i=1}^{N} [v(\mathbf{r}_i) - v'(\mathbf{r}_i)]. \tag{3.24}$$

Assume that the ground states of both Hamiltonians are non-degenerate and are represented by their corresponding ground-state wavefunctions Ψ_{gr} and Ψ'_{gr} with total ground energies E_{gr} and E'_{gr} and total electronic densities $\rho(\mathbf{r})$ and $\rho(\mathbf{r}')$ calculated using Eq. (3.21). Now, show that these two densities can not be identical. Since Ψ_{gr} and Ψ'_{gr} are the wavefunctions of the ground states of the corresponding Hamiltonians, it is evident that

$$\begin{aligned} &\langle \Psi_{gr}|\widehat{H}'|\Psi_{gr}\rangle > E'_{gr},\ \langle \Psi'_{gr}|\widehat{H}|\Psi'_{gr}\rangle > E_{gr}, \\ &\langle \Psi_{gr}|\widehat{H}|\Psi_{gr}\rangle = E_{gr},\ \langle \Psi'_{gr}|\widehat{H}'|\Psi'_{gr}\rangle = E'_{gr}. \end{aligned} \tag{3.25}$$

The relations in Eq. (3.25) can be rewritten

$$\langle \Psi_{gr}|\widehat{H} - \widehat{H}'|\Psi_{gr}\rangle - \langle \Psi'_{gr}|\widehat{H}' - \widehat{H}|\Psi'_{gr}\rangle > 0, \tag{3.26}$$

using Eq. (3.24) we get

$$\int [v'(\mathbf{r}) - v(\mathbf{r})]\rho(\mathbf{r})d^3r + \int [v(\mathbf{r}) - v'(\mathbf{r})]\rho'(\mathbf{r})d^3r > 0. \tag{3.27}$$

if we now assume that $\rho' = \rho$ the relation (3.27) becomes a contradiction, hence for each $v(\mathbf{r})$ there is a unique $\rho(\mathbf{r})$, that satisfies

$$\int \rho(\mathbf{r})d^3r = N. \tag{3.28}$$

and vice versa, each $\rho(\mathbf{r})$ determines $v(\mathbf{r})$. In turn, the external potential $v(\mathbf{r})$ uniquely determines (except when the ground state is degenerate) the ground state wavefunction Ψ_{gr}. Hence Ψ_{gr} is determined by $\rho(\mathbf{r})$, or in other words Ψ_{gr} is a functional of $\rho(\mathbf{r})$ and therefore the ground state kinetic and interaction energies that enter $\widehat{H}$ are also functionals of $\rho(\mathbf{r})$. Therefore we can conclude that the total ground state energy E_{gr} is a functional of $\rho(\mathbf{r})$. Now, given a potential $v(\mathbf{r})$ the energy $\langle \Psi_{gr}|\widehat{H}|\Psi_{gr}\rangle$ is a minimum when Ψ_{gr} is the exact ground state wavefunction, therefore $\delta E[\rho]$ vanishes when ρ is varied about its exact ground state density, therefore $E[\rho]$ is a minimum with respect to such variations and is equal to the ground state total energy E_{gr}.

3.2.3 The Kohn-Sham Equations

The Hohenberg-Kohn theorem does not give any prescriptions for how to calculate the ground state total energy E_{gr}. One way to do this is via Kohn-Sham equations [93]. A brief overview may be started from writing the two-particle density in (3.22) as

$$\rho_2(\mathbf{r}_1, \mathbf{r}_2) = \frac{1}{2}\left(\rho(\mathbf{r}_1)\rho(\mathbf{r}_2) + C_2(\mathbf{r}_1, \mathbf{r}_2)\right), \tag{3.29}$$

where $C_2(\mathbf{r}_1, \mathbf{r}_2)$ is usually called the two-electron correlation function. Then Eq. (3.19) may be written as

$$\begin{aligned} E = &\int \left[\left(-\frac{1}{2}\nabla^2\right)\rho(\mathbf{r}, \mathbf{r}')\right]_{\mathbf{r}=\mathbf{r}'} d^3r + \int v(\mathbf{r})\rho(\mathbf{r})d^3r \\ &+ \int\int \frac{\rho(\mathbf{r}_1)\rho(\mathbf{r}_2)}{r_{1,2}} d^3r_1 d^3r_2 + \int\int \frac{C(\mathbf{r}_1, \mathbf{r}_2)}{r_{1,2}} d^3r_1 d^3r_2. \end{aligned} \tag{3.30}$$

It was suggested by Kohn and Sham that Eq. (3.30) may be presented as

$$\begin{aligned} E = -\frac{1}{2}\sum_{i=1}^{N} \int \phi_i^*(\mathbf{r})\nabla^2\phi_i(\mathbf{r})d^3r + \int v(\mathbf{r})\rho(\mathbf{r})d^3r \\ + \int\int \frac{\rho(\mathbf{r}_1)\rho(\mathbf{r}_2)}{r_{1,2}} d^3r_1 d^3r_2 + E_{xc}[\rho], \end{aligned} \tag{3.31}$$

where $\phi_i(\mathbf{r})$ are the Kohn-Sham orbitals, that are required to satisfy

$$\sum_{i=1}^{N} \phi_i^*(\mathbf{r})\phi_i(\mathbf{r}) = \rho(\mathbf{r}), \tag{3.32}$$

where ρ is the exact one-electron density. It may be shown (se e.g., [91]) that the orbitals $\phi_i(\mathbf{r})$ satisfy the one-electron Kohn-Sham equations

$$\left\{-\frac{1}{2}\nabla^2 + v(\mathbf{r}) + v_C(\mathbf{r}) + v_{xc}(\mathbf{r})\right\}\phi_i(\mathbf{r}) = \varepsilon_i\phi_i(\mathbf{r}), \tag{3.33}$$

where $v_C(\mathbf{r}) = \int \frac{\rho(\mathbf{r})}{r_{12}} d^3r$ is the classical Coulomb potential, and $v_{xc}(\mathbf{r}) = \frac{\delta E_{xc}[\rho]}{\delta\rho(r)}$ is called the exchange-correlation potential which is generally unknown. Approximations such as local density approximation (LDA) derived from the homogeneous electron gas model are employed in practice to solve the Kohn-Sham equations. In Sec. 3.3.1 I will show that such approximations have

significant self-interaction errors that need to be accounted for (and are of pivotal importance), when considering single-electron charging and transport in molecular junctions.

3.3 Quasiparticle approximation

Table 3.1: Comparison between the calculations of energy $\varepsilon_{k\to k'}$ of the tunneling electron in the sodium atom and an OPE molecule, using two methods. In the "direct Kohn-Sham" method, these eigenenergies are calculated using the NRLMOL [83] software package after the explicit specification of level occupancies (see two right columns). In the second method, these energies are calculated from Eq. (3.36) after using NRLMOL to calculate the energy spectrum of the corresponding ions.

sodium			
$E_{k'}(n+1) - E_k(n)$		occupations	
direct Kohn-Sham	Eq. (3.36)	$p_i(n+1)$	$p_i(n)$
-4.0490 eV	-4.0490 eV	1111000	1110000
-2.1368 eV	-1.9128 eV	1110010	1110000
-0.5822 eV	-0.4544 eV	1111010	1111000
OPE			
-4.7648 eV	-4.7648 eV	1111000	1110000
-4.7648 eV	-5.0050 eV	1111000	1101000
-5.5770 eV	-5.5155 eV	1111000	1011000
-5.5770 eV	-5.6997 eV	1111000	011100
-7.6557 eV	-7.5954 eV	1111000	1010010

For the practical application of the master equations derived in Sec. 3.1.2, we need to know the tunneling electron energies $\varepsilon_{k\to k'}$ given by the natural generalization of Eqs. (2.1) and (2.2):

$$\varepsilon_{k\to k'} = W - e\gamma V, \tag{3.34}$$

and the corresponding tunneling rates $w^{s,d}_{k\to k'}$ for all essential pairs of states $k = n, i$ and[3] $k' = n \pm 1, i$. These energies may be readily calculated from the tunneling elasticity condition (see, e.g., Ref. [60]):

$$\varepsilon_{k\to k'} = E_{k'} - E_k, \tag{3.35}$$

[3]Here I assume that tunneling changes only a single occupation number p_i corresponding to the i-th orbital.

so we need to know "only" the energy eigenstates E_k. Generally, these energies depend on all quantum numbers characterizing the molecular excitation. However, I have found (see, e.g., Table A.1) that for some molecules[4] I have analyzed, the lowest excited states needed for calculations, satisfy, with the accuracy of the order of 10^{-1} eV, the following quasiparticle approximation:

$$E_k = E_{gr}(n) + \sum_{i>n} \varepsilon_i(n) p_i - \sum_{i \le n} \varepsilon_i(n)(1 - p_i), \tag{3.36}$$

where $E_{gr}(n)$ is the ground state energy of the molecule with the same number of electrons, the set of $\varepsilon_i(n)$ is its energy spectrum, and $p_i = 0, 1$ are the level occupation numbers whose sum over all i should equal n. This approximation is more general than Eq. (3.3) in two aspects:

(i) it uses the *ab initio* calculated values for the ground state energies $E_{gr}(n)$ rather than the simple quadratic dependence given by Eq. (3.2), and

(ii) the quasiparticle energy spectrum $\varepsilon_i(n)$ may be very much different for different n.

3.3.1 Correcting the DFT self-interaction deficiencies

As I have already mentioned, the DFT theory may provide a reasonably accurate ground state energy $E_{gr}^{\rm DFT}(n)$ and a single-particle spectrum $\varepsilon_i^{\rm DFT}(n)$ at a fraction of the computational cost of more correct *ab initio* methods. Unfortunately, for such strongly correlated electronic systems as molecules considered in this dissertation, results obtained using standard DFT software packages [5] have significant self-interaction errors [95].

Apparently, the source of such errors is that the approximate treatment of the exchange-correlation term in the Kohn-Sham Hamiltonian does not completely cancel the self-interaction energy present in the "Hartree term" of the Hamiltonian [6]. Indeed, the standard DFT approach leads to errors, in the key energies (2.1), of the order of the single-electron charging energy $e^2/2C$, where C is the effective capacitance of the island group — see Appendix A for details.

[4] Unfortunately, I do not have similar data for the more complex molecules analyzed in this work. A similar calculation for molecules used in the design of the resistive switch failed to converge in the SIESTA package, while for the NRLMOL package it has turned out to be a too computationally intensive.

[5] This is valid not only for the DFT packages based on the local spin density approximation (LSDA), such as the standard version of SIESTA. Another popular DFT functional, the generalized gradient approximation (GGA) [94], does not provide much improvement on these results

[6] In contrast, in the Hartree-Fock theory the exchange energy is exact (of course, in the usual sense of the first approximation of the perturbation theory), and the self-interaction errors are absent [95].

This error may be rather substantial; for example in the naphthalenediimide-based trap molecule (Fig. 2.1b), it is approximately equal to 1.8 eV. For this reason, the electron affinity $E_{gr}(n_0+1) - E_{gr}(n_0)$, calculated using the LSDA DFT for the singly-negatively charged ion of the molecular trap, is significantly (by ~ 3.2 eV) larger than the experimental value of similar molecules [96, 97]. The LSDA energies may be readily corrected to yield a much better agreement with experiments (see Table 1 in Appendix A). However, it is not quite clear how such a theory may be used for a self-consistent calculation of the corresponding working orbital $\psi_W(\mathbf{r})$.

A significant improvement may be achieved by using the recently proposed Atomic Self-Interaction Corrected DFT scheme (dubbed ASIC [74]) implemented in a custom version of the SIESTA software package. For the most important molecules that I have considered here, this approach gives the Kohn-Sham energy $\varepsilon_{n_0+1}(n_0+1)$ very close to the experimental electron affinity. However, using even this advanced approach for our task faces two challenges.

First, the algorithm gives (at least for my molecular trap states with $n = n_0+1$ and $n = n_0+2$ electrons) substantial deviations from the fundamental relation $\varepsilon_W = \varepsilon_{n+1}(n+1)$ for $n = n_0$ (which has to be satisfied in any exact theory [74, 98]), with the ground energy difference (2.1) close to the LSDA DFT results. This means that Eq. (3.35) cannot be directly used with the ASIC results; instead, for the electron transfer energy between adjacent ions n and $n-1$ I have used the following expression:

$$\varepsilon_{k\to k'} = \varepsilon_{i'}^{\mathrm{ASIC}}(n). \tag{3.37}$$

This relation implies that the differences $\varepsilon_{i'}^{\mathrm{ASIC}}(n) - \varepsilon_{n}^{\mathrm{ASIC}}(n)$ describe all possible single-particle excitations within the acceptor group, if the index i' is restricted to orbitals localized on the group. (Other orbitals, localized on the alkane chain are irrelevant for our transport and charging calculations since they do not directly contribute to the elastic tunneling between the molecular group and the electrode, and the cotunneling effects, described in 3.1.4 can be ignored).

In order to appreciate the second problem, look at Fig. 3.4 which shows the voltage-dependent Kohn-Sham spectra of the singly-negatively charged molecular trap, calculated using the ASIC SIESTA package for $T > 0$ K. Notice that above voltage $V_t \approx 13$V, and below voltage $V_t' \approx -7$V, the eigenenergy spectrum is virtually "frozen". (The LSDA SIESTA gives similar results.). As explained in Appendix B using a simple but reasonable model (similar to that used in Appendix A), at $V > V_t$ such "freezing" originates from the spurious self-interaction of an electron whose wavefunction cloud is gradually shifted from the top occupied orbital of the valence band of the chain, with

energy ε_v, into the initially empty group-localized orbital with energy ε_{W+1}. (A similar freeze at voltages $V < V_t'$, is due to the spurious gradual transfer of the electron wavefunction cloud from the working orbital, localized at the acceptor group, with energy ε_W, to the lowest orbital of the conduction band of the chain, with energy ε_c.) It is somewhat surprising that this spurious effect (which should not be present in any consistent quantum-mechanical approach — see Appendix B) is so strongly expressed in the ASIC version of the SIESTA code, which was purposely designed to get rid of the self-interaction in the first place. Being no SIESTA expert, I may only speculate that the nature of this artifact is related to the smoothing of the derivative discontinuity present in the ASIC method as the electron number passes through an integer value, which is mentioned in [74] — see also Fig. 7 in that paper.

Fortunately, there is a way to correct this error very substantially by following the iterative process of self-consistent energy minimization within ASIC SIESTA. Indeed, for a fixed temperature $T > 0$ K (when the program automatically populates molecular orbitals in accordance with the single-particle Fermi-Dirac statistics) and voltages $V > V_t \approx 13$ V and $V < V_t' \approx -7$ V, its iterative process converges to a wrong solution with the energy levels frozen at their V_t and V_t' values, as is discussed above — see Fig. 3.4. However, if the temperature in that program is fixed at $T = 0$ K, its iterative process ends up in quasi-periodic oscillations between different solutions — most of them with frozen levels (just like in Fig. 3.4), but some of them with the group localized energies like the working orbital energies ε_W, ε_{W+1} and the valence/conduction band edge energies ε_v, ε_c close to their expected (unfrozen) values. (Those values were obtained by a linear extrapolation of their voltage behavior calculated at $V_t' < V < V_t$.) Since such a solution is repeated almost exactly at each iterative cycle (see the vertical boxes in Fig. 3.5), we believe that it is close to the correct solution expected from the self-consistent quantum-mechanical theory — see Appendix B. These approximate solutions were used in our calculations both above V_t and below V_t'; they are illustrated in Fig. 2.4, where we have substituted the incorrect "frozen" solutions for $T > 0$ K with solutions for $T = 0$ K, with $\varepsilon_W \approx \varepsilon_W^{\rm fit}$, $\varepsilon_{W+1} \approx \varepsilon_{W+1}^{\rm fit}$ and $\varepsilon_c \approx \varepsilon_c^{\rm fit}$ at $V < V_t'$ or $\varepsilon_v \approx \varepsilon_v^{\rm fit}$ at $V > V_t$. Let me emphasize that the approximate nature of these solutions may have affected my calculations (I believe, rather insignificantly), only at $V > V_t \approx 13$ V and $V < V_t' \approx -7$ V, i.e. only the device recharging time results, but not the most important retention time calculations for smaller voltages — see Fig. 5.2.

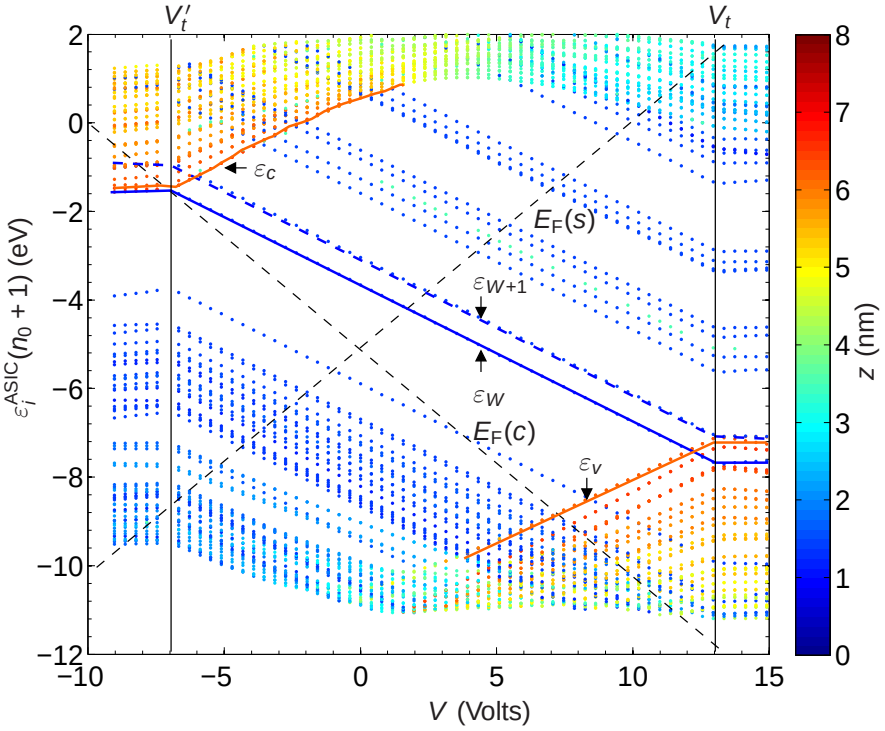

Figure 3.4: The Kohn-Sham spectra of the singly-negatively charged molecular trap, calculated with the ASIC SIESTA at $T = 10$ K. At voltages below $V_t' \approx -7$ V, the spectrum is virtually frozen due to a spurious gradual shift of the highest-energy electron from the "working" orbital (with energy ε_W, shown with a solid blue line) localized on the acceptor group, to the lowest orbital (with energy ε_c, shown with a solid red line) of the conduction band of the alkane chain. As a result, the calculated spectrum is virtually voltage-insensitive ("frozen"). In the voltage range $V_t' < V < V_t \approx 13$ V, ASIC SIESTA gives apparently correct solutions, with the working orbital ε_W fully occupied, and the next group-localized orbital (with energy ε_{W+1}, the dashed blue line) completely unoccupied. However, at $V > V_t$ the package describes a similar spurious gradual shift of the highest-energy electron from the highest level ε_v of the valence band of the chain to orbital ε_{W+1}, resulting in a similar spectrum "freeze". The spectrum evolution, calculated after the (approximate) correction of this spurious "freezing" effect, is shown in Fig. 2.4 in Sec. 2.2.1 above.

3.4 Calculation of tunneling electron rates

To evaluate the transport and charging properties in molecules, the master equations in Sec. 3.1.2 need to be supplied with tunneling rates $\Gamma_{k\to k'}^{s,d}$. These

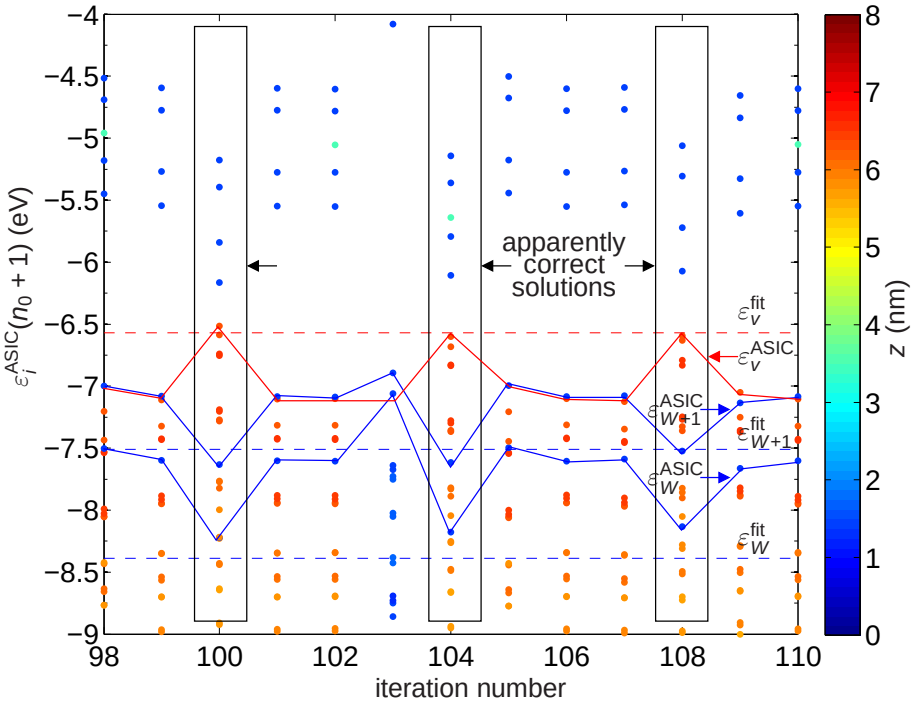

Figure 3.5: The Kohn-Sham energy spectrum of our trap molecule, as calculated by successive iterations within ASIC SIESTA for $T = 0$ K and $V = 14.9$ V, i.e. above the threshold voltage $V_t \approx 13$ V. Vertical boxes mark the apparently correct solutions with energies of the working orbital ($\varepsilon_W^{\rm ASIC}$), the next group-localized orbital ($\varepsilon_{W+1}^{\rm ASIC}$), and the highest orbital of the valence band of the alkane chain ($\varepsilon_v^{\rm ASIC}$) all close to their respective values $\varepsilon_W^{\rm fit}$, $\varepsilon_{W+1}^{\rm fit}$ and $\varepsilon_v^{\rm fit}$ obtained by a linear extrapolation of their voltage dependence calculated at $V_t' < V < V_t$. Just like in Figs. 4a, 5a and 6, point colors represent the spatial localization of the corresponding orbitals. Lines are only guides for the eye.

rates may be calculated using Fermi's Golden Rule:

$$\Gamma_{k\to k'}^{s,d} = \frac{2\pi}{\hbar} \sum_k |T_{k,k'}^{s,d}|^2 \nu^{s,d}, \tag{3.38}$$

where $\nu^{s,d}$ is the density of states in the corresponding electrode, and the sum is over all electronic states in the source or drain, with energy $\varepsilon_{k\to k'}$ given generally by Eq. (3.35) (or when ASIC DFT was used by Eq. (3.37)), i.e. essentially an integral over a half-sphere in the momentum space. Since the main condition (3.1) of single-electron tunneling is satisfied only if the overlap matrix elements $T_{k,k'}^{s,d}$ are much smaller than $\epsilon_{k\to k'}$, they may be calculated

using the Bardeen's approximation [99] — see Appendix C for the derivation of Eq. (3.39) [7]

$$T^{s,d}_{k\to k'} = \frac{\hbar^2}{2m}\int_S (\psi^*_{s,d}\frac{\partial\psi_i}{\partial z} - \psi_i\frac{\partial\psi^*_{s,d}}{\partial z})dS. \tag{3.39}$$

Here S is a plane in x, y which separates the single-electron island from the corresponding electrode, and $\psi_{s,d}$ is a wavefunction which describes the electron which is tunneling from the electrode into the island — see Fig. 3.6.

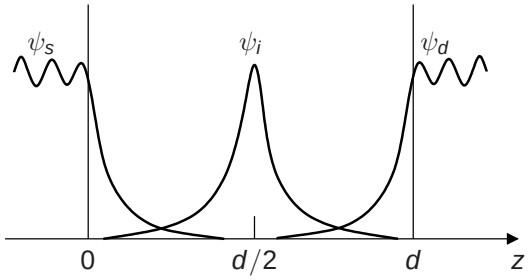

Figure 3.6: Wavefunctions ψ_i, ψ_s and ψ_d describing (schematically) the tunneling between the source or drain electrodes and the island of the molecular single-electron transistor.

3.5 Solving the Schrödinger equation for the wavefunction of the tunneling electron.

3.5.1 Boundary conditions for a direct, finite-difference solution.

Generally the tunneling electron wavefunctions ψ_s and ψ_d may be calculated by solving the effective Schrödinger equation:

$$(-\frac{\hbar^2}{2m}\nabla^2 + U_{KS} - \epsilon_{k\to k'})\psi_{s,d} = 0, \tag{3.40}$$

with the following boundary conditions:

$$\psi_{s,d} = (e^{ik_z z} - Re^{-ik_z z}), \text{ at } z = [0, d], \tag{3.41}$$

[7] The currently fashionable "nonequilibrium (Keldysh) Green function" (NEGF) formalism, while being more cumbersome, does not seem to provide any additional information, unless it is used to account for inelastic processes.

$$\psi_{s,d} = 0, \text{ at } z = d/2, \tag{3.42}$$

where R is a complex reflection coefficient (with $|R| \approx 1$). Such boundary conditions are justified by the fact that at small transparency of the effective potential barrier separating the single-electron island and source-drain electrodes, the wavefunction $\psi_{s,d}$ (Fig. 3.6) is constant inside the corresponding electrode and decays rapidly (exponentially) inside the barrier. As a result, one can neglect the effect of the molecule on the reflection coefficient R, and the non-zero value of the function in the center of the island, provided that the surface S along which integral (3.39) is taken somewhere in the barrier region. (In this region both ψ_i and $\psi_{s,d}$ decay exponentially, but in the different directions, so that the integral does not much depend on the exact position of this surface - see, e.g., Fig. 3.7).

The potential U_{KS} participating in Eq. (3.40) is the Kohn-Sham potential calculated for the ground state of the molecule with the number of electrons corresponding to the island state *without* the tunneling electron. The justification of this choice is that the bulk of the function $\psi_{s,d}$ is in the corresponding electrode, so that its contribution to the island charge is negligible. Reversing this argument, for calculation of the molecular orbital ψ_i the potential U_{KS} is used, which corresponds to the tunneling electron *inside* the molecule.

3.5.2 Analytical approximation for the wavefunction of the tunneling electron.

Numerically solving the three dimensional Schrödinger equation for $\psi_{s,d}$ is a computationally intensive task that for large molecules (such as those used in my final switch design) becomes impractical[8]. Fortunately the wavefunctions of electrons located inside the source or drain electrodes may be calculated in a simpler way. Namely, one of the key conditions of validity of the Bardeen formula for the tunneling matrix elements is that the result given by Eq. (3.39) is independent of the position of the surface S. Due to electrostatic screening of the electric field by the electrode (see Sec. 3.6 for details), the Kohn-Sham potential is very close to the vacuum potential at just a few Bohr radii a_{B} away from the interface with the electrode — see Fig. 3.8. Therefore, if the surface S is selected inside the vacuum gap between the molecule's end and the electrode surface, the effect of the molecule on wavefunctions $\psi_{s,d}$ is negligible with good accuracy (corresponding to a fraction of one order of magnitude in the resulting current). Hence, these wavefunctions may be calculated analytically

[8]For example an appropriately fine finite difference mesh for these molecules is too big and largely exceeds the compute node's memory that was available to me. Using a more cumbersome finite element mesh was not an option at the time.

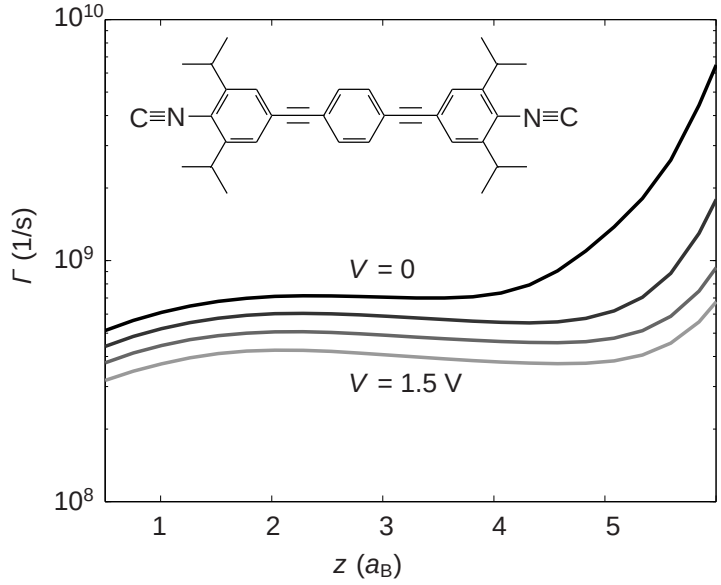

Figure 3.7: The tunneling rate as a function of the position of the integration plane S in Eq. (3.39), for four values of the source-drain voltage V, calculated for the early "toy model" transistor based on a 3-ring-OPE molecule (shown in the inset).

to describe the usual exponential 1D decay into vacuum:

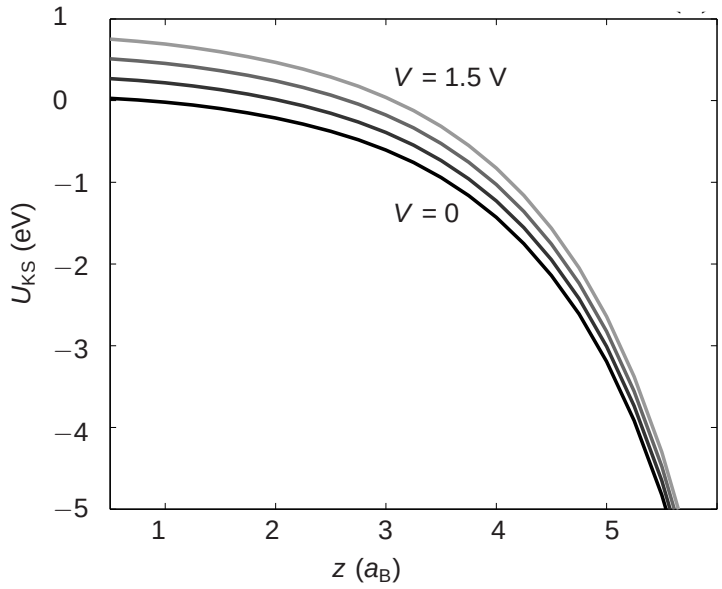

Figure 3.8: The image-corrected Kohn-Sham potential and for a 3-ring-OPE-based molecule (shown in the inset of Fig. 3.7) as a function of the center line coordinate

$$\psi(\mathbf{r}_\perp, z)_{s,d} = \sqrt{\frac{2}{V}} \frac{k_z}{\sqrt{\kappa_z^2 + k_z^2}} e^{i\mathbf{k}_\perp \mathbf{r}_\perp} e^{-\kappa_z z}, \tag{3.43}$$

where k_z and $\mathbf{k}_\perp$ are the wavevectors in z and perpendicular to z directions, κ_z is the wavevector under the barrier, and V is the total volume[9]. Then the expression for the matrix element in the Bardeen's approximation becomes:

$$|T_{k\to k'}|^2 = \left(\frac{\hbar^2}{2m}\right)^2 \frac{2}{V} \frac{k_z^2 e^{-2\kappa_z d_z}}{\kappa_z^2 + k_z^2} \left| \int_S \left(e^{-i\mathbf{k}_\perp \mathbf{r}_\perp} \frac{\partial \psi_i}{\partial z} + \kappa_z e^{i\mathbf{k}_\perp \mathbf{r}_\perp} \psi_i \right) dS \right|^2 . \tag{3.44}$$

And the rate of tunneling (using Fermi's Golden Rule):

[9]Extending infinitely into the source or drain electrodes. Note, that in the final expression (3.45) this volume naturally drops out.

$$\Gamma^{s,d}_{k\to k'} = \frac{2\pi}{\hbar}\sum_k |T_{k,k'}|^2\nu = \frac{2V}{\hbar(2\pi)^2}\int_0^{\pi/2} d\phi \int_0^{2\pi} d\theta (k_z^2 + k_\perp^2)\sin(\phi)|T_{k\to k'}|^2, \tag{3.45}$$

where θ and ϕ are the polar and azimuthal angles in the momentum space.

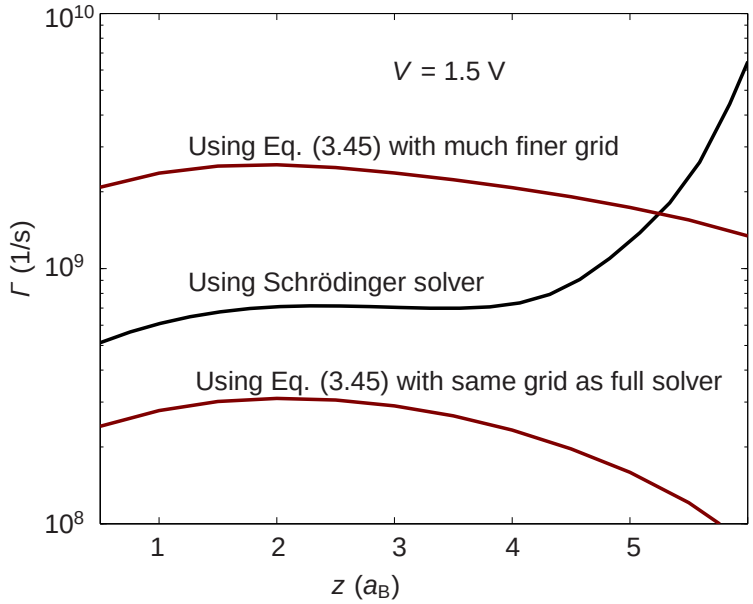

Figure 3.9: The tunneling rate as a function of the position of the integration plane S, calculated using the full Schrödinger solver for $\psi_{s,d}$ and compared to the tunneling rate calculated using the approximate Eq. (3.45), using two integration grids: same grid as used in the Schrödinger solver and a much finer grid (too fine for the Schrödinger solver to handle).

Figure 3.9 shows the comparison between tunnel rates calculated using the numerical solution of the Schrödinger equation for the $\psi_{s,d}$ described in Sec. 3.5.1 wavefunction and the 1D approximation given by Eq. 3.45.

3.6 Electrostatics

3.6.1 External Potentials

In this work, it was assumed that the environment of each molecule (that includes the electrodes as well as other molecules in the system) responds instantaneously to changes in the charge state of a molecule of interest, and

therefore the applied source-to-drain voltages, intermolecular Coulomb interaction, gate voltage (where applicable), and the image charge effects [87] may all be treated as parts of a total external electrostatic potential. Indeed the most important polarization response of typical metals (given by the plasmon frequency) is $\sim 10^{-15}$s, i.e. 5 orders of magnitude faster than the "fastest" electron tunnel time $\sim 10^{-10}$s in single-electron molecular devices analyzed here.

Another assumption is that molecules are embedded between plane, infinite surfaces of source and drain/control electrodes. (This assumption is natural for the eventual SAM implementation of the resistive switches see Sec. 5.2.) In such geometry, the source-drain voltage V creates an electrostatic potential with a linear gradient:

$$\varphi_{sd} = -V\frac{z - d/2}{d}, \tag{3.46}$$

where z is the coordinate perpendicular to the source and drain surfaces (with the origin at the source electrode), and d is the distance between the electrodes. For a single-electron transistor calculations (described in Chapter 4) with a gate not too close to the single-electron island, its potential in this geometry may be well approximated by a quadratic parabola[10]:

$$\varphi_g = \alpha V_g \left[1 - \left(\frac{z - d/2}{d/2}\right)^2\right], \tag{3.47}$$

where $\alpha \ll 1$ is a coupling constant.

The approximations (3.46) and (3.47) imply that the electrostatic screening length λ of the source, drain and gate materials are much smaller than $d \sim$ few nm. For metallic electrodes (with $\lambda \sim 0.1$ nm) the requirement $\lambda \ll d$ is well fulfilled.

3.6.2 Intermolecular electrostatics and image charge effects.

The electrostatic interaction between the two molecules is taken into account by an iterative incorporation of the numerically calculated Coulomb potential created by both molecules (as well as by the series of their charge images in

[10] Consider the solution of the Laplace equation in a box of size $a \times b \times d$ with $d \ll a \ll b$ with the bottom side in the d, a plane at a constant potential V_g and all other sides taken at a zero potential. The solution will be $\varphi_g(x, y, z)/V_g \propto sin(\pi x/a)sin(\pi z/d)exp(-\pi y/d)$ assuming that the molecule lies flat in the y, z and is located at $x \approx a/2$ then to the first order I get Eq. (3.47).

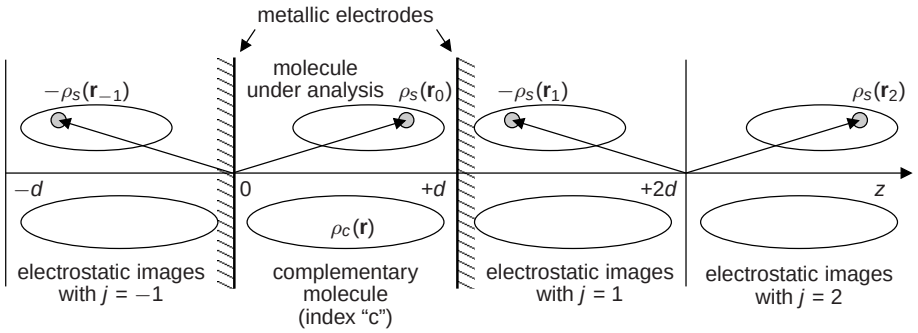

Figure 3.10: A schematic view of charge densities participating in Eq. (3.48).

the metallic electrodes of the system — see Fig. 3.10) into the Kohn-Sham potentials[11]. From elementary electrostatics, this potential may be expressed as

$$\begin{aligned}\varphi_s(\mathbf{r}) &= \int \frac{\rho_c(\mathbf{r_0})}{|\mathbf{r}-\mathbf{r_0}|} d^3 r_0 \\ &\quad + \sum_{j\neq 0} (-1)^j \int \frac{\rho_c(\mathbf{r_j}) + \rho_s(\mathbf{r_j})}{|\mathbf{r}-\mathbf{r_j}|} d^3 r_j, \\ \mathbf{r}_j &\equiv \mathbf{r}_0 + \mathbf{n}_z \times \begin{cases} jd, \text{ for } j \text{ even}, \\ (j+1)d - 2z, \text{ for } j \text{ odd}. \end{cases}\end{aligned} \tag{3.48}$$

where $\rho_s(\mathbf{r}_0)$, $\rho_c(\mathbf{r}_0)$ are the total charge distributions of the molecule under analysis and the complementary molecule, and $\rho_s(\mathbf{r}_j)$, $\rho_c(\mathbf{r}_j)$ are the corresponding charge images in the source ($j > 0$) and the drain ($j < 0$) electrodes — see Fig. 3.10. The first term in Eq. (3.48) is the potential created by the complement molecule and the second term describes the potential of the infinite set of charge images of both molecules in the source and control/drain electrodes. The total electrostatic potential is then:

$$\varphi = \varphi_s + \varphi_{sd} + \varphi_g \tag{3.49}$$

At the 0-th iteration, the first term is taken equal to zero. Fortunately, the iterations give rapidly converging results, so that there was actually no need to go beyond the second iteration — see Fig. 3.11.

[11]The same equation is used in calculations in Chapter 4, where the transport properties of a three terminal molecular single-electron transistor are evaluated, with terms due to the complement molecule in Eq. (3.48) set to zero.

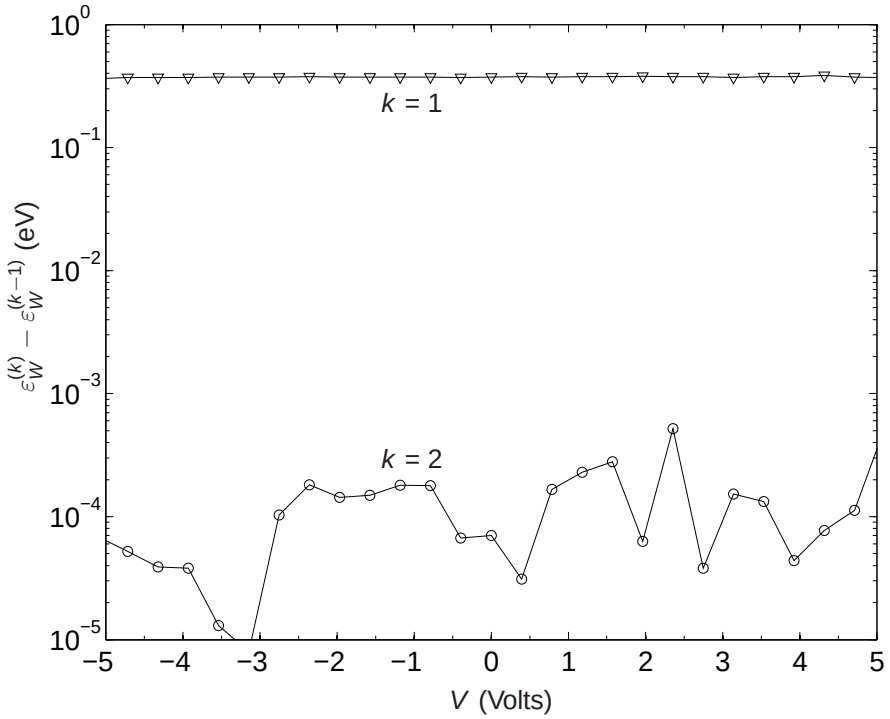

Figure 3.11: Differences between the energies of the working orbital of the molecular trap, calculated with ASIC SIESTA at the k-th and $(k-1)$-th iterations of the Coulomb interaction potential, given by Eq. (3.48), as functions of the applied voltage.

3.7 Parasitic discharge of the trap molecule

As was already mentioned in Sec. 2.2.1, the trap and transistor molecules have to be placed sufficiently far from each other at a distance d_p (see Fig. 2.1b to prevent a parasitic discharge of the trap via the elastic cotunneling through the transistor island, into one of the electrodes. This effect may be estimated using the same formula for $\Gamma^{\rm cot}$ (3.17), used in Sec. 3.1.4 to describe elastic cotunneling between the acceptor island of the trap molecule and its tail.

In this context, Δ is the matrix element of electron tunneling between the trap and the transistor islands (that exponentially depends on the distance d_p between the molecules), ε is the difference between eigenenergies of these states, and Γ is the rate of tunneling between the source and drain electrodes and the transistor's island. The process is schematically shown in Fig. 3.12

The parasitic cotunneling rates $\Gamma^{\rm cot}_{\rightarrow}$ were calculated for all possible escape routes (such as electron escape from the trap via an excited states of the transistor). It was found that in order for the cotunneling rate $\Gamma^{\rm cot}_{\rightarrow}$ to be

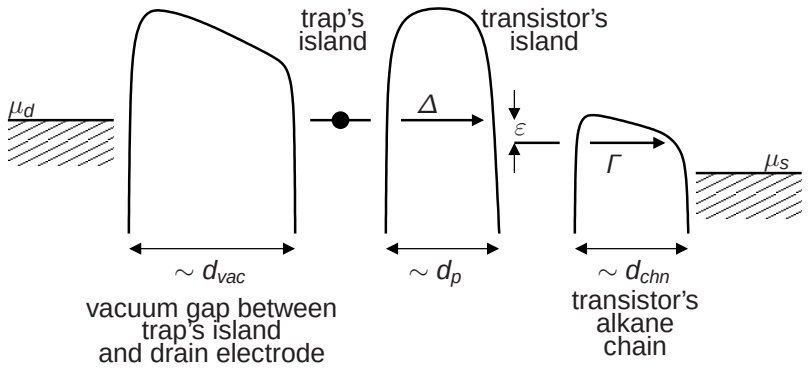

Figure 3.12: Parasitic discharge of the trap molecule via the elastic cotunneling through the transistor island, into the source electrode (schematically).

below the retention rate of the trap Γ_r, the distance d_p between the trap and the transistor molecular islands should not be lower than $\sim$ 1.5 nm. Such relatively large separation justifies separate DFT calculations of the electronic structures of the trap and the transistor, related only by their electrostatic interaction described in Sec. 3.6.2.

3.8 Geometry relaxation

The molecular geometry of each component molecule was relaxed, using the LSDA SIESTA package, only for isolated neutral molecules, at no applied bias voltage and without accounting for image charge effects. In the relaxed geometry all force components on atoms are smaller than 0.05 eV/$\mathring{A}$.

To justify this procedure, I have verified that the most important trap charging and discharging rates are little affected by changes in the molecular geometry induced by a high constant external electric field. For example Fig. (3.13) shows electron tunnel rates in and out of the molecular trap calculated using two geometries: one, relaxed in the presence of a high (8 V) external bias voltage, and the other, relaxed at $V = 0$. The resulting curves differ so insignificantly that there hardly is any sense in performing a computationally demanding geometry minimization loop at every voltage step.

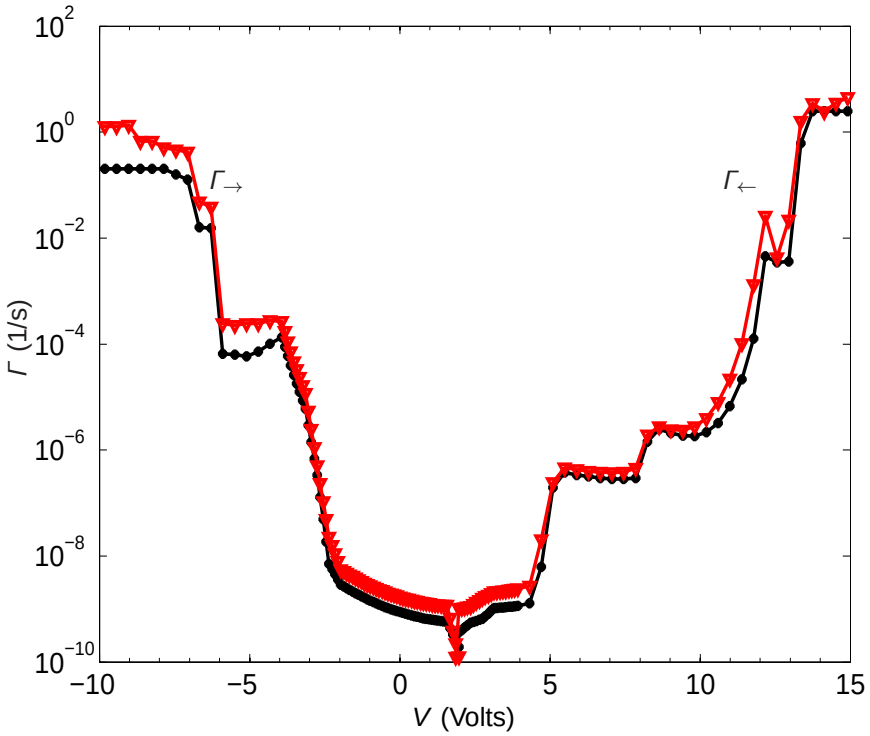

Figure 3.13: The trap switching rates; in red — calculated using the traps geometry relaxed at no applied external bias voltage (without the level "freezing" correction), in black — using the geometry, relaxed at V=$\sim$ 8 Volts also without the level "freezing" correction).

Chapter 4

Negative differential resistance at sequential single-electron tunneling through atoms and molecules

4.1 NDR in a single atom, single-electron transistor

The approach described in Chapter 3 was first applied to a very simple model of an atomic single-electron transistor - a single sodium atom positioned in the middle of a 1.45-nm gap between two gold electrodes. This model is of course not too realistic, because it does not describe the additional chemical groups necessary to fix the atom in such position - see, e.g., experiments [100] with a single-Co-atom transistor. The particular choice of the atom in these calculations was a certain compromise: a desire to avoid very simple atoms which cannot be adequately described by the DFT approach, as well as very complex atoms which would be well described by the simple charging model (3.2). (As Fig. 3.1 shows, in Na the deviations from this simple behavior are still very strong.)

The self-interaction corrections that are discussed at length in Sec. 3.3.1 were not included into this calculation, and the NRLMOL software package was used to calculate the quasiparticle energies and corresponding Kohn-Sham orbitals, directly as was discussed in Sec. 3.3[1].

[1]The single-electron transistors, described in this chapter, consist of either a single Na atom or a simple OPE molecular chain. The main effect of self-interaction in these transis-

First, the ground state energies $E_{gr}(n)$ and the Kohn-Sham orbitals $\psi_i(n)$ for a limited set of charged states (ions) of the atom were calculated. Knowledge of $E_{gr}(n)$ allows sketching the approximate position of the lowest diamond of Coulomb diagram $[V_g, V]$ of the system (see Sec. 1.3.3), neglecting the effects of the source-drain and gate voltages on the atom, in particular its polarization. For that, it is sufficient to mark the Coulomb blockade node points [61, 101]

$$\alpha e V_g(n) = E_{gr}(n+1) - E_{gr}(n) \tag{4.1}$$

on the gate voltage axis, and pass through each of them two straight lines with slopes $dV/d(\alpha V_g) = \pm 1/2$ - see Fig. 4.1. The equal factors 1/2 reflect the equal division of the source-drain voltage between two similar halves of the device; for asymmetric devices (such as atoms placed away from the middle of the gap between the two electrodes or asymmetric molecules) the slopes would be different. This sketch, which is actually pretty close to the finally calculated diagram, allows the selection of the appropriate range of source and gate voltages and the necessary set of states k participating in the transport[2], for the exact calculations of the diamond diagram (shown in Fig. 4.1) as well as a set of $I - V$ curves in Fig. 4.2.

The dashed lines in Fig. 4.1 show the Coulomb diamond diagram of the sodium-atom transistor for moderate positive values of the gate voltage. The regions below the lowest lines correspond to the Coulomb blockade, i.e. stable ions of the Na atom, without noticeable current [82, 101]. When the source-drain voltage is negligible, the change of V_g results in the transition from one ion (with, say, n electrons) to the adjacent ion (with, e.g., $n+1$ electrons) in each of special points $V_g(n)$ given by Eq. (4.1). If the source-drain voltage V is increased, the transition occupies a finite gate voltage range $[\alpha V_g(n) - V/2 < V_g < \alpha V_g(n) + V/2]$, within which the atom cycles quasi periodically between the two ion states, with one electron per period transferred through the system [61, 101].[3] Note that this process involves only the ground states of both ions. On the other hand, in the language of orbitals, the transport corresponds to a periodic tunneling in and out of one quasiparticle state with a fixed number i (either n or $n+1$). As the source-drain voltage is further increased, other transfer channels open, involving orbitals with other values of i. On the $[V_g, V]$ plane, boundaries of the channel openings are almost linear

tors is a simple shift of energy levels (as described in Appendix A), which may be readily compensated by the applied gate voltage V_g. Hence, the omission of the self-interaction corrections here is not as crucial.

[2]The larger is the voltage range, and the more complex is the junction, the larger is the latter set.

[3]In the chemical language, this is just a quasi-periodic redox reaction.

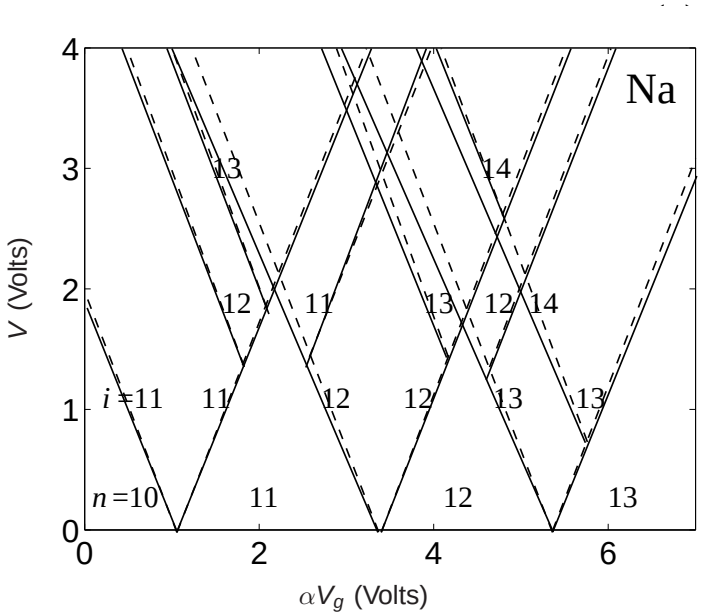

Figure 4.1: The Coulomb diamond diagrams for a single-Na-atom transistor: Solid lines show the "exact" (DFT) results that include the effects of image charges, gate and source-drain electric fields on the atom (including its polarization), while dashed lines correspond to the approximation in which these effects are ignored.

- see Fig. 4.1.

Figure 4.2 shows a set of calculated $I - V$ curves corresponding to three values of the gate voltage: one very close to a special point $V_g(n)$ (in this case, $n = 10$) and two values separated by that point by nearly equal increments up and down from that point. As was expected, crossing the Coulomb blockade threshold, i.e. opening the first transport channel, leads to a sharp current step. What was unexpected is the *reduction* of the current with a further increase of the applied voltage V. Each of these regions of negative differential resistance (NDR) with $dI/dV < 0$, is extended almost to the next current step.

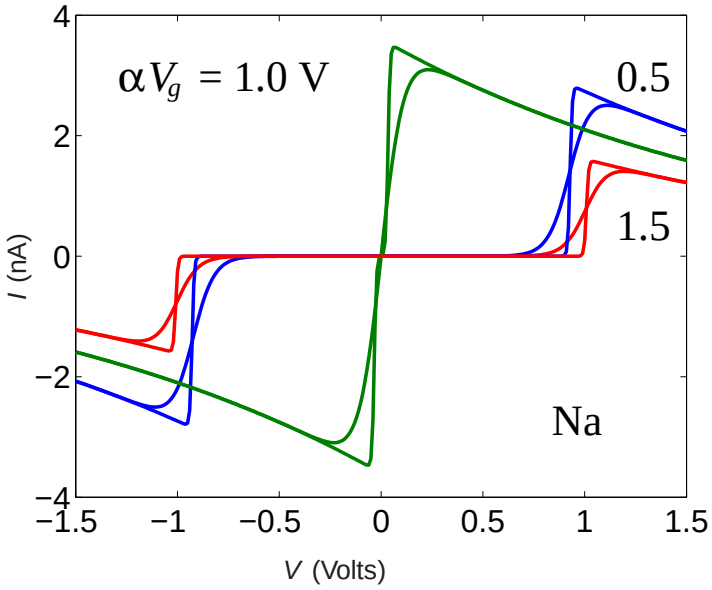

Figure 4.2: A set of the $I - V$ curves for a Na-atom-based transistor for three values of gate voltage, each for two values of temperature (30 and 300 K). Within the shown range of voltages, either none or just a single transport channel is open, corresponding to an alternating occupation of the $3S_1$ orbital (i=11), which is the HOMO level for a neutral Na atom and the LUMO level for its singly-positive ion.

4.2 NDR in single-electron transistors based on OPE molecules

In order to verify that this effect is not accidental or atom-specific, the calculations have been extended to single-electron transistors based on short,

isocyanide-terminated OPE chains (Fig. 5a) with three and four benzene rings. (At the time of this work, such molecules were considered the leading candidates for the future implementation of molecular single-electron latching switches [18].) The Kohn-Sham spectrum and orbital structure of these two molecules are rather similar - see Fig. 4.3. For our study, the ends of such molecules were separated from gold electrodes by vacuum gaps. The width of the gaps was selected rather large, $\Delta z \approx 0.35$ nm, to provide currents of practical interest (below one nA). As a result, the role of the single-electron island was played by the molecule as a whole (cf. Refs. [102, 103]). A change of Δz within reasonable limits ($\Delta z \geq 0.2$ nm) changes only the current scale, but not the shape of the $I - V$ curves.

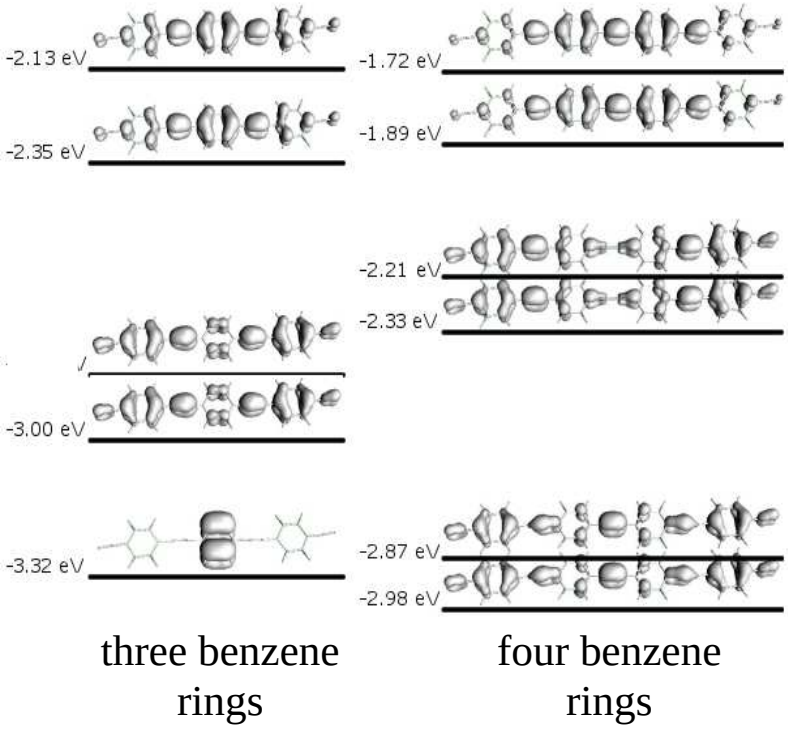

Figure 4.3: The energy spectrum and orbital structure of neutral OPE molecules with (left column) three and (right column) four benzene rings.

The Coulomb diamond diagrams of single-electron transistors based on these two OPE molecules are shown in Fig. 4.4, while Fig. 4.5 shows a set of $I - V$ curves of one of them (with three benzene rings). Due to the more complex structure of the molecule (compared to the single atom), more channels open as the source-drain voltage is increased, but the NDR effect is similar to that calculated for the single-atom transistor.

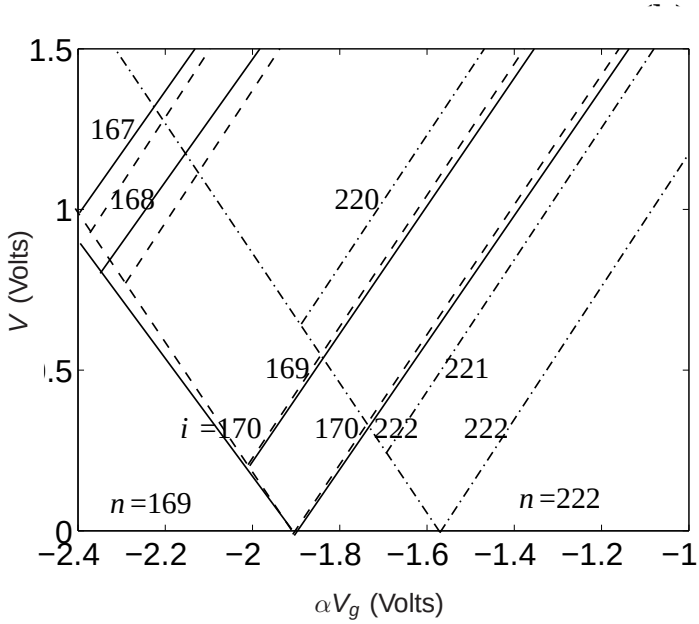

Figure 4.4: The Coulomb diamond diagrams for two (3-ring and 4-ring) single OPE molecules: Solid lines show the "exact" (DFT) results (without the self-interaction corrections), while dashed lines correspond to the approximation in which the effects of the gate and source-drain electric fields on the molecules (i.e., its polarization) are ignored.

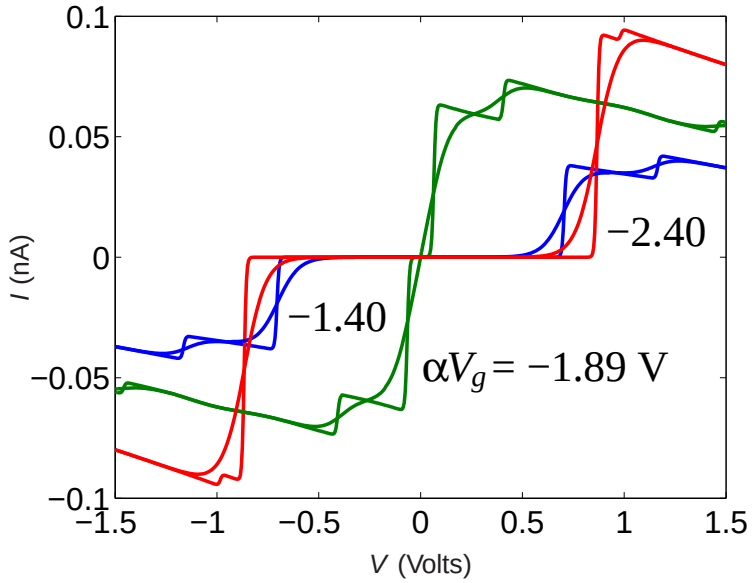

Figure 4.5: A family of $I-V$ curves of a transistor based on a three-ring OPE molecule, for three values of αV_g and two values of temperature (30 and 300 K). Each current step corresponds to opening of one more transport channel, i.e., crossing one more line on the Coulomb diamond $[V_g, V]$ diagram shown in Fig. 4.4.

4.3 Universal NDR mechanism

After careful examination, we have been able to interpret the effect as follows, see Fig. 4.6. At sequential tunneling, an additional electron first tunnels through one barrier of the system, and then through another one. In accordance with this physical picture, the formulas of Sec. 3.1 show that the transistor current beyond the Coulomb blockade threshold is always of the order of

$$I \sim e\frac{\Gamma^s\Gamma^d}{\Gamma^s+\Gamma^d} = e\left(\frac{1}{\Gamma^s}+\frac{1}{\Gamma^d}\right)^{-1}, \tag{4.2}$$

and thus crudely corresponds to the serial connection of tunneling resistances of the two barriers. Figure 4.6 shows that, since the eigenenergy of the electron on the island is fixed (quantized), the increase of the source-drain voltage leads both to a *suppression* of the height of one of the barriers, and to an *increase* of the height of the other barrier, so that one of the Γs in Eq. (4.2) grows, while the other one decreases. Evidently, as Eq. (4.2) shows, the current roughly follows the *lower* transparency (i.e. the *larger* tunnel resistance) and thus drops with increasing voltage.

Generally the NDR effect has been observed in quite a few measurements of electron transport through molecules. Typically it takes place at the back of sharp current peaks, which have been attributed to electron transfer between two energy levels (or narrow energy bands) which are aligned at a certain voltage, and then misaligned at its increase. On the contrary, the NDR mechanism discussed above takes place within broad ranges of voltages, and may be quite resilient. Such NDR effect has already been observed experimentally by at least two groups:

First, Grobis *et al.* [104] observed $I-V$ curves similar to those in Fig. 4.2 and 4.5, while doing scanning tunneling spectroscopy of double C_{60} layers on a metallic surface. Their interpretation, basically the same as ours, was generously credited by the authors to an older paper by Esaki and Stiles [105] which actually describes a rather different situation. Grobis *et al.* have made an approximate calculation for the case of a highly asymmetric system, with one tunnel barrier much more transparent than another one. In this case the NDR effect is much simpler than in our symmetric case, because the situation is reduced to tunneling, from a Fermi sea continuum, through a single barrier, into a set of discrete energy levels. In that asymmetric case the barrier increases with V, and hence NDR takes place, only for one polarity of the applied voltage. (A similar situation has been briefly mentioned in Ref. [106].)

Second, Khondaker *et al.* [107] have observed (though not explained) similar NDR effects for *both* polarities of applied voltage through a short phenylene-

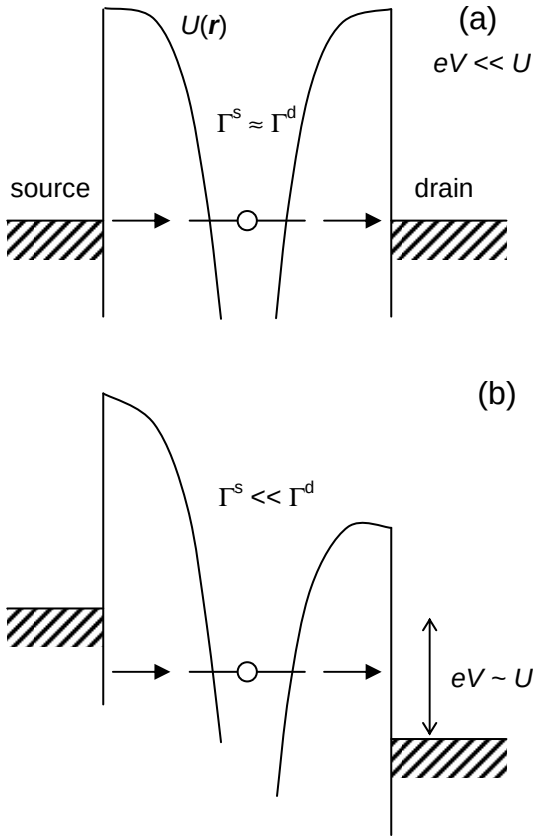

Figure 4.6: A schematic conduction band edge diagram of the simplest system with one quasiparticle energy level, explaining the mechanism of the negative differential resistance in our systems: the increase of one of the tunnel barriers by the source-drain voltage V.

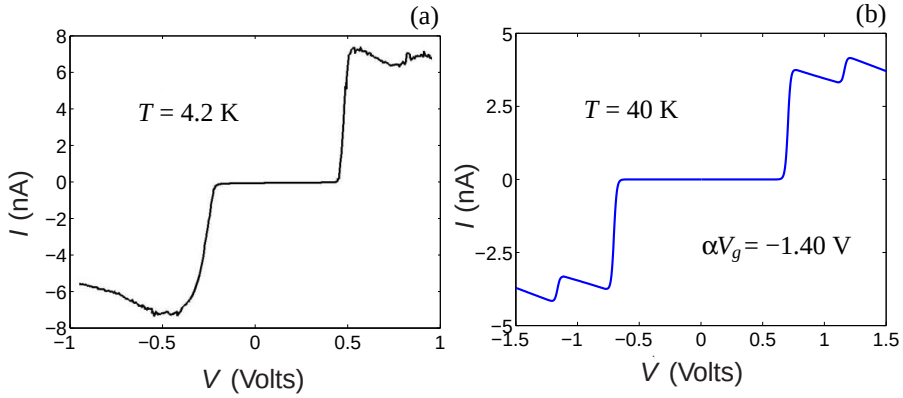

Figure 4.7: (a) Experimental $I-V$ curve for a phenylene-ethynylene molecule with four benzene rings (copied, with permission, from Fig. 2b of Ref. [107]) for $T = 4.2$ K, and (b) a result of our calculations for a three-ring OPE molecule for $T = 40$ K, with the current scaled up by a factor of 100. Such scaling corresponds to the reduction of the molecule-electrode gap Δz from 0.35 nm down to approximately 0.23 nm.

ethynylene chain, very similar to our OPE chains. Figure 4.7 shows a comparison of their data with a typical result of our simulation for a three-ring OPE molecule. Given the fact that the molecules are somewhat different, and no attempt has been made to fit the value of V_g and the gaps between the molecule and the electrodes at calculations, it is striking how strong the similarity is. The slight asymmetry of the experimental curve may be readily explained by the possible asymmetry of the molecule attachment to electrodes.

An important question is why the NDR effect is not observed in other molecular conduction experiments. (In a typical experiment, current through a molecule increases monotonically with voltage.) There could be several reasons.

First, our calculations pertain only to sequential tunneling at which the molecule (or its part), playing the role of the single-electron island, is separated from electrodes by tunnel barriers with small transparencies - see Eq. (3.1). Second, the effect appears only when the applied source-drain voltage becomes comparable with the tunnel barrier height. Though the molecular field may suppress the barrier considerably below the electrode work function level of 4 to 5 eV, its typical height is still above 1 eV, so that the NDR effect may hardly show up at voltages much below that value, and some molecular junctions may not be strong enough mechanically to endure such fields. Next, the more complex is the molecule, the more eigenstates it has within a certain energy interval, so that the increasing voltage opens more and more transport

channels (compare, for example, the $I-V$ curves of the single-atom transistor shown in Fig. 4.2 with those of the more complex OPE chains - Fig. 4.5 and with the complex single-electron transitors in Chapter 5 Fig. 5.1). As the molecule complexity grows, the increased number of current steps will mask, and eventually completely overwhelm the NDR effect. In particular, this effect is completely absent in the "orthodox" theory of single-electron tunneling [101] which considers the set of island eigenstates as a continuum.

Despite these qualifiers, I believe that the NDR effect with the mechanism described in this work may be implemented in single-electron transistors based on many relatively simple molecules suitable for their incorporation into reproducible SAM-based crosspoint devices. This is why possible applications of this effect in the hybrid semiconductor/nanoelectronic (e.g., CMOL) circuits [108, 109] should be carefully analyzed. The most immediate opportunity is to connect crosspoint devices into the so-called Goto pairs [110] with two stable states which may be used for coding binary zeros and ones. Logic circuits based on such pairs (see, e.g., Ref. [111]) may enable the digital signal restoration without help from the semiconductor-transistor subsystem, used in the current generation of hybrid logic circuits [78]. This may boost the circuit density very substantially. (Rose and Stan have proposed [112] a three-level crossbar to integrate nanoscale Goto pairs into hybrid circuits, but this structure would require nanoscale alignment of the layers and hence is hardly practicable.)

Chapter 5

Simulations of molecular nonvolatile single-electron resistive switches

5.1 Simulation results for a single resistive switch

Unlike devices that were considered in Chapter 4, the calculation of transport and charging properties in the molecular resistive switches requires a more careful approach that includes self-interaction corrections described in detail in Sec. 3.3.1.

Figures 5.1 and 5.2 show the main results of a simulation of the resistive switch shown in Fig. 2.1b, for a temperature $T = 300$ K. Figure 5.1 shows the dc $I - V$ curves of the transistor, plotted for both charge states of the trap. These plots show that the $I - V$ curves fit the initial specifications rather well, with a broad voltage window (from ~ 2.0 to ~ 2.5 V) for the trap state readout, with a large ON/OFF current ratio (inset in Fig. 5.1), and a very reasonable ON current $I \sim 0.2$ pA.

Fig. 5.2 shows the rates of transitions between the neutral and single-negatively charged states of the trap, with and without accounting for the transistor effect on the trap molecule. The plots show that the trap features a high retention time, $\tau_r > 10^8$s, for both charge states, within a broad voltage range, $-2\text{V} < V < +5\text{V}$ (it is somewhat surprising how little the trap retention is affected by the electrostatic "shot noise" generated by fast, quasi-periodic charging and discharging of the transistor island, which is taken into account by the theory in Chapter 3.). The range includes point $V = 0$, so that the device may be considered a nonvolatile memory cell.

At the same time, the device may be switched between its states relatively

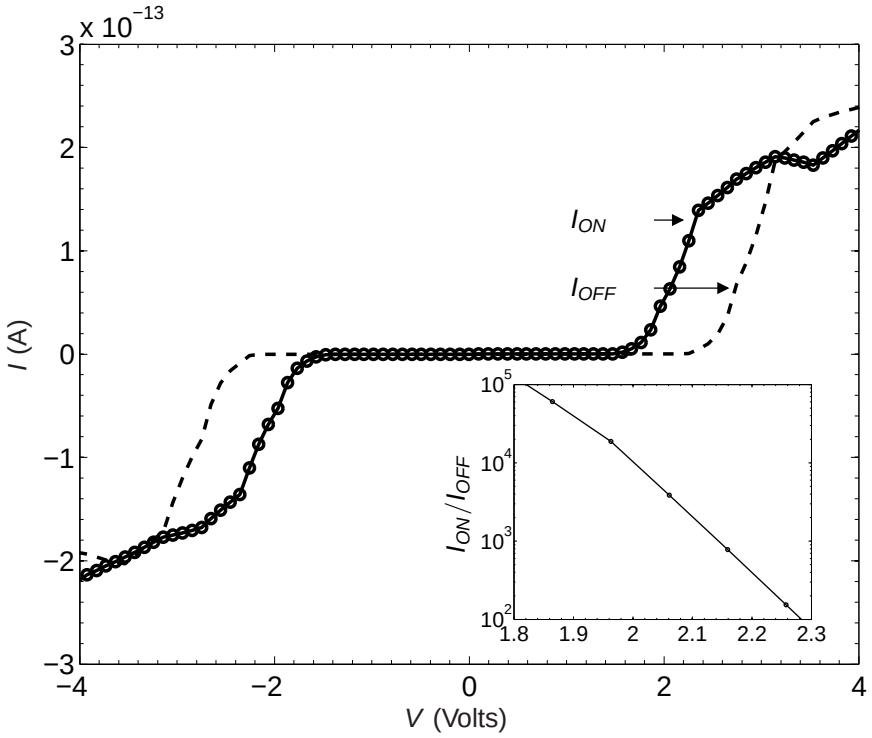

Figure 5.1: Calculated dc $I-V$ curves of the transistor for two possible charge states of the trap molecule. The inset shows the ON/OFF current ratio of the transistor on a semi-log scale, within the most important voltage interval.

quickly by applied voltages outside of this window. The price being paid for using alkane chains with their large HOMO-LUMO gap is that the voltages necessary for fast switching are rather large — they must align the valence or conduction band of the alkane chain with the group-localized working orbital — see Fig. 2.4.

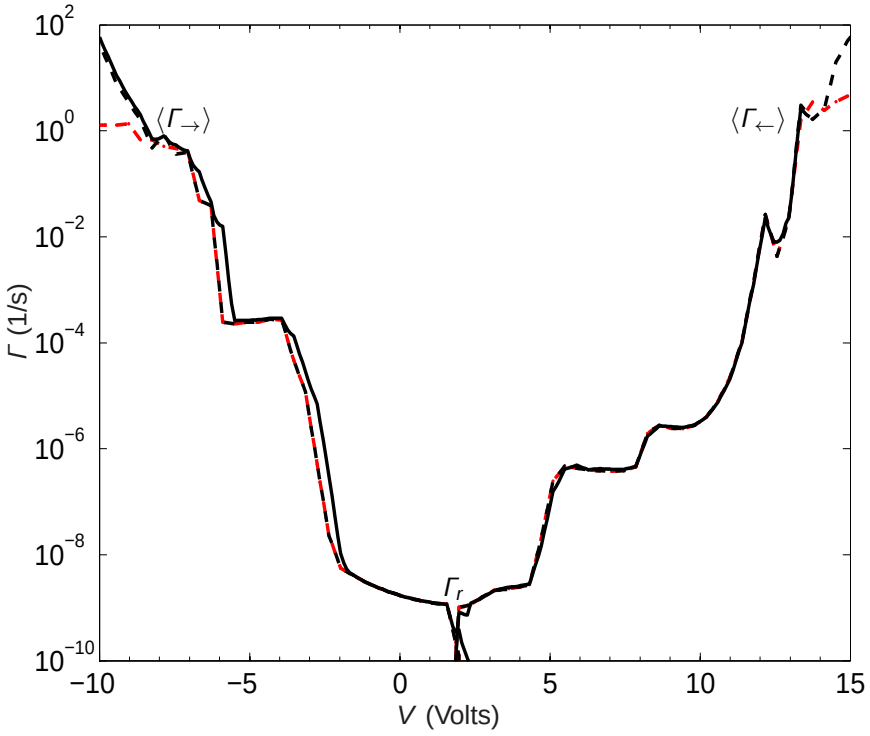

Figure 5.2: The trap switching rates, calculated with (solid lines) and without (black dashed lines) the account of transistor's back action, as functions of the applied voltage. Red dashed lines show the trap switching rates calculated without the level "freezing" correction (Sec. 3.3.1 and Appendix B) and without taking into the account transistors back action.

5.2 SAMs of resistive switches

Probably the largest problem of molecular electronics [67, 68] is the low reproducibility of interfaces between molecules and metallic electrodes. However, recent results [113] indicate that this challenge may be met at least for self-assembled monolayers (SAMs) encapsulated using special organic counter-electrodes. This is why I have explored properties of SAMs consisting of square

arrays of $N \times N$ resistive switches described above — see Fig. 1.4. In order to increase the tolerance of the resulting SAM devices to self-assembly defects and charged impurities, it is beneficial to place the component molecular assemblies (Fig. 2.1b) as close to each other as possible, say at distances comparable to that (~ 1.5 nm) between the trap and transistor. In this case, the Coulomb interactions between the component molecules are very substantial, and properties of the system have to be calculated taking these interactions into account.

A system of $N \times N$ resistive switches has $2N \times 2N$ single-electron islands and hence at least $2^{2N \times 2N}$ possible charge states, which would require solving that many master equations for their exact description. Even for relatively small N, this approach is impracticable, and virtually the only way to explore the properties of the system is to perform Monte Carlo simulations [66, 72].

5.2.1 Monte Carlo algorithm

Generally, a Monte Carlo simulation requires prior calculation of tunnel rates in all molecular devices for all possible charge states of a $N \times N$ resistive switch SAM (it will be shown in Sec. 5.2.2 that for our uniform system this requirement may be relaxed.). Let K be some charge state of the SAM.[1] Rewriting our notation in Sec. 3.1.2 to fit a more general problem, let $w^{s,d}_{K,\leftrightarrows}(i)$ be an in/out ($\leftrightarrows$) tunnel rate from the i'th molecule in the SAM in its K'th global charge state. Assuming that each tunnel rate $w^{s,d}_{K,\leftrightarrows}(i)$ pertains to a random independent event of a single-electron charge change at the i-th molecule, a well-known equation for the exponential decay of the initial state probability can be used to calculate the time interval between two such events:

$$\tau_l = \frac{-log(rand_1)}{\sum_i (w^s_{K,\leftrightarrows}(i) + w^d_{K,\leftrightarrows}(i))}, \tag{5.1}$$

where $rand_1$ is a random number, with the probability distributed uniformly between 0 and 1.

Then a second, independent random number $rand_2$, with the same probability distribution, may be used to decide which specific tunneling event takes place, by finding j' such that:

$$\frac{\sum_j^{j'-1} w_K(j)}{\sum_i^{4N^2} w_K(j)} \leq rand_2 < \frac{\sum_j^{j'} w_K(j)}{\sum_i^{4N^2} w_K(j)}, \tag{5.2}$$

[1] The single index K represents a charge state of *all* molecules in the SAM, i.e. $K = \{k_1, k_2 ..., k_i, ...k_{4N^2}\}$ where k_i is a charge state of *each* molecule.

where the index j is over all indices in w: s, d, $\leftrightarrows$, i. Thus $w_K(j')$ gives a particular rate of tunneling from/into the i-th molecule into/from either source or drain.

As was discussed in Sec. 3.1.3, the peculiarity of my system is that it features two very different time scales: the first one (for our devices, $\tau_t \approx e/I_{ON} \sim 10^{-4} - 10^{-6}$ s) characterizes the fast charge tunneling through single-electron transistors, while the second one corresponds to the lifetimes of trap states ($\tau_r = 1/\Gamma \sim 10^8 - 10^{-2}$ s). In order to gather reasonable statistics of the switching rates, the data accumulation time (for each parameter set) corresponded to a physical time of up to 10 s, i.e., included up to a million transition tunneling events in the system's transistors, i.e. the Monte Carlo simulation loop was run L times before the condition $\sum_l^L \tau_l > 10$ s was met. At each step l, the number of electrons that arrived from the source electrode $n^s_{\leftarrow}$ and the number of electrons that left back to the source electrode $n^s_{\rightarrow}$ were recorded. The total current through the SAM is then:

$$I/e = (n^s_{\leftarrow} - n^s_{\rightarrow}) \Big/ \sum_{l=1}^{L} \tau_l \, . \tag{5.3}$$

As a check of the validity of the procedure, the Monte Carlo algorithm was first applied to a single resistive switch, and it indeed gave virtually the same result as the master equation solution. The approach was then used for a direct simulation of SAM fragments with two and more coupled resistive switches.

5.2.2 Nearest neighbor approximation

As the fragment is increased beyond a 2×2 switch array, even the Monte Carlo method runs into computer limitations, because of the exponentially growing number of the possible charge configurations. The calculations may be very significantly sped up by using the approximation in which each molecule's state affects the potential of only its nearest neighbors. This approximation has turned out to be very reasonable and may be justified by the fact that metallic electrodes of the system substantially screen the Coulomb potential of the charges of distant molecules: the distance between the acceptor group centers and the electrodes, $d/2 \approx 4$ nm, is of the same order as the 3-nm distance between the molecule and its next-next neighbors (Fig. 5.3). In this nearest-neighbor approximation, each molecule (a trap or a transistor) is still affected by 8 other molecules.

In order to limit the number of the charge configurations even further, all

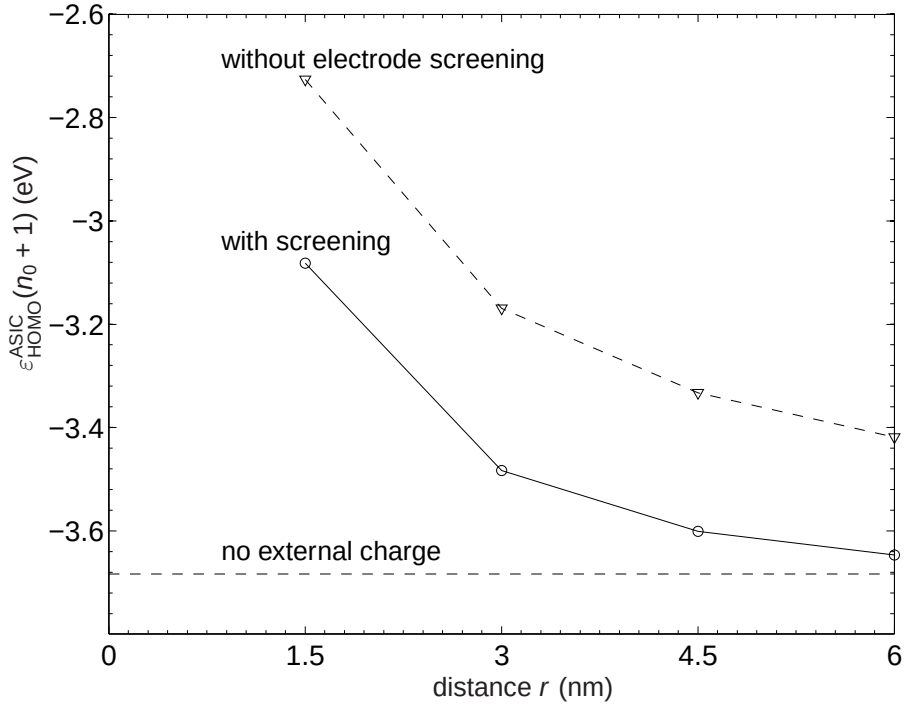

Figure 5.3: Effect of a single charge of a trap molecule on the electron affinity of another molecule, located at distance r without and with the account of the electric field screening by the common metallic electrodes.

"essentially similar" of them (having charge pairs at equal distances, irrespective of their angular position) were treated as identical. As Fig. 5.4 shows, this is a very reasonable approximation.

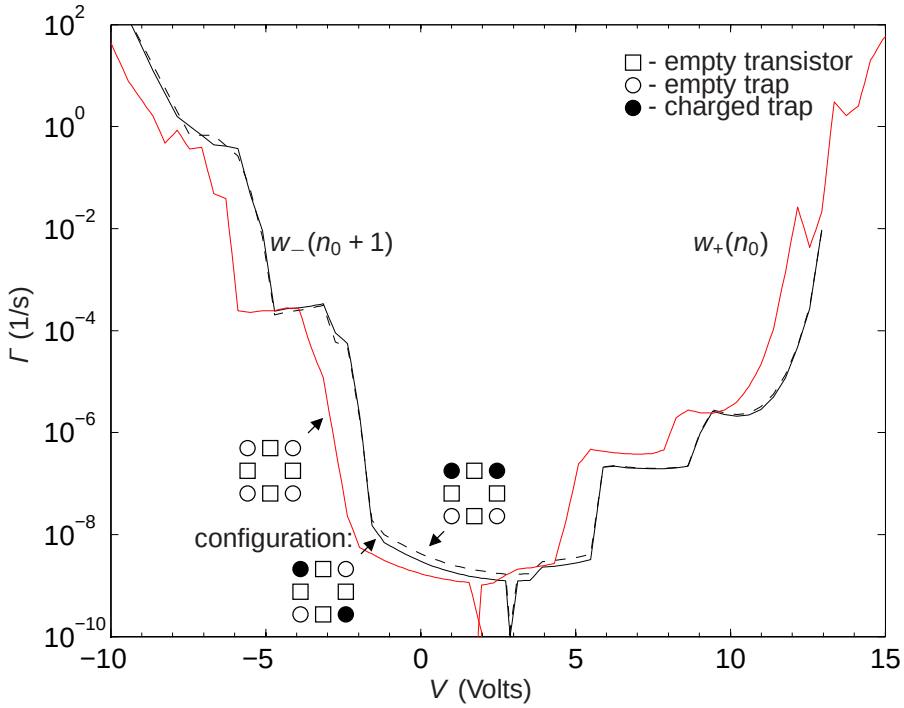

Figure 5.4: Trap tunnel rates as functions of the applied voltage for two quasi-similar nearest-neighbor charge configurations shown in the insets. Trap tunnel rates with all nearest neighbour charges set neutral is shown for a reference (in red).

Even with the significant charge configuration reductions outlined above, the calculation of the remaining configurations still required massive computational resources — about 100,000 node-hours on fast IBM P6 4.2 GHz processors.

5.2.3 Monte Carlo results

Figure 5.5 shows the results of calculations, based on this approach, for a 5×5-switch SAM, with the total area close to 10×10 nm^2. The switching and state readout properties are very comparable with those of a single switch (Fig. 5.1), despite a significant mutual repulsion between single electrons charging neighboring traps.

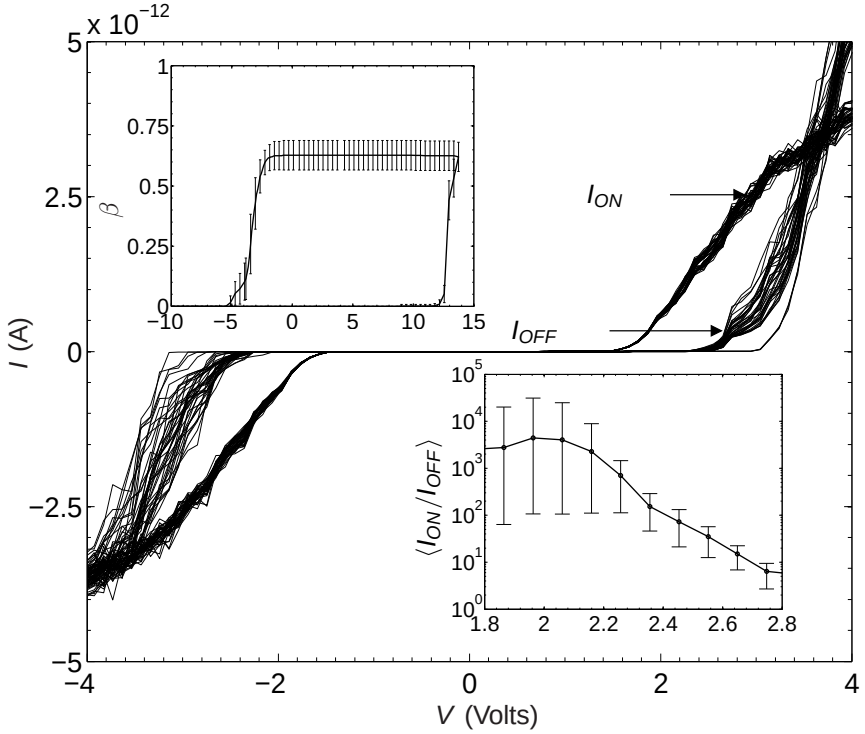

Figure 5.5: Monte-Carlo simulated dc $I - V$ curves of a 25-switch SAM. The top inset shows the fraction β of single-negatively charged traps, averaged over 40 sweeps of applied voltage between -8V and 13V. The bottom inset shows the ON/OFF current ratio averaged over the voltage sweeps, and its maximum sweep-to-sweep spread.

In order to better understand why such a repulsion does not have adverse effects on the operation of the SAM as a whole, I have calculated the correlation coefficients $K(r)$ of charging of two (same type) molecules A and B as a function of the distance between them. The correlation coefficient (at a constant V) may be calculated using the following formula (for its derivation, see Appendix D):

$$K(r) = \frac{P_{A,B} - P_A P_B}{\sqrt{P_A(1-P_A)P_B(1-P_B)}}, \tag{5.4}$$

where $P_{A,B}$ is the probability of both molecules A and B to be simultaneously charged (the joint probability), and P_A is the total probability that the molecule A is charged (and similarly for B).

At voltages above the transistor Coulomb blockade, the transistor molecules switch their charge state quickly and the correlation coefficient $K(r)$ between two transistors was calculated directly from their time evolution records at each fixed voltage. On the other hand, trap molecules have quasi-stationary charge states, so that the correlation between two trap molecules had to be calculated from a set of snapshots of their charge states (at some voltage of interest) taken at repeated, slow sweeping of the applied voltage throughout the whole voltage range.

Figure 5.6 shows the resulting average correlation between molecules (and its fluctuations) as a function of the distance between them in the 5×5-switch SAM. The charge states of neighboring traps are significantly anticorrelated, while the next-next neighbor charge states are positively correlated. This means that the switching is due to a nearly-simultaneous entry of electrons into roughly every other trap [2]. This explains why in the top inset in Fig. 5.5 the average fraction of charged traps is close to 1/2. Thus the only adverse effect of the Coulomb interaction between individual resistive switches is the approximately two-fold reduction of the average ON current per device. Figure 5.7 presents a summary characterization of the SAM operation as a function of its size (and hence its area).

5.2.4 SAM defect tolerance

The fact that even the fractional charging of traps in SAMs is sufficient for a very good modulation of their net current suggests that these devices should have a high tolerance to defects and stray electric charges [66]. In order to verify this, I have carried out a preliminary evaluation of the defect tolerance

[2] There is virtually no correlation between the transistor molecules, just as with their autocorrelation in time [114], because at least two transition channels are open at any time.

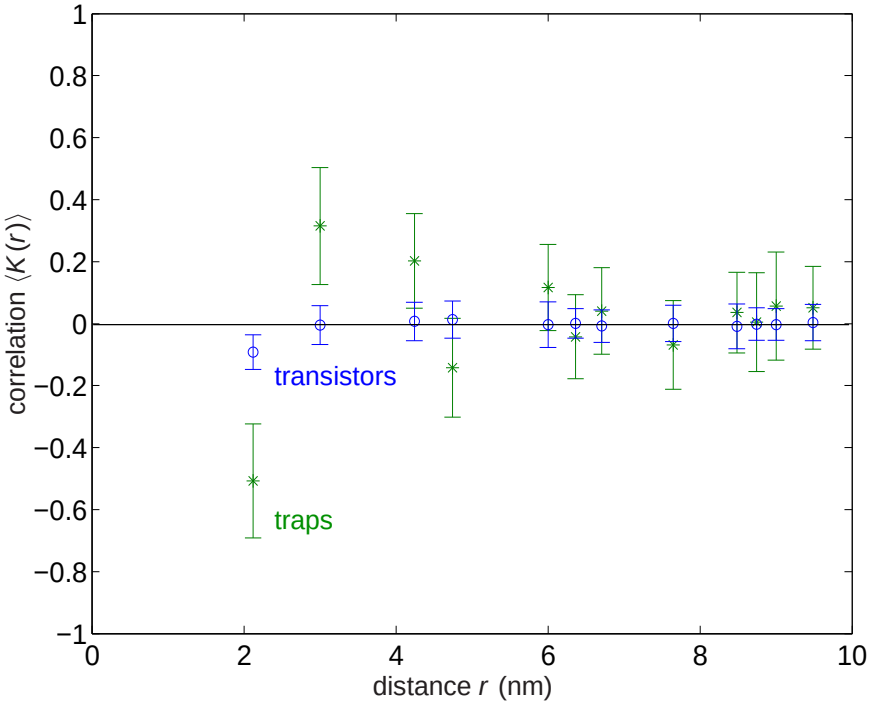

Figure 5.6: The average correlation between two traps (green) and two transistors (blue) as a function of distance between them in a 5×5 device SAM.

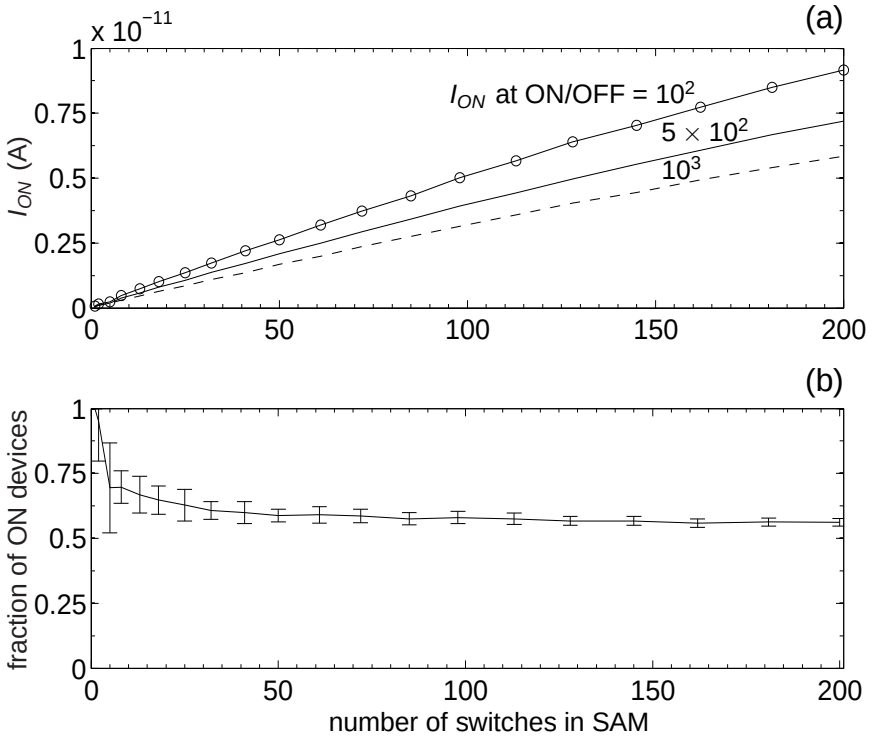

Figure 5.7: Summary of Monte Carlo simulations of SAMs of various area: (a) the average ON currents at voltages providing certain ON/OFF ratios; (b) the average fraction of negatively charged traps at the equilibrating voltage V_e.

by artificially fixing charge states of certain, randomly selected component molecules. The results, shown in Fig. 5.8, are rather encouraging, implying that the switches may provide the ON/OFF current ratios above 100 at defective switch fractions up to $\sim 10\%$, and at a comparable concentration of random offset charges.

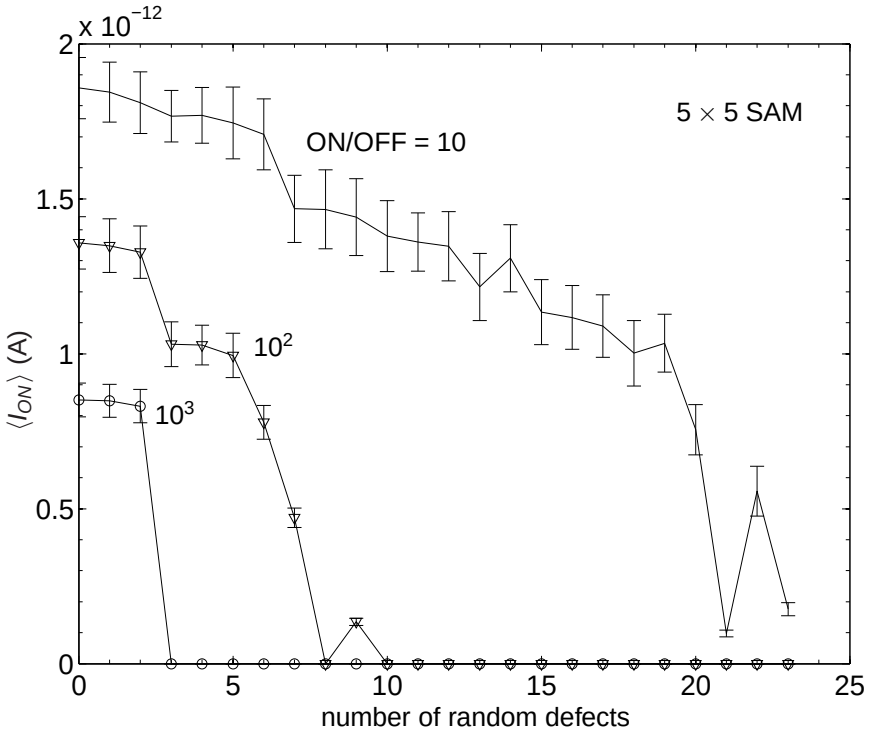

Figure 5.8: Defect tolerance of the 5×5 SAM switch: ON current as a function of a number of molecules held artificially in a fixed, random charge state, at random locations, at the applied voltage values necessary to ensure a certain level of the ON/OFF current ratio. Error bars show the r.m.s. spread of results.

Chapter 6

Summary

The main objective of this work was to explore possibilities of using single-electron tunneling effects in molecular assemblies for the implementation of bistable memristive devices ("resistive switches").

6.1 Design of switch components

The original molecular switch design (see Fig. 2.1a) featured OPE chains that linked the transistor and the trap acceptor groups to the metal electrodes. My DFT calculations have shown that OPE chains can hardly provide a tunnel barrier high enough to ensure sufficiently long electron retention times in traps with acceptable lengths. I have instead proposed to use alkane chains that feature a much larger HOMO-LUMO gap, and designed a molecular resistive switch (see Fig. 2.1b) based on such chains and suitable acceptor groups.

Instead of following the conventional design of the single-electron trap, which is based on the incorporation of several additional single-electron islands into the trap charging path[1], I proposed to use the non-conducting alkane chains performing two roles simultaneously: those of tunnel barriers and intermediate islands. The results show that this idea does indeed work, and may be used in future designs of molecular single-electron devices.

6.2 Theoretical model

In this dissertation a novel approach to the *ab initio* calculation of electron transport through molecular-scale single-electron transistors and charging of molecular single-electron traps was presented. The approach was based on

[1] Making the trap molecule unreasonably long and complex.

a (generalized to molecular structures) combination of the Averin-Korotkov theory of single-electron tunneling [22], Bardeen's formula [99] for tunneling rates, and the DFT approximation [115] for electronic structure. Initially the approach was tested on a toy model of a single-Na-atom transistor, and on a more realistic model of short (three- and four-ring) OPE chains stretched between two gold electrodes.

During this work, two serious shortcomings of the density-functional theory for the description of single-electron charging have been uncovered; they are described in detail in Appendices A and B. Despite these difficulties, I have managed to combine the advanced (ASIC) version of the DFT code to analyze the possibility of using single-electron tunneling effects in designed molecular assemblies for the implementation of bistable memristive devices ("resistive switches").

6.3 Results

The first (unexpected) important finding was a general mechanism for negative differential resistance described in Sec. 4.3, caused by the enhancement of one of the tunnel barriers by the applied source-drain field. Apparently, this effect has been observed in at least two experiments [104, 107] with single molecules.

The results presented in Chapter 5 indicate that chemically-plausible molecules and self-assembled monolayers of such molecules may indeed operate, at room temperature, as nonvolatile resistive switches which would combine multi-year retention times with sub-second switching times, and have ON/OFF current ratios in excess of 10^3. Moreover, strong evidence that operation of the SAM version of the device may be tolerant to a rather high concentration of defects and randomly located charged impurities was obtained. The ON current of a single device (~ 0.1 pA at $V \approx 2$ V) corresponds to a very reasonable density (~ 4 W/cm^2) of the power dissipated in an open SAM switch, potentially enabling 3D integration of hybrid CMOS/nano circuits [116]. In this context it is important to note that the average power density in a crossbar is at least 4 times lower than the cited number, because of the necessary crosspoint device spacing (Fig. 1.1b); besides that, in most applications, at least 50% of the switches (and frequently much more) are closed, decreasing the power even further.

6.4 Future work

Even the best design developed in this thesis (Fig. 2.1b) still requires additional work. First, proper spatial positions of the functional molecules have to be enforced by some additional molecular support groups which have not been taken into account. If the spacer groups, fixing the relative spatial arrangement of the islands, can be constructed from saturated molecular units similar to the alkane chains used to separate the islands from the electrodes, then the calculations presented here should be applicable to complete devices, but this expectation still has to be verified.

There is also a substantial room for improvement in the choice of molecular chains used as tunnel barriers and intermediate islands. For example, the low calculated effective mass, $m_{\text{eff}} \approx 0.1 m_0$, of electrons tunneling along alkane chains makes it necessary to use rather long chains, despite their large HOMO-LUMO gaps (which, in turn, require large switching voltages — see Figs. 2.4, 5.2). The use of a molecular chain with a higher m_{ef} and a narrower gap would decrease switching voltages (and hence energy dissipation at switching), and also reduce the total device length, resulting in shorter switching times (at the same charge retention).

Also, the theoretical model presented in Chapter 3 ignores the possible strong excitation of molecule vibrations by tunneling electrons, whose evidence has been seen in several experiments with molecular single-electron transistors - see, e.g., Refs. [10, 11, 100, 102, 117]. They show that additional current steps may appear in the $I - V$ curve at voltages corresponding to phonon energy multiples. The incorporation of a theoretical description of such effects (see, e.g., Refs. [118, 119]) into the *ab initio* framework presented in this dissertation is one of possible future research topics.

The defect tolerance of SAM-based switches should be evaluated in more detail, for charged impurities located not only on the molecular acceptor groups, but also between them — say, inside the (still unspecified) support groups.

Finally, an experimental verification of the predictions in this thesis looks imperative for the further progress of work towards practical molecular resistive switches.

Appendix A

Single-electron charging correction

Let us consider a simple but reasonable model of a well-conducting (say, metallic) island, of a size well above the Thomas-Fermi screening length, in which the single-electron addition energies are simply

$$\Delta E(i) = K_i - e\phi_i, \tag{A.1}$$

where K_i is i-th electron's kinetic energy (which, as well as the island capacitance C, is assumed to be independent of other electron state occupancies, but is an arbitrary function of i), and the second term describes the potential energy of that electron in the net electrostatic potential of all other charges,

$$\phi_i = \phi_0 - (i-1)\frac{e}{C}, \tag{A.2}$$

where ϕ_0 is the background potential of the nuclei, and the second term is due to the previously added electrons. In this model the total ground-state energy of an n-electron ion (besides the electron-independent contributions) is

$$\begin{aligned} E_{gr}(n) &= \sum_{i=1}^{n} \Delta E(i) \\ &= \sum_{i=1}^{n} K_i - en\phi_0 + \frac{e^2}{2C} n(n-1), \end{aligned} \tag{A.3}$$

so that the energy difference created by the last charging is

$$\begin{aligned}\Delta E(n) &= E_{gr}(n) - E_{gr}(n-1) \\ &= K_n - e\phi_0 + \frac{e^2}{C}(n-1). \end{aligned} \tag{A.4}$$

On the other hand, in a hypothetical naïve DFT theory, without the partial self-interaction corrections present in its LSDA, GGA and ASIC versions, the single-particle (Kohn-Sham) energies of ion n of this model are written as

$$\varepsilon_i^{\rm DFT}(n) = K_i - e\phi_n, \;\; \phi_n = \phi_0 - \frac{e}{C}n. \tag{A.5}$$

For the calculation of the full ground-state energy of ion n, such generic DFT sums up these energies from $i = 1$ to $i = n$, adding the "double-counting correction" term [115], in the Gaussian units equal to

$$E_{\rm corr} = -\frac{1}{2}\int d^3r \int d^3r' \frac{\rho(\mathbf{r})\rho(\mathbf{r}')}{|\mathbf{r}-\mathbf{r}'|}, \tag{A.6}$$

where $\rho(\mathbf{r})$ is the total electron charge density at point $\mathbf{r}$. For our simple model, this correction is just $e^2n^2/2C$, so that

$$\begin{aligned} E_{gr}^{\rm DFT} &= \sum_{i=1}^{n} \varepsilon_i^{\rm DFT}(n) - \frac{e^2n^2}{2C} \\ &= \sum_{i=1}^{n} K_i - en\phi_0 + \frac{e^2n^2}{2C}, \end{aligned} \tag{A.7}$$

and

$$\begin{aligned} \Delta E^{\rm DFT}(n) &\equiv E_{gr}^{\rm DFT}(n) - E_{gr}^{\rm DFT}(n-1) \\ &= K_n - e\phi_0 + \frac{e^2}{C}\left(n - \frac{1}{2}\right). \end{aligned} \tag{A.8}$$

Comparing this result with Eq. (A.4), we obtain the following relation:

$$\Delta E(n) = \Delta E^{\rm DFT}(n) - \frac{e^2}{2C}. \tag{A.9}$$

Thus in the naïve DFT theory, the single-electron addition energy differs from the correct expression (A.4) by $e^2/2C$. Moreover, it does not satisfy the

fundamental Eq. (2.1). Indeed, for $i = n$, Eq. (A.5) gives the following result,

$$\varepsilon_n^{\rm DFT}(n) = K_n - e\phi_0 + \frac{e^2}{C}n \tag{A.10}$$

which, according to Eqs. (A.4) and (A.8) may be rewritten either as

$$\Delta E(n) = \varepsilon_n^{\rm DFT}(n) - \frac{e^2}{C}, \tag{A.11}$$

or as

$$\Delta E^{\rm DFT}(n) = \varepsilon_n^{\rm DFT}(n) - \frac{e^2}{2C}. \tag{A.12}$$

This error is natural, because such DFT version ignores the fundamental physical fact that an electron does not interact with itself, even if it is quantum-mechanically spread over a finite volume. This difference can become quite substantial in small objects such as molecular groups. For example, Table 1 shows the results using LSDA SIESTA calculations for two different ions of our trap molecule (Fig. 2.1b), with $n = n_0 + 1$ and $n = n_0 + 2$, where $n_0 = 330$ is the total number of protons in the molecule. The results show that the inconsistency described by Eq. (A.12) is indeed very substantial and is independent (as it should be) of the applied voltage V in the range keeping the working orbital's energy inside the HOMO-LUMO gap of the alkane chain. The two last columns of the table show the values of $e^2/2C$, calculated in two different ways: from the relation following from Eq. (A.5):

$$\frac{e^2}{2C} = \frac{\varepsilon_n^{\rm DFT}(n) - \varepsilon_n^{\rm DFT}(n-1)}{2}, \tag{A.13}$$

and from the direct electrostatic expression

$$\frac{e^2}{2C} = \frac{1}{2}\int \phi_n(\mathbf{r}) \left|\psi_n^{\rm DFT}(\mathbf{r})\right|^2 d^3r, \tag{A.14}$$

where $\phi_n(\mathbf{r})$ is the part of the electrostatic potential, created by the electron of the n-th orbital of the n-th ion. The values are very close to each other and correspond to capacitance $C \approx 4.5 \times 10^{-20}$ F which a perfectly conducting sphere of diameter $d \approx 0.8$ nm would have. The last number is in a very reasonable correspondence with the size of the acceptor group of the molecule — see Fig. 2.1b.

The second and third columns of the table present the genuine electron addition energies $\Delta E(n)$ calculated from, respectively, Eq. (A.9) and (A.11), using the average of the above values of $e^2/2C$. Not only do these values coincide very well; they are in a remarkable agreement with experimentally

Table A.1: Columns 2 and 3: values of the single-electron transfer energy $\Delta E(n)$ for the trap molecule ions with $n = n_0 + 1$ and $n = n_0 + 2$ electrons, calculated in LSDA SIESTA and then self-interaction corrected as discussed in Appendix A, as functions of the applied voltage (Column 1). Columns 3 and 4 list the values of parameter e^2/C , calculated as discussed in Appendix A.

Voltage V (V)	$\Delta E(n)$ from Eq. (A.9) (eV)	$\Delta E(n)$ from Eq. (A.11) (eV)	$e^2/2C$ from Eq. (A.13) (eV)	$e^2/2C$ from Eq. (A.14) (eV)
		$n = n_0 + 1$		
-2.36	-3.08	-3.01	1.84	1.79
-1.18	-3.38	-3.37	1.84	1.79
0.00	-3.73[(a)]	-3.73[(a)]	1.84	1.79
1.18	-4.07	-4.10	1.84	1.79
2.36	-4.42	-4.46	1.84	1.79
3.53	-4.77	-4.82	1.84	1.79
		$n = n_0 + 2$		
7.07	-1.91	-2.02	1.82	1.79
8.24	-2.29	-2.39	1.82	1.79
9.42	-2.61	-2.75	1.82	1.79
10.60	-2.97	-3.11	1.82	1.79
11.78	-3.32	-3.47	1.82	1.79

[(a)] The numbers to be compared with experimental values of electron affinity: -3.31 eV Ref. [96] and -3.57 eV Ref. [97].

measured electron affinities [96, 97] of molecules similar to our molecular trap.

We believe that these results show that, first, LSDA SIESTA provides very small compensation of the self-interaction effects in the key energy $\Delta E(n)$ and, second, that (at least for the lowest negative ions of our trap molecules), an effective compensation may be provided using any of the simple relations (A.9) and (A.11).

Appendix B

Level freezing in DFT

For the analysis of the fictitious "level freezing" predicted by a naïve DFT at $V > V_t$ (see Fig. 3.4), let us consider the following simple model: a molecule consisting of a small acceptor group with just one essential energy level, and a spatially separated chain with a quasi-continuous valence band. Figure B.1 shows the energy spectrum of the system at $V < V_t$. (As before, the occupied levels are shown in black, while the unoccupied ones are shown in green.)

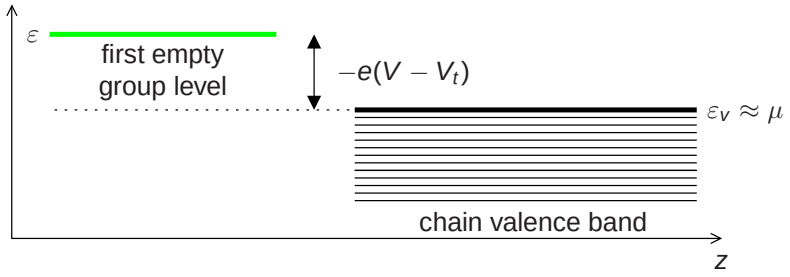

Figure B.1: The schematic energy spectrum of our model at a voltage V below voltage V_t that aligns the group localized level ε with the valence band edge ε_v.

The edge ε_v of the band is separated from the first unoccupied level in the group by energy $-e(V - V_t)$, where V is the fraction of the voltage drop between the centers of the group and the tail of a molecule, and V_t is its value which aligns the level with ε_v. Now let V be close to V_t, so that the occupancy p of the discrete level is noticeable. If the effect of group charging on the exchange-correlation energy is negligible, a generic DFT theory (e.g., LSDA) would describe the system energy as

$$\begin{aligned} E &= E_0 - e(V - V_t)p \\ &+ \frac{e^2}{2}\int d^3r \int d^3r' \frac{\rho(\mathbf{r})\rho(\mathbf{r}') - \rho_0(\mathbf{r})\rho_0(\mathbf{r}')}{|\mathbf{r}-\mathbf{r}'|}, \end{aligned} \tag{B.1}$$

where index 0 marks the variable values at $p = 0$.

Now let me simplify Eq. (B.1) by assuming that due to a small size of the acceptor group, the Coulomb interaction of electrons localized on it is much larger than that on the chain, so that the latter may be neglected. (For the trap molecule shown in Fig. 2.1b, this assumption is true within ∼5%.) Then Eq. (B.1) is reduced to

$$\begin{aligned} E &\approx E_0 - e(V - V_t)p - \frac{e}{2}\int_{\text{group}} \phi(\mathbf{r})\,|\psi(\mathbf{r})|^2\, d^3r, \\ p &= \int_{\text{group}} |\psi(\mathbf{r})|^2\, d^3r, \end{aligned} \tag{B.2}$$

where $\phi(\mathbf{r})$ is the electrostatic potential created by the part of the electronic wavefunction that resides on the group.

$$\phi(\mathbf{r}) = -e\int_{\text{group}} dr' \frac{|\psi(\mathbf{r}')|}{|\mathbf{r}-\mathbf{r}'|} \tag{B.3}$$

In the simple capacitive model of the group (used in particular in Appendix A), $\phi(\mathbf{r}) = -ep/C$, where C is the effective capacitance of the group, so that

$$E \approx E_0 - e(V - V_t)p + \frac{e^2p^2}{2C}. \tag{B.4}$$

On the other hand, in accordance with Eq. (A.7), the total energy in the DFT may generally be presented in the form

$$E = \sum_i p_i\varepsilon_i - \frac{e^2}{2}\int d^3r \int d^3r' \frac{\rho(\mathbf{r})\rho(\mathbf{r}')}{|\mathbf{r}-\mathbf{r}'|}, \tag{B.5}$$

where ε_i are all occupied (or partially occupied) single particle energies and ρ is the total electronic density. Then in our simple model the index i may be dropped and we get

$$E \approx E_0 + (\varepsilon - \varepsilon_v)p - \frac{e^2p^2}{2C}. \tag{B.6}$$

Comparing Eqs. (B.4) and (B.6), we arrive at the following expression:

$$\varepsilon - \varepsilon_v \approx -e(V - V_t) + \frac{e^2 p}{C}. \tag{B.7}$$

In most DFT packages, level occupancies p_i are calculated from the single-particle Fermi distribution,

$$p_i = \frac{1}{\exp\{(\varepsilon_i - \mu)/k_{\mathrm{B}}T\} + 1}; \tag{B.8}$$

for our simple model, and (due to the valence band multiplicity) $\mu \approx \varepsilon_v$.

As is evident from the sketch of Eqs. (B.7) and (B.8), in Fig. B.2, if the thermal fluctuation scale $k_{\mathrm{B}}T$ is much lower than the charging energy scale e^2/C, then almost within the whole range $V_t < V < V_t + e/C$, the approximate solution of the system of these equations is

$$p \approx \frac{C}{e}(V - V_t), \ \varepsilon \approx \varepsilon_v. \tag{B.9}$$

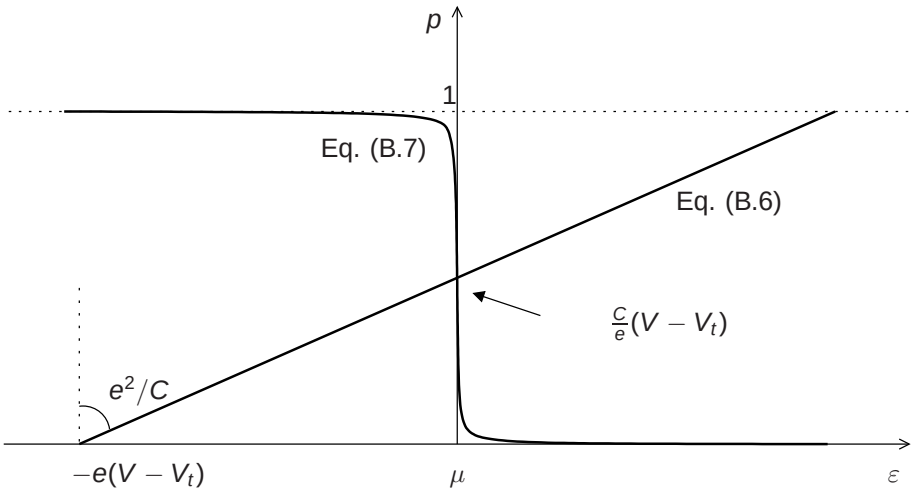

Figure B.2: A sketch of Eqs. (B.7) and (B.8).

Panel (a) in Fig. B.4 shows (schematically) the resulting dependence of the energy spectrum of our model system on the applied voltage V, with level freezing in the range $V_t < V < V_t + e/C$. The dashed black-green line indicates the region with a partial occupancy $0 < p < 1$ of the group-localized orbital. In panel (b) in (Fig. B.4) we show the evolution which should follow from the correct quantum-mechanical theory, in which electrons do not self-interact and as a result there is the usual anticrossing of energy levels ε and ε_v at $V = V_t$.

For clarity, Fig. B.4 strongly exaggerates the anticrossing width, which is less than 10^{-3} eV for our trap. A direct SIESTA calculation — see. Fig B.3 has shown that the anticrossing energy splitting is less than the calculation error (of the order of 10^{-3} eV). An indirect calculation using Eq. (3.39), with ψ_W and ψ_v substituted instead of ψ_i and $\psi_{s,c}$, suggests that this overlap is as small as $\sim 10^{-8}$ eV.

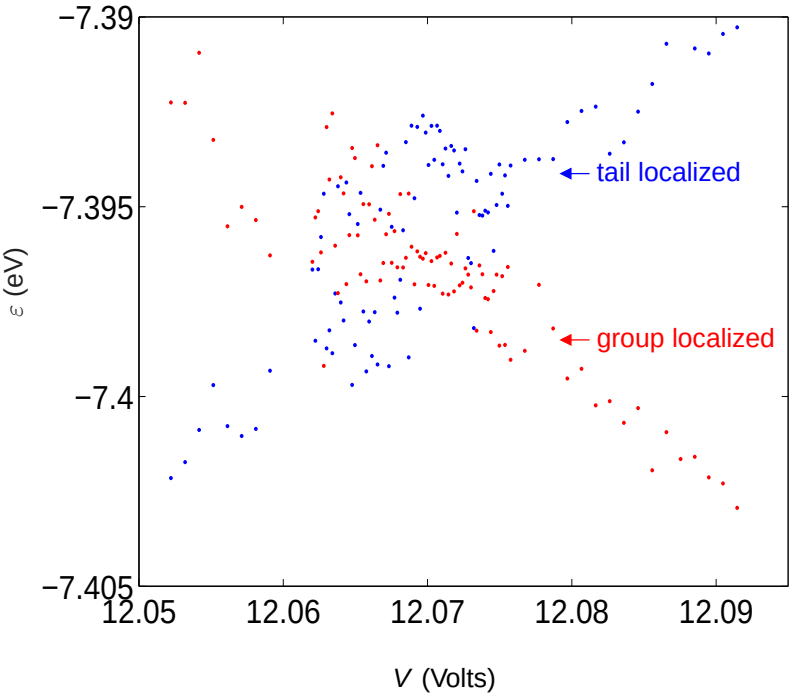

Figure B.3: The energy anticrossing of a group localized working orbital and the tail localized (valence band orbital). Evidently the anticrossing energy width is smaller than the DFT precision (of the order of 10^{-3} eV.)

The actual spectrum of our molecular trap is somewhat more complex than that of the simple model above — see Figs. 2.4 and 3.4. First, not only the valence energy band of the alkane chain, but also its conduction band is important for electron transfer in our voltage range. Second, the molecular group has not one, but a series of discrete energy levels, with the most important of them corresponding to the working orbital (energy ε_W), and one more group-localized orbital with energy $\varepsilon_{W+1} \approx \varepsilon_W + 0.7$ eV.

Nevertheless, the behavior of the spectrum, predicted by uncorrected versions of DFT (Fig. 3.4) may still be well understood using our model. Just as was discussed above, for voltages V above the threshold value V_t (which now corresponds to the alignment of ε_v with ε_{W+1} rather than ε_W), it describes a

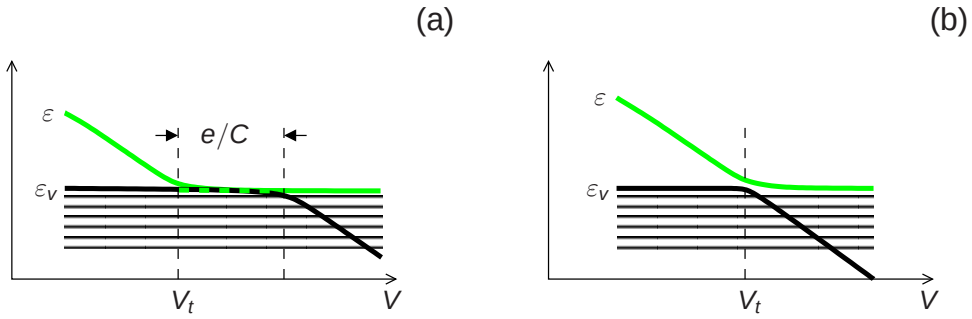

Figure B.4: (a) A sketch of the evolution of the energy spectrum from Fig. B.1 as a function of the applied voltage V, illustrating how the self-interaction errors give rise to a spurious level freezing in the $V_t < V < V_t + e/C$ voltage range. The dashed black-green line indicates the region with a partial occupancy $0 < p < 1$ of the group-localized orbital. (b) A sketch of the evolution of the same energy spectrum in a correct quantum-mechanical theory, in which electrons do not self-interact.

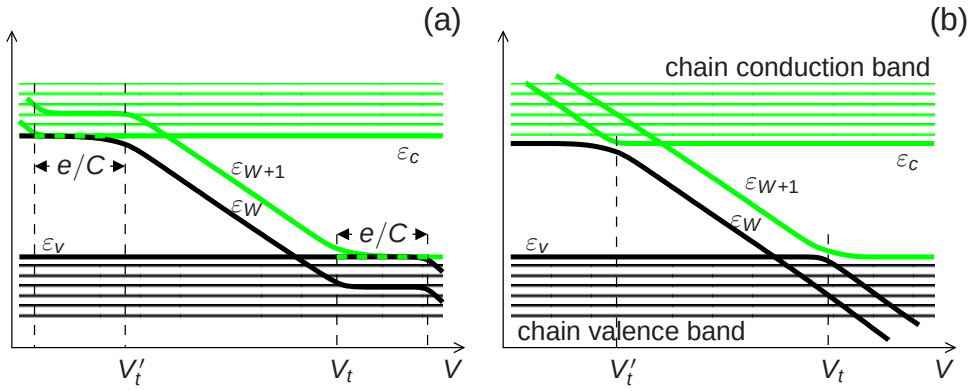

Figure B.5: (a) A sketch of the evolution of the molecular energy spectrum of our trap molecule as a function of the applied voltage V, illustrating how the self-interaction errors give rise to a spurious level freezing in voltage ranges $V_t' - e/C < V < V_t'$ and $V_t < V < V_t + e/C$. As if Fig. B.4, dashed black-green line indicate the regions with a partial occupancy $0 < p < 1$ of the group-localized orbitals with energies ε_W or ε_{W+1}. (b) A sketch of the evolution of the molecular energy spectrum but in a correct quantum-mechanical theory, in which electrons do not self-interact.

gradual transfer of an electron between the top level of the valence band and the second group-localized orbital, with its occupation number p_{W+1} gradually growing in accordance with Eq. (B.9) — see panel (a) in Fig. B.5. Similarly, at voltages V below V_t' (which corresponds to the alignment of the working

orbital's energy ε_W with the lowest level ε_c of the chain's conduction band), there is a similar spurious gradual transfer of an electron between the corresponding orbitals. In both voltage ranges, a spurious internal electrostatic potential is created; as is described by Eq. (B.9), it closely compensates the changes of the applied external potential, thus "freezing" all orbital energies of the system at their levels reached at thresholds V_t' and V_t — see panel (a) in Fig. B.5.

Figure B.6 shows that results of both the LSDA and ASIC DFT calculations at $V > V_t$ agree well with Eq. (B.9), with the value $C = 4.5 \times 10^{-20}$ F calculated as discussed in Appendix A, indicating that the electron self-interaction effects remain almost uncompensated in these software packages, at least for complex molecules such as our trap.

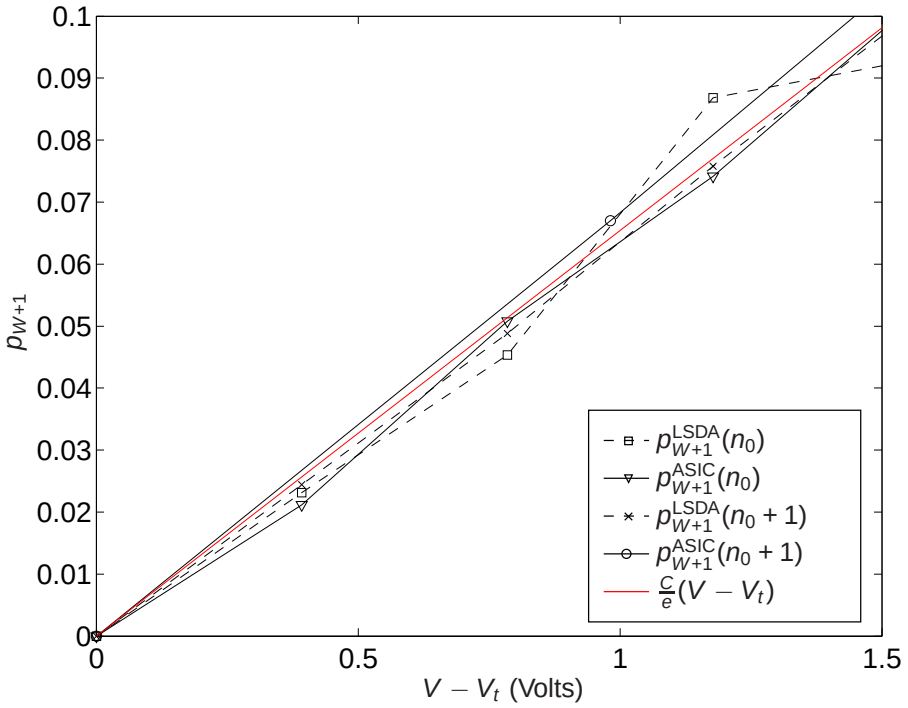

Figure B.6: The DFT-calculated occupancy p_{W+1} of the $(W+1)$st orbital of the acceptor group of the trap molecule at voltages above the threshold voltage V_t of the alignment of its energy ε_{W+1} with alkane chain's valence band edge ε_v. Black lines show results of two versions of DFT theory, for two ion states: the singly-negatively charged ion and the neutral molecule, while the red line shows the result given by Eq. (B.9) with $C = 4.5 \times 10^{-20}$ F.

Again, in the correct quantum-mechanical theory, there should be a simple (and in our molecules, extremely narrow) anticrossing between the effective

single-particle levels of the acceptor group and the alkane chain — see panel (b) in Fig. B.5. As described in Sec. III of the main text, we have succeeded to describe this behavior rather closely, using the internal iteration dynamics of ASIC SIESTA with $T = 0$ K.

Appendix C

Bardeen's Approximation

Figure C.1a shows a schematic potential profile of a molecular island attached to a metallic electrode via a non-conducting molecular chain is shown. The potential well of the metallic electrode is assumed to be constant and expanding infinitely into the negative z direction. Let wavefunctions $\psi'_{s,d}$ and ψ'_i be the eigenfunctions of the potentials $U'_{s,d}$ and U'_i (both with the same eigenenergy ε'), as schematically shown in Figs. C.1b,c.

If the two potential wells are now brought close together as shown in Fig. C.1a, the small probability of tunneling between the two wells must be taken into account. This may be done by means of setting the off-diagonal terms in the expectation value of the Hamiltonian matrix of the system equal to $\Delta\varepsilon/2$:

$$\langle H \rangle = \begin{pmatrix} \varepsilon' & \Delta\varepsilon/2 \\ \Delta\varepsilon/2 & \varepsilon' \end{pmatrix} \tag{C.1}$$

The Hamiltonian in Eq. (C.1) can be diagonalized by eigenfunctions $\psi_+ = 1/\sqrt{2}(\psi'_{s,d} + \psi'_i)$ and $\psi_- = 1/\sqrt{2}(\psi'_{s,d} - \psi'_i)$ with the corresponding eigenergies equal to $\varepsilon' - \Delta\varepsilon/2$ and $\varepsilon' + \Delta\varepsilon/2$.

I want to express the unknown $\Delta\varepsilon$ through the known quantities. Let us assume that the wavefunction $\psi'_{s,d}$ is vanishingly small in the potential well created by the molecular island, similarly the wavefunction ψ'_i is vanishingly small in the potential well of the metallic electrode. Therefore the product $\psi'_{s,d}\psi'_i$ is vanishingly small everywhere. Then let us write the following Schröedinger equations:

$$\begin{aligned} \nabla^2\psi'_i + \frac{2m}{\hbar^2}(\varepsilon' - U')\psi'_i = 0 \\ \nabla^2\psi^*_+ + \frac{2m}{\hbar^2}(\varepsilon_+ - U)\psi^*_+ = 0, \end{aligned} \tag{C.2}$$

Multiplying the first equation by ψ_+^* and the second equation by ψ_i' and subtracting the first of the from the second one yields

$$\psi_i'\nabla^2\psi_+^* - \psi_+^*\nabla^2\psi_i' = \frac{2m}{\hbar^2}\left((\varepsilon' - U')\psi_i'\psi_+^* - (\varepsilon_+ - U)\psi_+^*\psi_i'\right). \tag{C.3}$$

Now let us integrate this equation over the volume V where the potentials U and U' coincide:

$$\int_V \nabla\cdot\left(\psi_i'\nabla\psi_+^* - \psi_+^*\nabla\psi_i'\right)d^3V = \frac{2m}{\hbar^2}\int_V\left(\varepsilon'\psi_i'\psi_+^* - \varepsilon_+\psi_+^*\psi_i'\right)d^3V. \tag{C.4}$$

where I have used the relation

$$\int_V\left(U'\psi_i'\psi_+^* - U\psi_+^*\psi_i'\right)d^3V \approx 0$$

(that holds because the wavefunction ψ_i' in the region where $U' \neq U'$ is negligibly small), together with the relation

$$\left(\psi_i'\nabla^2\psi_+^* - \psi_+^*\nabla^2\psi_i'\right) = \nabla\cdot\left(\psi_i'\nabla\psi_+^* - \psi_+^*\nabla\psi_i'\right).$$

Next, we can apply the divergence theorem to a box so large that only the side of the box between the two potential wells gives a non-vanishing component (at other sides the wavefunctions ψ_i' and ψ_+^* are equal to zero). Taking into account the definition eigenenergy definition, we get

$$\int_S \mathbf{n}\cdot\left(\psi_i'\nabla\psi_+^* - \psi_+^*\nabla\psi_i'\right)d^2S = \frac{2m}{\hbar^2}\frac{1}{2}\left(\varepsilon' - \varepsilon_+\right). \tag{C.5}$$

where S is an arbitrary surface separating the left and right wells, and $\mathbf{n}$ is the normal to this surface, in particular it can be taken to be a plane in x, y, then (assuming that ψ_i' is real) we arrive at

$$\frac{\hbar^2}{2m}\int_S\left(\psi_{s,d}^*\frac{d\psi_i'}{dz} - \psi_i'\frac{d\psi_{s,d}^*}{dz}\right)dS = \Delta\varepsilon/2 \equiv T_{k\to k'}^{s,d}. \tag{C.6}$$

where the integral is taken on a plane S in x, y at $z = z_0$ (in the the gap between the two wells — see Fig. C.1).

Eq. (C.6) allows the calculation of matrix elements $T_{k,k'}^{s,d}$ and hence of the tunneling rates $\Gamma_{k\to k'}^{s,d}$ given by Eq. (3.38) in the main text.

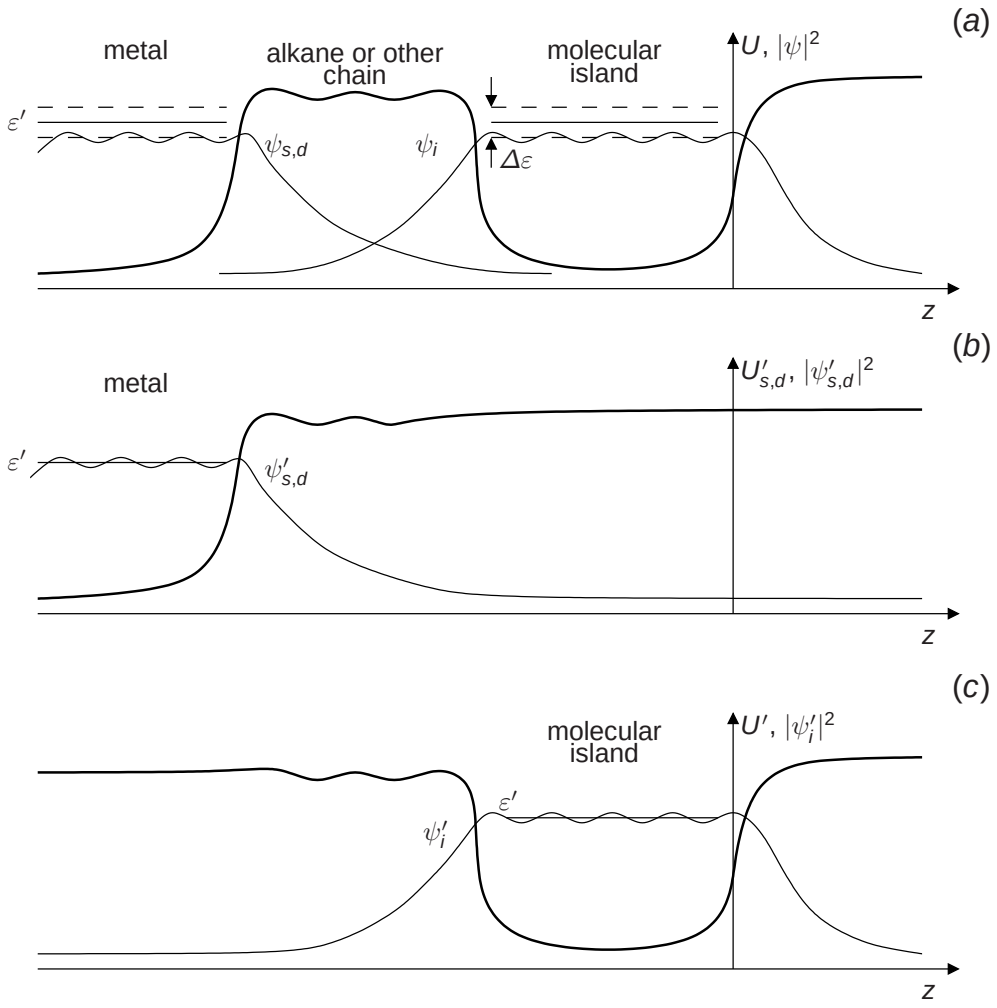

Figure C.1: In (a) the schematic potential profile along the molecule's axis with a potential well of the metallic electrode in the left and the potential well of the molecular island, attached to the metallic electrode via a non-conducting molecular chain in the right. The energy ε' is the electron eigenenergy if the two wells are infinitely far away, as shown in (b) and (c). When the small probability of tunneling is taken into account, the level ε' splits into two levels with a splitting width corresponding to $\Delta\varepsilon$, schematically shown in (a).

Appendix D

Correlation between charge states of two molecules

By definition, the coefficient of correlation between two independent random variables A and B is:

$$K(A,B) = \frac{cov(A,B)}{\sigma(A)\sigma(B)}, \tag{D.1}$$

where $cov(A,B)$ is the covariance between A and B. For discrete variables (where $E(X)$ is the expected value of the discrete random variable X),

$$\begin{aligned} cov(A,B) &= E(A,B) - E(A)E(B) \\ &= \sum_i A_i B_i P(A_i,B_i) - \left(\sum_i A_i P(A_i)\right)\left(\sum_i B_i P(B_i)\right), \end{aligned} \tag{D.2}$$

where $P(A_i), P(B_i)$ are the probabilities of random variables A, B to have values A_i, B_i, and $P(A_i,B_i)$ is their joint probability. The r.m.s. fluctuations σ_A, σ_B can be calculated from

$$\sigma(A) = \sqrt{var(A)} = \sqrt{\sum_i (A_i - \mu(A))^2 P(A_i)}, \tag{D.3}$$

where $\mu(A) = \sum_i A_i P(A_i)$, and similarly for $\sigma(B)$.

In the simplest case of just two states (i.e., our electric charge states), each of variables A, B has only two values: 0(the molecular group is neural), and 1(the group is charged), we have:

$$
\begin{aligned}
\mu(A) &= 0 * P_A(0) + 1 * P_A(1) = P_A(1), \\
\mu(B) &= 0 * P_B(0) + 1 * P_B(1) = P_B(1), \\
cov(A,B) &= P(1,1) - P_A(1)P_B(1), \\
\sigma(A) &= \sqrt{P_A(1) - P_A(1)^2}, \\
\sigma(B) &= \sqrt{P_B(1) - P_B(1)^2}.
\end{aligned} \tag{D.4}
$$

In order to write the final result more compact, let us define $P_A \equiv P_A(1)$, $P_B \equiv P_B(1)$ and $P_{A,B} \equiv P(1,1)$; then the correlation coefficient is

$$
K(A,B) = \frac{P_{A,B} - P_A P_B}{\sqrt{P_A(1-P_A)P_B(1-P_B)}}, \tag{D.5}
$$

as used in Eq. (5.4) of the main text.

Bibliography

[1] D.J. Frank, R.H. Dennard, E. Nowak, P.M. Solomon, Y. Taur, and Hon-Sum Philip Wong. Device scaling limits of si mosfets and their application dependencies. *Proceedings of the IEEE*, 89(3):259–288, 2001. doi: 10.1109/5.915374.

[2] V.A. Sverdlov, T.J. Walls, and K.K. Likharev. Nanoscale silicon mosfets: A theoretical study. *IEEE Transactions on Electron Devices*, 50(9):1926–1933, 2003. doi: 10.1109/TED.2003.816523.

[3] W. Haensch, E. J. Nowak, R. H. Dennard, P. M. Solomon, A. Bryant, O. H. Dokumaci, A. Kumar, X. Wang, J. B. Johnson, and M. V. Fischetti. Silicon cmos devices beyond scaling. *IBM Journal of Research and Development*, 50(4.5):339–361, 2006. doi: 10.1147/rd.504.0339.

[4] Thomas J. Walls and Konstantin K. Likharev. Two-dimensional quantum effects in ultimate nanoscale metal-oxide-semiconductor field-effect transistors. *Journal of Applied Physics*, 104(12):124307, 2008. doi: 10.1063/1.3039959.

[5] L. A. Bumm, J. J. Arnold, M. T. Cygan, T. D. Dunbar, T. P. Burgin, L. Jones, D. L. Allara, J. M. Tour, and P. S. Weiss. Are single molecular wires conducting? *Science*, 271(5256):1705–1707, 1996. doi: 10.1126/science.271.5256.1705.

[6] M. A. Reed. Conductance of a molecular junction. *Science*, 278(5336):252–254, 1997. doi: 10.1126/science.278.5336.252.

[7] C. Kergueris, J.-P. Bourgoin, S. Palacin, D. Esteve, C. Urbina, M. Magoga, and C. Joachim. Electron transport through a metal-molecule-metal junction. *Physical Review B*, 59(19):12505–12513, 1999. doi: 10.1103/PhysRevB.59.12505.

[8] Jiwoong Park, Abhay N. Pasupathy, Jonas I. Goldsmith, Connie Chang, Yuval Yaish, Jason R. Petta, Marie Rinkoski, James P. Sethna, Hctor D.

Abrua, Paul L. McEuen, and Daniel C. Ralph. Coulomb blockade and the kondo effect in single-atom transistors. *Nature*, 417(6890):722–725, 2002. doi: 10.1038/nature00791.

[9] Sergey Kubatkin, Andrey Danilov, Mattias Hjort, Jrme Cornil, Jean-Luc Brdas, Nicolai Stuhr-Hansen, Per Hedegrd, and Thomas Bjrnholm. Single-electron transistor of a single organic molecule with access to several redox states. *Nature*, 425(6959):698–701, 2003. doi: 10.1038/nature02010.

[10] A. N. Pasupathy, J. Park, C. Chang, A. V. Soldatov, S. Lebedkin, R. C. Bialczak, J. E. Grose, L. A. K. Donev, J. P. Sethna, D. C. Ralph, and P. L. McEuen. Vibration-assisted electron tunneling in c_{140} transistors. *Nano Letters*, 5(2):203–207, 2005. doi: 10.1021/nl048619c.

[11] Dong-Hun Chae, John F. Berry, Suyong Jung, F. Albert Cotton, Carlos A. Murillo, and Zhen Yao. Vibrational excitations in single trimetal-molecule transistors. *Nano Letters*, 6(2):165–168, 2006. doi: 10.1021/nl0519027.

[12] Andrey Danilov, Sergey Kubatkin, Sergey Kafanov, Per Hedegard, Nicolai Stuhr-Hansen, Kasper Moth-Poulsen, and Thomas Bjornholm. Electronic transport in single molecule junctions: Control of the molecule-electrode coupling through intramolecular tunneling barriers. *Nano Letters*, 8(1):1–5, 2008. doi: 10.1021/nl071228o. URL http://pubs.acs.org/doi/abs/10.1021/nl071228o. PMID: 18085806.

[13] Changsheng Wang, Andrei S. Batsanov, Martin R. Bryce, Santiago Martin, Richard J. Nichols, Simon J. Higgins, Victor M. Garcia-Suarez, and Colin J. Lambert. Oligoyne single molecule wires. *Journal of the American Chemical Society*, 131(43):15647–15654, 2009. doi: 10.1021/ja9061129.

[14] Konstantin K. Likharev. Hybrid cmos/nanoelectronic circuits: Opportunities and challenges. *Journal of Nanoelectronics and Optoelectronics*, 3(3):203–230, 2008.

[15] R. Waser, R. Dittmann, G. Staikov, and K. Szot. Redox-based switching memories - nanoionic mechanisms, prospects, and challenges. *Adv. Materials*, 21:2632, 2009.

[16] D.B. Strukov and H. Kohlstedt. Resistive switching phenomena in thin films: Materials, devices, and applications. *MRS Bulletin*, 37(02):108–114, 2012. doi: 10.1557/mrs.2012.2.

[17] James R. Heath, Philip J. Kuekes, Gregory S. Snider, and R. Stanley Williams. A defect-tolerant computer architecture: Opportunities for nanotechnology. *Science*, 280(5370):1716–1721, 1998.

[18] Konstantin K. Likharev, Andreas Mayr, Ibrahim Mucra, and Ozgur Turel. Crossnets high-performance neuromorphic architectures for cmol circuits. *Annals of the New York Academy of Sciences*, 1006:146–163, 2003.

[19] K. K. Likharev. Correlated discrete transfer of single electrons in ultrasmall junctions. *IBM J. Res. Develop.*, 32:144–158, 1988.

[20] D. V. Averin and A. N. Korotkov. Correlated single-electron tunneling via mesoscopic metal particles: Effects of the energy quantization. *Journal of Low Temperature Physics*, 80(3-4):173–185, 1990. doi: 10.1007/BF00683484.

[21] C. W. J. Beenakker. Theory of coulomb-blockade oscillations in the conductance of a quantum dot. *Phys. Rev. B*, 44(4):16461656, 1991.

[22] Dmitri. V. Averin, Alexander. N. Korotkov, and Konstantin K. Likharev. Theory of single-electron charging of quantum wells and dots. *Phys. Rev. B*, 44(12):61996211, 1991.

[23] C. J. Amsinck, N. H. Di Spigna, D. P. Nackashi, and P. D. Franzon. Scaling constraints in nanoelectronic random-access memories. *Nanotechnology*, 16:2251–2260, 2005.

[24] D. B. Strukov and K. K. Likharev. Defect-tolerant architectures for nanoelectronic crossbar memories. *J. of Nanosci. and Nanotech.*, 7:151–167, 2007.

[25] International technology roadmap for semiconductors. 2012 edition. available online at http://www.itrs.net/links/2012ITRS/.

[26] Fushan Li, Tae Whan Kim, Wenguo Dong, and Young-Ho Kim. Formation and electrical bistability properties of zno nanoparticles embedded in polyimide nanocomposites sandwiched between two c[sub 60] layers. *Applied Physics Letters*, 92(1):011906, 2008. doi: 10.1063/1.2830617.

[27] Nathaniel G. Portney, Alfredo A. Martinez-Morales, and Mihrimah Ozkan. Nanoscale memory characterization of virus-templated semiconducting quantum dots. *ACS Nano*, 2(2):191–196, 2008. doi: 10.1021/nn700240z.

[28] S. Kolliopoulou, P. Dimitrakis, P. Normand, Hao-Li Zhang, Nicola Cant, Stephen D. Evans, S. Paul, C. Pearson, A. Molloy, M. C. Petty, and D. Tsoukalas. Hybrid siliconorganic nanoparticle memory device. *Journal of Applied Physics*, 94(8):5234, 2003. doi: 10.1063/1.1604962.

[29] Jae Hun Jung, Jae-Ho Kim, Tae Whan Kim, Mun Seop Song, Young-Ho Kim, and Sungho Jin. Nonvolatile organic bistable devices fabricated utilizing cu[sub 2]o nanocrystals embedded in a polyimide layer. *Applied Physics Letters*, 89(12):122110, 2006. doi: 10.1063/1.2355465.

[30] Wei Lin Leong, Nripan Mathews, Subodh Mhaisalkar, Yeng Ming Lam, Tupei Chen, and Pooi See Lee. Micellar poly(styrene-b-4-vinylpyridine)-nanoparticle hybrid system for non-volatile organic transistor memory. *Journal of Materials Chemistry*, 19(39):7354, 2009. doi: 10.1039/B911493A.

[31] Won Tae Kim, Jae Hun Jung, Tae Whan Kim, and Dong Ick Son. Current bistability and carrier transport mechanisms of organic bistable devices based on hybrid ag nanoparticle-polymethyl methacrylate polymer nanocomposites. *Applied Physics Letters*, 96(25):253301, 2010. doi: 10.1063/1.3453661.

[32] J.Billen, R.Muller, J.Genoe, and P.Heremans. *Proc. of ICMTD*, page 135, 2007.

[33] L. P. Ma, J. Liu, and Y. Yang. Organic electrical bistable devices and rewritable memory cells. *Applied Physics Letters*, 80(16):2997, 2002. doi: 10.1063/1.1473234.

[34] Anirban Bandhopadhyay and Amlan J. Pal. Large conductance switching and binary operation in organic devices: Role of functional groups. *The Journal of Physical Chemistry B*, 107(11):2531–2536, 2003. doi: 10.1021/jp027369q.

[35] Jianyong Ouyang, Chih-Wei Chu, Charles R. Szmanda, Liping Ma, and Yang Yang. Programmable polymer thin film and non-volatile memory device. *Nature Materials*, 3(12):918–922, 2004. doi: 10.1038/nmat1269.

[36] Ralf Thomas Weitz, Andreas Walter, Reimund Engl, Recai Sezi, and Christine Dehm. New charge-transfer salts for reversible resistive memory switching. *Nano Letters*, 6(12):2810–2813, 2006. doi: 10.1021/nl0619204.

[37] T. W. Hickmott. Low-frequency negative resistance in thin anodic oxide films. *Journal of Applied Physics*, 33(9):2669, 1962. doi: 10.1063/1.1702530.

[38] H.Schröder and D.S.Jeong. *Microel. J.*, 84:1982, 2007.

[39] Zhiyong Li, Matthew D Pickett, Duncan Stewart, Douglas A A Ohlberg, Xuema Li, Wei Wu, Warren Robinett, and R Stanley Williams. Experimental demonstration of a defect-tolerant nanocrossbar demultiplexer. *Nanotechnology*, 19(16):165203, 2008. doi: 10.1088/0957-4484/19/16/165203.

[40] J. Joshua Yang, Matthew D. Pickett, Xuema Li, Douglas A. A. Ohlberg, Duncan R. Stewart, and R. Stanley Williams. Memristive switching mechanism for metal/oxide/metal nanodevices. *Nature Nanotechnology*, 3(7):429–433, 2008. doi: 10.1038/nnano.2008.160.

[41] I.G. Baek, D.C. Kim, M.J. Lee, H.-J. Kim, E.K. Yim, M.S. Lee, J.E. Lee, S.E. Ahn, S. Seo, J.H. Lee, J.C. Park, Y.K. Cha, S.O. Park, H.S. Kim, I.K. Yoo, U. Chung, J.T. Moon, and B.I. Ryu. Multi-layer cross-point binary oxide resistive memory (oxrram) for post-nand storage application. In *IEEE InternationalElectron Devices Meeting, 2005. IEDM Technical Digest.*, pages 750–753. IEEE, 2005. doi: 10.1109/IEDM.2005.1609462.

[42] An Chen, S. Haddad, Yi-Ching Wu, Tzu-Ning Fang, Zhida Lan, S. Avanzino, S. Pangrle, M. Buynoski, M. Rathor, Wei Cai, N. Tripsas, C. Bill, M. Van Buskirk, and M. Taguchi. Non-volatile resistive switching for advanced memory applications. In *IEEE InternationalElectron Devices Meeting, 2005. IEDM Technical Digest.*, pages 746–749. IEEE, 2005. doi: 10.1109/IEDM.2005.1609461.

[43] T.N.Fang, S.Kaza, S.Haddad, A.Chen, Y.C.Wu, Z.Lan, S.Avanzino, D.Liao, C.Gopalan, S.Mahdavi, M.Buynoski, C.Marrian, M.VanBuskirk, and M.Taguchi. In *2nd International Conference on Memory Technology and Design - ICMTD*, page 143. IMEC, 2007.

[44] Christina Schindler, Sarath Chandran Puthen Thermadam, Rainer Waser, and Michael N. Kozicki. Bipolar and unipolar resistive switching in cu-doped SiO_2. *IEEE Transactions on Electron Devices*, 54(10):2762–2768, 2007. doi: 10.1109/TED.2007.904402.

[45] Rainer Waser and Masakazu Aono. Nanoionics-based resistive switching memories. *Nature Materials*, 6(11):833–840, 2007. doi: 10.1038/nmat2023.

[46] K. Terabe, T. Hasegawa, T. Nakayama, and M. Aono. Quantized conductance atomic switch. *Nature*, 433(7021):47–50, 2005. doi: 10.1038/nature03190.

[47] Naoki Banno, Toshitsugu Sakamoto, Noriyuki Iguchi, Hisao Kawaura, Shunichi Kaeriyama, Masayuki Mizuno, Kozuya Terabe, Tsuyoshi Hasegawa, and Masakazu Aono. Solid-electrolyte nanometer switch. *IEICE TRANSACTIONS on Electronics*, E89-C(11):1492–1498, 2006.

[48] L. Courtade, Ch. Turquat, D Goguenheim, Ch. Muller, J.G. Lisoni, L. Goux, D.J. Wouters, and D. Goguenheim. Resistive switching and microstructure of nio binary oxide films developed for oxrram non-volatile memories. In *2nd International Conference on Memory Technology and Design - ICMTD*, pages 147–150. IMEC, 2007.

[49] M H Zhai, K B Yin, L Shi, J Yin, and Z G Liu. Conductance switching effect in the cu/cui. *Journal of Physics D: Applied Physics*, 40(12): 3702–3706, 2007. doi: 10.1088/0022-3727/40/12/024.

[50] Chad Johns, Doug A. A. Ohlberg, Shih-Yuan Wang, R. Stanley Williams, and M. Saif Islam. Nanoscale switching junctions based on an organic monolayer of molecules and solid electrolytes. In *2007 7th IEEE Conference on Nanotechnology (IEEE NANO)*, pages 1306–1308. IEEE, 2007. doi: 10.1109/NANO.2007.4601422.

[51] Weihua Guan, Shibing Long, Rui Jia, and Ming Liu. Nonvolatile resistive switching memory utilizing gold nanocrystals embedded in zirconium oxide. *Applied Physics Letters*, 91(6):062111, 2007. doi: 10.1063/1.2760156.

[52] Y.Dong, G.Yu, M.C.McAlpine, W.Lu, and C.M.Lieber. Si/a-si core/shell nanowires as nonvolatile crossbar switches. *Nano Lett.*, 8:386, 2008. doi: 10.1021/nl073224p.

[53] Weihua Guan, Shibing Long, Qi Liu, Ming Liu, and Wei Wang. Nonpolar nonvolatile resistive switching in cu doped zro_2. *IEEE Electron Device Letters*, 29(5):434–437, 2008. doi: 10.1109/LED.2008.919602.

[54] S.H.Jo and W.Lu. Cmos compatible nanoscale nonvolatile resistance switching memory. *IEEE Electron Device Letters*, 8(2):392397, 2008. doi: 10.1021/nl073225h.

[55] C. P. Collier, E. W. Wong, M. Belohradsky, F. M. Raymo, J. F. Stoddart, P. J. Kuekes, R. S. Williams, and J. R. Heath. Electronically configurable

molecular-based logic gates. *Science*, 285(5426):391–394, 1999. doi: 10.1126/science.285.5426.391.

[56] Charles P. Collier, Gunter Mattersteig, Eric W. Wong, Yi Luo, Kristen Beverly, Jose Sampaio, Francisco M. Raymo, J. Fraser Stoddart, and James R. Heath. A [2]catenane-based solid state electronically reconfigurable switch. *Science*, 289(5482):1172–1175, 2000. doi: 10.1126/science.289.5482.1172.

[57] W. R Dichtel, J. R Heath, and J Fraser Stoddart. Designing bistable [2]rotaxanes for molecular electronic devices. *Philosophical Transactions of the Royal Society A: Mathematical, Physical and Engineering Sciences*, 365(1855):1607–1625, 2007. doi: 10.1098/rsta.2007.2034.

[58] John Lambe and R. Jaklevic. Charge-quantization studies using a tunnel capacitor. *Physical Review Letters*, 22(25):1371–1375, 1969. doi: 10.1103/PhysRevLett.22.1371.

[59] I. O. Kulik and R. I. Shekhter. Kinetic phenomena and charge discreteness effects in granular media. *Sov. Phys. - JETP*, 41:308–316, 1975.

[60] Likharev K.K. and Averin D.V. Coulomb blockade of tunneling, and coherent oscillations in small tunnel junction. *J. Low Temp. Phys.*, 62 (3/4):345–372, 1986.

[61] Likharev K.K. New results of the theory of SET and bloch oscillations in small tunnel junctions. *IEEE Trans. Magn.*, 23(2):1138–1141, 1987.

[62] T. Fulton and G. Dolan. Observation of single-electron charging effects in small tunnel junctions. *Physical Review Letters*, 59(1):109–112, 1987. doi: 10.1103/PhysRevLett.59.109.

[63] Yu. A. Pashkin, Y. Nakamura, and J. S. Tsai. Room-temperature al single-electron transistor made by electron-beam lithography. *Applied Physics Letters*, 76(16):2256, 2000. doi: 10.1063/1.126313.

[64] P. Dresselhaus, J. Li, S. Han, L. Ji, J.E. Lukens, and K.K. Likharev. Single electron lifetimes in a multijunction trap. *Phys. Rev. Lett.*, 72: 3226–3229, 1994.

[65] L. Ji, P.D. Dresselhaus, S. Han, K. Lin, W. Zheng, and J. Lukens. Fabrication and characterization of single-electron transistors and traps. *J. Vac. Sci. Technol. B*, 12:3619–3622, 1994.

[66] Konstantin K. Likharev. Single-electron devices and their applications. *Proceedings of the IEEE*, 87:606–632, 1999.

[67] James M. Tour. *Molecular Electronics*. World Scientific, Singapore, 2003.

[68] Gianaurelio Cuniberti and Giorgos Fagas. Introducing molecular electronics. In Klaus Richter, editor, *Lecture Notes In Physics*, volume 680. Springer, Berlin, 2005.

[69] Andreas Mayr, Muthialu Srisailas, Qun Zhao, Yuan Gao, Heidi Hsieh, Mahsa Hoshmand-Kochi, and Natalie St. Fleur. Synthesis of oligo(phenyleneethynylene)s containing central pyromellitdiimide or naphthalenediimide groups and bearing terminal isocyanide groups: molecular components for single-electron transistors. *Tetrahedron*, 63: 8206, 2007.

[70] San-Huang Ke, Harold U. Baranger, , and Weitao Yang. Contact transparency of nanotube-molecule-nanotube junctions. *Phys. Rev. Lett.*, 99: 146802, 2007.

[71] Wenyong Wang, Takhee Lee, and Mark A. Reed. Electronic transport in self-assembled alkanethiol monolayers. *Physica E: Low-dim. Sys. and Nanostructures*, 19:117–125, 2003.

[72] K. K. Likharev, N. S. Bakhvalov, G. S. Kazacha, and S. I. Serdyukova. Single-electron tunnel junction array: An electrostatic analog of the josephson transmission line. *IEEE Trans. Magn.*, 25:1436–1439, 1989.

[73] A L Efros and B I Shklovskii. Coulomb gap and low temperature conductivity of disordered systems. *Journal of Physics C: Solid State Physics*, 8(4):L49–L51, 1975. doi: 10.1088/0022-3719/8/4/003.

[74] C. D. Pemmaraju, T. Archer, D. Sánchez-Portal, and S. Sanvito. Atomic-orbital-based approximate self-interaction correction scheme for molecules and solids. *Phys. Rev. B*, 75:045101, 2007. doi: 10.1103/PhysRevB.75.045101.

[75] Shane McDermott, Christopher B. George, Giorgos Fagas, James C. Greer, and Mark A. Ratner. Tunnel currents across silane diamines/dithiols and alkane diamines/dithiols: A comparative computational study. *J. Phys. Chem. C*, 113:744–750, 2009.

[76] Dmitri B Strukov and Konstantin K Likharev. Prospects for terabit-scale nanoelectronic memories. *Nanotechnology*, 16(1):137–148, 2005. doi: 10.1088/0957-4484/16/1/028.

[77] Dmitri B Strukov and Konstantin K Likharev. Defect-tolerant architectures for nanoelectronic crossbar memories. *J. of Nanosci. and Nanotech.*, 7:151–167, 2007.

[78] Dmitri B Strukov and Konstantin K Likharev. Cmol fpga: a reconfigurable architecture for hybrid digital circuits with two-terminal nanodevices. *Nanotechnology*, 16(6):888–900, 2005. doi: 10.1088/0957-4484/16/6/045.

[79] C. J. Amsinck, N. H. Di Spigna, D. P. Nackashi, and P. D. Franzon. Scaling constraints in nanoelectronic random-access memories. *Nanotechnology*, 16:2251–2260, 2005.

[80] S.J. Krausea, T.B. Haddocka, D.L. Veziea, P.G. Lenhertb, W.-F. Hwang, G.E. Pricec, T.E. Helminiakd, J.F. O'Briend, and W.W. Adams. Morphology and properties of rigid-rod poly(p-phenylene benzobisoxazole) (pbo) and stiff-chain poly(2,5(6)-benzoxazole) (abpbo) fibres. *Polymer*, 29(8):1354–1364, 1988.

[81] Likharev K. K. and Strukov D. B. Cmol technology development roadmap. In *Proc. of the 4th Workshop on Non-Silicon Computing.* IEEE, Piscataway, NJ, 2007.

[82] Likharev K. K. Electronics below 10 nm. In Greer J. *et al.*, editor, *Giga and Nano Challenges in Microelectronics.* Elsevier, Amsterdam.

[83] M.R. Pederson, D.V. Porezag, J. Kortus, and D.C. Patton. Strategies for massively parallel local-orbital-based electronic structure methods. *Phys. Stat. Sol. (b)*, 217(1):219–230, 2000.

[84] J. M. Soler, E. Artacho, J.D. Gale, A. Garcia, J. Junquera, P. Ordejon, and D. Sanchez-Portal. The siesta method for ab initio order-n materials simulation. *J. Phys.: Condens. Matter*, 14:2745–2779, 2002.

[85] C. Toher, A. Filippetti, S. Sanvito, and Kieron Burke. Self-interaction errors in density-functional calculations of electronic transport. *Physical Review Letters*, 95(14):146402, 2005. doi: 10.1103/PhysRevLett.95.146402.

[86] Y. Q. Feng, Zhang R. Q., and Lee S. T. Simulation of gate-controlled coulomb blockades in carbon nanotubes. *Journal of Applied Physics*, 95 (10):5729, 2004. doi: 10.1063/1.1704851.

[87] Per Hedegard and Thomas Bjornholm. Charge transport through image charged stabilized states in a single molecule single electron transistor device. *Chemical Physics*, 319(1-3):350–359, 2005. doi: 10.1016/j.chemphys.2005.05.035.

[88] Klessinger M and Michl J. *Excited States and Photochemistry of Organic Molecules*. VCH, New York, 1995.

[89] T. H. Stoof and Yu. V. Nazarov. Time-dependent resonant tunneling via two discrete states. *Phys. Rev. B*, 53(3):10501053, 1996.

[90] D. V. Averin, J. R. Friedman, and J. E. Lukens. Macroscopic resonant tunneling of magnetic flux. *Phys. Rev. B*, 62:11802, 2000.

[91] Jens P. Dahl. *Introduction to the Quantum Worlds of Atoms and Molecules*. World Scientific, Singapore, 2002.

[92] P. Hohenberg and Kohn W. Inhomogeneous electron gas. *Physical Review*, 136(3B):B864–B871, 1964. doi: 10.1103/PhysRev.136.B864.

[93] W. Kohn and L. J. Sham. Self-consistent equations including exchange and correlation effects. *Physical Review*, 140(4A):A1133–A1138, 1965. doi: 10.1103/PhysRev.140.A1133.

[94] John P. Perdew, Kieron Burke, and Matthias Ernzerhof. Generalized gradient approximation made simple. *Physical Review Letters*, 77(18): 3865–3868, 1996. doi: 10.1103/PhysRevLett.77.3865.

[95] J. P. Perdew and Alex Zunger. Self-interaction correction to density-functional approximations for many-electron systems. *Phys. Rev. B*, 23: 5048–5079, 1981. doi: 10.1103/PhysRevB.23.5048.

[96] S. V. Bhosale, C. H. Jani, and S. J. Langford. Chemistry of naphthalene diimides. *Chem. Soc. Rev.*, 37:331342, 2008.

[97] T. B. Singh, S. Erten, S. Günes, C. Zafer, G. Turkmen, B. Kuban, Y. Teoman, N.S. Sariciftci, and S. Icli. Soluble derivatives of perylene and naphthalene diimide for n-channel organic field-effect transistors. *Organic Electronics*, 7:480489, 2006.

[98] J. F. Janak. Proof that $\delta e/\delta n_i = \varepsilon$ in density-functional theory. *Phys. Rev. B*, 18:7165–7168, 1978.

[99] J. Bardeen. Tunnelling from a many-particle point of view. *Phys. Rev. Lett.*, 6(2):5759, 1961.

[100] Jiwoong Park, Abhay N. Pasupathy, Jonas I. Goldsmith, Connie Chang, Yuval Yaish, Jason R. Petta, Marie Rinkoski, James P. Sethna, Hector D. Abruna, Paul L. McEuen, and Daniel C. Ralph. Electron tunneling through alkanedithiol self-assembled monolayers in large-area molecular junctions. *Nature*, 417:722, 2002.

[101] Averin D V and Likharev K K. Coulomb blockade of single-electron tunneling, and coherent oscillations in small tunnel junctions. *J. Low Temp. Phys.*, 62:345—373, 1986.

[102] Park H, Park J, Lim A K L, Anderson E H, Alivisatos P, and McEuen. Nanomechanical oscillations in a single-c60 transistor. *Nature*, 407:57—60, 2000.

[103] Sergey Kubatkin, Andrey Danilov, Mattias Hjort, Jerome Cornil, Jean-Luc Bredas, Nicolai Stuhr-Hansen, and Per Hedegard Thomas Bjornholm. Single-electron transistor of a single organic molecule with access to several redox states. *Nature*, 425:698–701, 2003.

[104] M. Grobis, A. Wachowiak, R. Yamachika, and M. F. Crommie. Tuning negative differential resistance in a molecular film. *Applied Physics Letters*, 86(20):204102, 2005. doi: 10.1063/1.1931822.

[105] L. Esaki and P. Stiles. New type of negative resistance in barrier tunneling. *Physical Review Letters*, 16(24):1108–1111, 1966. doi: 10.1103/PhysRevLett.16.1108.

[106] G.-C. Liang and A. Ghosh. Identifying contact effects in electronic conduction through c60 on silicon. *Physical Review Letters*, 95(7):076403, 2005. doi: 10.1103/PhysRevLett.95.076403.

[107] Saiful I. Khondaker, Zhen Yao, Long Cheng, Jay C. Henderson, Yuxing Yao, and James M. Tour. Electron transport through single phenyleneethynylene molecular junctions at low temperature. *Applied Physics Letters*, 85(4):645, 2004. doi: 10.1063/1.1773915.

[108] Strukov D V and Likharev K K. Cmol: Devices, circuits, and architectures. In Cuniberti G, editor, *Introduction to Molecular Electronics*, pages 447—477. Springer, Berlin, 2005.

[109] Likharev K K. Hybrid semiconductor/nanoelectronic circuits. *Proc. of Nanotech 2007 (NSTI, Cambridge, MA)*, pages 552—555, 2007.

[110] Goto E. Esaki diode high speed logical circuits. *IRE Trans. Elect. Comp.*, 9:25—29, 1960.

[111] Mathews R H, Sage J P, Sollner T C L G, Calawa S D, Chen C L, Mahoney L J, Maki P A, and Molvar KM. A new rtd-fet logic family. *Proc. IEEE*, 87:596—605, 1999.

[112] Rose G S and Stan M R. Memory arrays based on molecular rtd devices. *Proc. of IEEE-NANO-2003*, pages 453–456, 2003.

[113] Hylke B. Akkerman, Paul W. M. Blom, Dago M. de Leeuw, and Bert de Boer. Towards molecular electronics with large-area molecular junctions. *Nature*, 441:69–72, 2006.

[114] A. N. Korotkov. Intrinsic noise of the single-electron transistor. *Phys. Rev. B*, 49:10381–10392, 1994.

[115] R. O. Jones and O. Gunnarsson. The density functional formalism, its applications and prospects. *Rev. Mod. Phys.*, 61(3):689746, 1989.

[116] K.-T. Cheng and D.B. Strukov. 3d cmos-memristor hybrid circuits: Devices, integration, architecture, and applications. *Proceedings of ISPD'12*, 2012.

[117] Zhitenev N B, Meng H, and Bao Z. Conductance of small molecular junctions. *Phys. Rev. Lett.*, 88:226801, 2002.

[118] A. Mitra, I. Aleiner, and A. Millis. Phonon effects in molecular transistors:quantal and classical treatment. *Physical Review B*, 69(24):245302, 2004. doi: 10.1103/PhysRevB.69.245302.

[119] Michael Galperin, Mark A Ratner, and Abraham Nitzan. Molecular transport junctions: vibrational effects. *Journal of Physics: Condensed Matter*, 19(10):103201, 2007. doi: 10.1088/0953-8984/19/10/103201.